TECHNICAL REPORT R-2

SLENDER-BODY THEORY BASED ON APPROXIMATE SOLUTION OF THE TRANSONIC FLOW EQUATION

By JOHN R. SPREITER and ALBERTA Y. ALKSNE

Ames Research Center
Moffett Field, Calif.

CONTENTS

TECHNICAL REPORT R-2

SLENDER-BODY THEORY BASED ON APPROXIMATE SOLUTION OF THE TRANSONIC FLOW EQUATION

By JOHN R. SPREITER and ALBERTA Y. ALKSNE

SUMMARY

Approximate solutions of the nonlinear equations of the small disturbance theory of transonic flow are found for the pressure distribution on pointed slender bodies of revolution for flows with free-stream Mach number 1, and for flows that are either purely subsonic or purely supersonic. These results are obtained by application of a method based on local linearization that was introduced recently in the analysis of similar problems in two-dimensional flows. The theory is developed for bodies of arbitrary shape, and specific results are given for cone-cylinders and for parabolic-arc bodies at zero angle of attack. All results are compared either with existing theoretical results or with experimental data.

INTRODUCTION

This paper is concerned with the prediction of the pressure distribution on slender pointed bodies of revolution in flight at zero angle of attack at high subsonic Mach numbers, at low supersonic Mach numbers, and at Mach numbers near 1. The solution of such problems is of interest not only because of the frequent use of bodies of revolution in practical applications but also because knowledge of the aerodynamic properties of a body of revolution in axisymmetric flow taken together with the transonic area rule and equivalence rule described in references 1, 2, 3, and elsewhere permits the ready calculation of the aerodynamic properties of a wide class of wings, bodies, wing-body combinations, etc., having the same longitudinal distribution of cross-section area as the body of revolution.

The analysis is based throughout on the small disturbance theory of transonic flow. This theory, at least as formulated in this paper and in several earlier papers of the present authors, is not restrictive in its range of applicability as might be inferred from its name, but is equally applicable to subsonic and supersonic flows. It is, moreover, the simplest theory proposed to date that is capable of yielding reliable results throughout this entire speed range. Difficulties arise in the solution of the equations of transonic flow theory, however, because the governing partial differential equation is nonlinear and of mixed elliptic-hyperbolic type if regions of subsonic and supersonic flow both appear in a single flow field. Inasmuch as the mathematical theory of such equations is still in a rather early state of development and methods have not yet been discovered for the exact solution of such equations, the engineer is forced to turn either to experiment or to approximate methods for the solution of practical problems. Of the various methods that have been proposed for the approximate solution of the equations of transonic flow theory, the most successful and also the most versatile method is that described recently for two-dimensional flows in reference 4. This was demonstrated in reference 4 by the presentation of results for a large number of specific applications for which experimental and other theoretical results were available for comparison. Additional results for both two-dimensional and axisymmetric flows with free-stream Mach number 1 are given in reference 5. The latter account is brief, however, and it is the purpose of the present paper to provide a more detailed account of the extension and application to axisymmetric flows of the method described originally in reference 4. Inasmuch as this method of approximation is of somewhat novel character and the mathematical basis for the procedure is only incompletely understood, the results are again

evaluated by extensive comparisons with experimental results and also with other theoretical results whenever available.

PRINCIPAL SYMBOLS

a parameter defined in equation (50)

C Euler's constant $\approx 0.577215665\ldots$

C_D pressure drag coefficient, $\dfrac{D}{(\rho_\infty/2)U_\infty^2 S_m}$

C_p pressure coefficient, $\dfrac{p-p_\infty}{(\rho_\infty/2)U_\infty^2}$

D pressure drag

d maximum diameter of body of revolution

h interval between successive values of x in numerical integration

k $\dfrac{M_\infty^2(\gamma+1)}{U_\infty}$

l length of body

M local Mach number

M_∞ free-stream Mach number

p local static pressure

p_∞ free-stream static pressure

R radius of body

S area of body cross section, πR^2

U_∞ free-stream velocity

u,v perturbation velocity components parallel to x and r axes, respectively

u_E value of u obtained by solution of equation (16)

u_H value of u obtained by solution of equation (35)

u_P value of u obtained by solution of equation (47)

x,r cylindrical coordinates where x extends in the direction of the free-stream velocity

γ ratio of specific heats, 1.4 for air

Δ difference between "predictor" and "corrector" for numerical integration (see eqs. (23) and (24))

λ_E $1-M_\infty^2-ku$

λ_H M_∞^2-1+ku

λ_P $k\dfrac{\partial u}{\partial x}$

ρ_∞ free-stream density of air

τ thickness ratio, $\dfrac{d}{l}$

φ perturbation velocity potential

SUBSCRIPTS

cr values associated with critical Mach number

i values associated with incompressible flow or with $M_\infty=0$

m values associated with maximum diameter of body

x,r differentiation with respect to the variable in question

FUNDAMENTAL EQUATIONS AND BOUNDARY CONDITIONS

STATEMENT OF PROBLEM

Consider the steady axisymmetric flow of an inviscid compressible gas past an arbitrary slender pointed body of revolution, and introduce cylindrical coordinates x and r with the x axis parallel to the direction of the free stream, as illustrated in

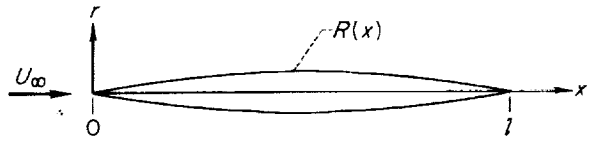

FIGURE 1.—View of body and coordinate system.

figure 1. Let the free-stream velocity and density be U_∞ and ρ_∞, the perturbation potential be φ, and the perturbation velocity components parallel to the x and r axes be φ_x or u, and φ_r or v, where the subscript indicates differentiation. The boundary conditions require that the perturbation velocities vanish at infinity, and that the flow be tangential to the body surface. The first condition indicates that φ is constant at infinity. The second condition can be approximated for smooth slender bodies by

$$(r\varphi_r)_{r=0}=U_\infty R\frac{dR}{dx}=\frac{U_\infty}{2\pi}\frac{dS}{dx} \tag{1}$$

where R and S represent, respectively, the ordinates and cross-section area of the body. The relation between the pressure coefficient C_p and the perturbation velocity components is likewise approximated and reduces to the following form for points near the body surface:

$$C_p=\frac{p-p_\infty}{\frac{\rho_\infty}{2}U_\infty^2}=-2\frac{\varphi_x}{U_\infty}-\frac{\varphi_r^2}{U_\infty^2} \tag{2}$$

The corresponding expression for points on the body surface is

$$C_p=-2\frac{\varphi_x}{U_\infty}-\left(\frac{dR}{dx}\right)^2 \tag{3}$$

These relations are familiar from linear theory but apply equally for transonic theory. The differential equation for φ is not the same as in linear theory, however, but is

$$(1-M_\infty{}^2)\varphi_{xx}+\frac{1}{r}\varphi_r+\varphi_{rr}=\frac{M_\infty{}^2(\gamma+1)}{U_\infty}\varphi_x\varphi_{xx}\equiv k\varphi_x\varphi_{xx} \tag{4}$$

where M_∞ is the Mach number of the undisturbed flow and γ is the ratio of specific heats (1.4 for air). It is useful to note that the total coefficient of φ_{xx}, that is, $1-M_\infty{}^2-k\varphi_x$, corresponds in the present approximation to $1-M^2$ where M is the local Mach number.

In transonic and supersonic flows, it is also necessary, in general, to provide appropriate relations for the discontinuous changes in velocity that occur at shock surfaces. The necessary equations, when simplified to the form consistent with the approximations of transonic flow theory, reduce to

$$\left.\begin{aligned}(1-M_\infty{}^2)(u_a-u_b)^2+(v_a-v_b)^2&\\ =\frac{M_\infty{}^2(\gamma+1)}{U_\infty}\left(\frac{u_a+u_b}{2}\right)(u_a-u_b)^2&\\ \varphi_a=\varphi_b&\\ u_a>u_b&\end{aligned}\right\} \tag{5}$$

where the subscripts a and b refer to the values immediately upstream and downstream of the shock surfaces.

Solutions for problems of transonic flow theory must satisfy not only equations (1) through (5), but certain additional requirements concerning the regions of influence and dependence associated with subsonic and supersonic flows. Although a detailed discussion of these conditions is complicated by the presence of both subsonic and supersonic flows in a single flow field, the principal conclusion is that the usual conditions apply locally and must be satisfied in order to obtain solutions that are physically realistic (see ref. 6, pp. 448–453, for an elementary discussion of this matter).

SIMILARITY RULES

The equations for axisymmetric transonic flow enumerated above contain a similarity rule that associates the pressure fields of affinely related families of bodies. Various members of such a family of bodies may be of different length l and thickness ratio τ, but must have ordinates given by an expression of the form

$$R\left(\frac{x}{l}\right)=\tau f\left(\frac{x}{l}\right) \tag{6}$$

where f is the same function of x/l for all members of a single family. If the subscripts 1 and 2 refer to different members of a given family, the similarity rule states that the pressure coefficients C_P at corresponding points defined by

$$\frac{x_2}{l_2}=\frac{x_1}{l_1}, \qquad \frac{r_2}{l_2}=\sqrt{\frac{M_{\infty_1}{}^2(\gamma_1+1)}{M_{\infty_2}{}^2(\gamma_2+1)}}\frac{\tau_1 r_1}{\tau_2 l_1} \tag{7}$$

are related according to

$$C_{p_2}=\left(\frac{\tau_2}{\tau_1}\right)^2 C_{p_1} \tag{8}$$

provided the free-stream Mach numbers of the two flows are in accordance with the following expression:

$$\frac{1-M_{\infty_2}{}^2}{M_{\infty_2}{}^2(\gamma_2+1)}=\left(\frac{\tau_2}{\tau_1}\right)^2\frac{1-M_{\infty_1}{}^2}{M_{\infty_1}{}^2(\gamma_1+1)} \tag{9}$$

The similarity rule given above cannot be used directly to relate the surface pressures on bodies having different thickness ratios because the ordinates of related bodies given by equation (6) do not conform with the relationship for corresponding points given by equation (7). Thus the r coordinate of a point in the vicinity of body 2 that corresponds to a point on the surface of body 1 is given by

$$\frac{r_2}{R_2}=\sqrt{\frac{M_{\infty_1}{}^2(\gamma_1+1)}{M_{\infty_2}{}^2(\gamma_2+1)}}\left(\frac{\tau_1}{\tau_2}\right)^2 \tag{10}$$

Oswatitsch and Berndt have shown (ref. 7) that a similarity rule can be established for the surface pressures on affinely related bodies of revolution if it is assumed that the longitudinal perturbation velocity component u is given by an expression of the form

$$u=\frac{U_\infty}{2\pi}\frac{d^2S}{dx^2}\ln r+g(x) \tag{11}$$

in the vicinity of the body. This relation permits the calculation of the difference in pressure

between the point r_2 and the surface of body 2. The similarity rule for the surface pressures follows immediately. It states that

$$C_{p_2}=\left(\frac{\tau_2}{\tau_1}\right)^2\left\{C_{p_1}+\frac{1}{\pi}\frac{d^2S_1}{dx^2}\ln\left[\left(\frac{\tau_1}{\tau_2}\right)^2\sqrt{\frac{M_{\infty_1}{}^2(\gamma_1+1)}{M_{\infty_2}{}^2(\gamma_2+1)}}\right]\right\} \tag{12}$$

provided still that the free-stream Mach numbers are in accordance with equation (9). A similarity rule for drag D can be obtained by combination of equation (12) and the following expression for the drag coefficient C_D:

$$C_D=\frac{D}{\frac{\rho_\infty}{2}U_\infty{}^2S_m}=\frac{1}{S_m}\int_0^l C_p\frac{dS}{dx}\,dx \tag{13}$$

It is

$$C_{D_2}=\left(\frac{\tau_2}{\tau_1}\right)^2\left[C_{D_1}+\frac{S_1{}'^2(l)}{2\pi S_{m_1}}\ln\frac{\tau_1{}^2\sqrt{M_{\infty_1}{}^2(\gamma_1+1)}}{\tau_2{}^2\sqrt{M_{\infty_2}{}^2(\gamma_2+1)}}\right] \tag{14}$$

where the prime indicates differentiation with respect to x and S_m refers to the maximum cross-section area. This relation simplifies if the body is either pointed or cylindrical at the base, since then $S'(l)$ is zero.

It should be observed that the relation given by equation (11) follows as a direct consequence of the assumption implicit in the use of the slender-body boundary condition given by equation (1) that at any given x the product $r\phi_r$ is constant between the x axis and points in the vicinity of the body surface. The error introduced into the analysis by the use of equation (11) is thus of the same order of magnitude as that already present in the fundamental relations of the small disturbance theory of transonic flow enumerated in equations (1) through (5). It is important to recognize, however, that equations (11), (12), and (14) must be regarded as approximate relations within the framework of analysis specified by equations (1) through (5), and that exact solutions of the latter equations will not obey the similarity rules perfectly. This situation may be contrasted with that for the similarity rule for airfoils or for wings of finite span for which the similarity rules are exact relations within the framework of the small disturbance theory for transonic flow.

A much stronger limitation that affects the general applicability of the similarity rules for axisymmetric flows, and to which attention does not appear to have been directed previously, is concerned with the regions of influence and dependence. This limitation arises because the extent and even the existence of a region of supersonic flow imbedded in a subsonic flow, or of a subsonic region imbedded in a supersonic flow, are not determined by the value of the similarity parameter $(M_\infty{}^2-1)/[M_\infty{}^2(\gamma+1)\tau^2]$ alone, as in flows around thin wings, but by the values for the Mach number and thickness ratio individually. These effects are small at Mach numbers near unity for which the sonic line is inclined at a steep angle to the body surface, but become large as the inclination of the sonic line approaches that of the body surface at Mach numbers near the lower and upper critical. The latter Mach numbers are defined, respectively, as the lowest subsonic Mach number and the highest supersonic Mach number at which sonic velocity (i.e., $u/U_\infty=(1-M_\infty{}^2)/[M_\infty{}^2(\gamma+1)]$) occurs at the surface of the body. Consider, as an example of a case for which these effects are large, that results are available for a certain body at the lower critical Mach number and that it is desired to use the similarity rule to determine the flow around an affinely related body that is more slender than the first body. The flow past the second body will be found to contain a supersonic region, but since there are no shock waves in the flow around the first body there will be no shock waves indicated in the flow around the second body. If, on the other hand, results are available for a body at a Mach number somewhat greater than the lower critical, and the flow contains a shock wave, application of the similarity rule to compute the flow around an affinely related body of sufficiently greater thickness that the flow is purely subsonic leads to the completely unacceptable result that there are discontinuities in a purely subsonic flow. It is evident that equally unacceptable results are indicated by the similarity rule for drag, and that related difficulties with both the details of the flow field and the drag are encountered at Mach numbers in the vicinity of the upper critical.

The properties of the similarity rule discussed

in the preceding paragraph require the imposition, for free-stream Mach numbers other than 1, of certain rather definite restrictions on the values for τ, or for M_∞, for which the surface pressures and drag are related by equations (12) and (14). It is clear such a restriction is necessary because the similarity rules contain no mechanism for the subtraction or addition of shock waves and the associated contributions to drag, as there should be in any proper relationship between subcritical and supercritical flows. These and related points will be examined further in the course of the following discussion.

The remainder of this paper is concerned with the presentation of a method for the approximate solution of the problem described by equations (1) through (5), application to a number of specific bodies, and comparison with existing theoretical and experimental results. Purely subsonic flows are discussed first, purely supersonic flows next, and flows with free-stream Mach number near unity are treated last.

SUBSONIC FLOWS

APPROXIMATE SOLUTION OF EQUATIONS

It is convenient in the analysis of subsonic flows to introduce the symbol λ_E as an abbreviation for the coefficient of φ_{xx}

$$\lambda_E=1-M_\infty{}^2-M_\infty{}^2\frac{\gamma+1}{U_\infty}\varphi_x=1-M_\infty{}^2-ku>0 \quad (15)$$

and rewrite equation (4) in the form

$$\lambda_E\varphi_{xx}+\frac{1}{r}\varphi_r+\varphi_{rr}=0 \quad (16)$$

It is now assumed that λ_E is neither zero nor infinite and that it varies sufficiently slowly that its derivatives can be disregarded so that it can be considered, temporarily, as a constant. At this stage, the problem is equivalent to that encountered in linearized theory of subsonic flow around slender bodies of revolution (it is identical if λ_E is replaced by $1-M_\infty{}^2$). The solution for φ is thus well known (see, e.g., ref. 8, p. 188) and is given by

$$\varphi_E=-\frac{U_\infty}{4\pi}\int_0^l\frac{S'(\xi)d\xi}{\sqrt{(x-\xi)^2+\lambda_E r^2}} \quad (17)$$

where the subscript E denotes that the solution refers to equation (16) of elliptic type with λ_E constant. The corresponding expression for u_E follows immediately by differentiation. It can be approximated for points on the surface of a smooth slender body by

$$\frac{u_E}{U_\infty}=\frac{S''(x)}{4\pi}\ln\frac{\lambda_E S}{4\pi x(l-x)}+\frac{1}{4\pi}\int_0^l\frac{S''(x)-S''(\xi)}{|x-\xi|}d\xi$$
$$=\frac{S''(x)}{4\pi}\ln\lambda_E+\frac{u_i}{U_\infty} \quad (18)$$

where the subscript i refers to the values for incompressible flow, or for $M_\infty=0$. Differentiation yields

$$\frac{d(u_E/U_\infty)}{dx}=\frac{S(x)'''}{4\pi}\ln\lambda_E+\frac{d(u_i/U_\infty)}{dx} \quad (19)$$

If, now, $1-M_\infty{}^2-ku$ is restored in place of λ_E so that, in effect, the local value for λ_E is used at each point, and the subscript E on u is dropped, equation (19) becomes

$$\frac{d(u/U_\infty)}{dx}=\frac{S'''(x)}{4\pi}\ln(1-M_\infty{}^2-ku)+\frac{d(u_i/U_\infty)}{dx} \quad (20)$$

Equation (20) is a nonlinear ordinary differential equation for u on the body surface. This equation is of first order and the necessary value for the constant of integration is determined by assuming that u equals u_E at the point on the forebody where $S''(x)$ vanishes, since u_E is indicated by equation (18) to be independent of λ_E and hence of Mach number at this point. Thus

$$u=u_i \quad \text{where} \quad S''(x)=0 \quad (21)$$

The calculation of u on the surface of a body of revolution of specified shape is thus reduced to the solution of an equation of the form

$$\frac{du}{dx}=F(x,u) \quad (22)$$

which can be solved, at least approximately, by application of any of a number of standard techniques. The corresponding values for the surface pressures follow directly upon insertion of the results into equation (3).

The particular method used to calculate the results presented in the following section of this report is that of Milne (ref. 9, p. 135). It is a step-by-step process in which the values of the dependent variable u are calculated one after the other for a sequence of equally spaced values of

the independent variable x. The successive values of x are denoted by $x_0, x_1, x_2, \ldots$, the interval is denoted by h, and the corresponding values of u are denoted by $u_0, u_1, u_2, \ldots$. Differentiation with respect to x is indicated by a prime. The actual calculations proceed by alternate use of the formula

$$u_{n+1}=u_{n-3}+\frac{4}{3}h(2u_n'-u_{n-1}'+2u_{n-2}') \quad (23)$$

as a "predictor" and Simpson's rule

$$u_{n+1}=u_{n-1}+\frac{1}{3}h(u_{n+1}'+4u_n'+u_{n-1}') \quad (24)$$

as a "corrector." Both expressions are approximate, but the error in the result given by the corrector is roughly equal to $\Delta/29$ when Δ is the difference between the results given by the two formulas. It is assumed that the value given by equation (24) is correct so long as $\Delta/29$ is not significant. Abrupt fluctuations in the values of Δ indicate the presence of errors and the calculations should be checked. If the error $\Delta/29$ proves to be larger than the desired accuracy permits, it is necessary to shorten the interval h. Cutting the interval in half will divide the error by about 32.

The computation is started at the point where $S''(x)$ is zero and requires four consecutive known values for u. One of these is given by equation (21), the remaining three are determined by use of the first six terms of a Taylor's series for u about the point where $S''(x)$ vanishes. This requires evaluation of the first five derivatives of u with respect to x at the point where $S''(x)$ vanishes. The first of these is calculated directly by use of equations (20) and (21). The remaining four are calculated similarly by use of corresponding expressions derived from equation (20) by successive differentiation with respect to x.

APPLICATION TO PARABOLIC-ARC BODY

As an application of the foregoing results, consider subsonic flow past a parabolic-arc body of revolution of length l and maximum diameter d. The ordinates R of this body are given by

$$R=2\tau l\left[\frac{x}{l}-\left(\frac{x}{l}\right)^2\right] \quad (25)$$

where τ represents the thickness ration d/l. The variation of cross-section area S with x is thus

$$S=\pi R^2=4\pi\tau^2 l^2\left[\frac{x}{l}-\left(\frac{x}{l}\right)^2\right]^2 \quad (26)$$

and the points at which $S''(x)$ vanishes are located at

$$x_{S''=0}=\frac{l}{2}\left(1\pm\frac{\sqrt{3}}{3}\right) \quad (27)$$

The expression for u at zero Mach number can be determined directly upon substitution of the above relation for $S(x)$ into equation (18) and carrying out the indicated operations. The result can be expressed simply as

$$\frac{u_i}{U_\infty}=\frac{S''(x)}{4\pi}\left[3+\ln\frac{\tau R(x)}{2l}\right] \quad (28)$$

where $R(x)$ and $S(x)$ now refer to the radius and cross-section area of a parabolic-arc body of revolution, and are defined as functions of x by equations (25) and (26). Substitution of equation (28) into equation (20) leads to the following ordinary nonlinear differential equation of first order for u on the surface of a parabolic-arc body of revolution in subsonic flow.

$$\frac{d(u/U_\infty)}{dx}=\frac{S'''}{4\pi}\ln(1-M_\infty^2-ku)+\frac{d}{dx}\left[\frac{S''}{4\pi}\left(3+\ln\frac{\tau R}{2l}\right)\right] \quad (29)$$

The constant of integration is evaluated by imposing the condition derived from equations (21), (27), and (28) that

$$u=0 \text{ at } x=\frac{l}{2}\left(1-\frac{\sqrt{3}}{3}\right) \quad (30)$$

The problem described by equations (26), (29), and (30) has been solved numerically for several subcritical Mach numbers for a body of fineness ratio l/d of 10. The resulting values of u/U_∞ are tabulated in table I together with the values for the error term $\Delta/29$. Results are given for only the front half of the body since the solution is symmetric around the center of the body, and the calculated values at x and $l-x$ should be identical. It can be seen from inspection of the values for $\Delta/29$ that the size of the interval h, which was maintained at 2 percent of the body length throughout all of the calculations, is sufficiently

small that inaccuracies incurred in the numerical solution are negligible.

The corresponding values for C_p on the body surface can be calculated directly from the values for u/U_∞ by means of equation (3). The resulting values are tabulated in table I, and are shown graphically in figure 2. The corresponding results indicated by linearized compressible flow theory are shown in figure 3.

The latter results are calculated by means of the following expression derived from equations (3), (18), and (25) with λ_E replaced by $1-M_\infty^2$.

$$C_{p_1}=-\frac{S''}{2\pi}\left(3+\ln\frac{\sqrt{1-M_\infty^2}\tau R}{2l}\right)-R'^2 \qquad (31)$$

It can be seen that the values for C_p obtained by application of the present theory are qualitatively similar to those indicated by linear theory, although somewhat more negative at all points. This trend is similar to that shown in reference 4 to result upon application of the same procedures to two-dimensional subsonic flows.

The results presented in table I and figures 2 and 3 are repeated in figure 4 together with the corresponding results indicated by the second-order approximation to the solution of the equations of transonic flow theory for flow past a slender parabolic-arc body of revolution. The

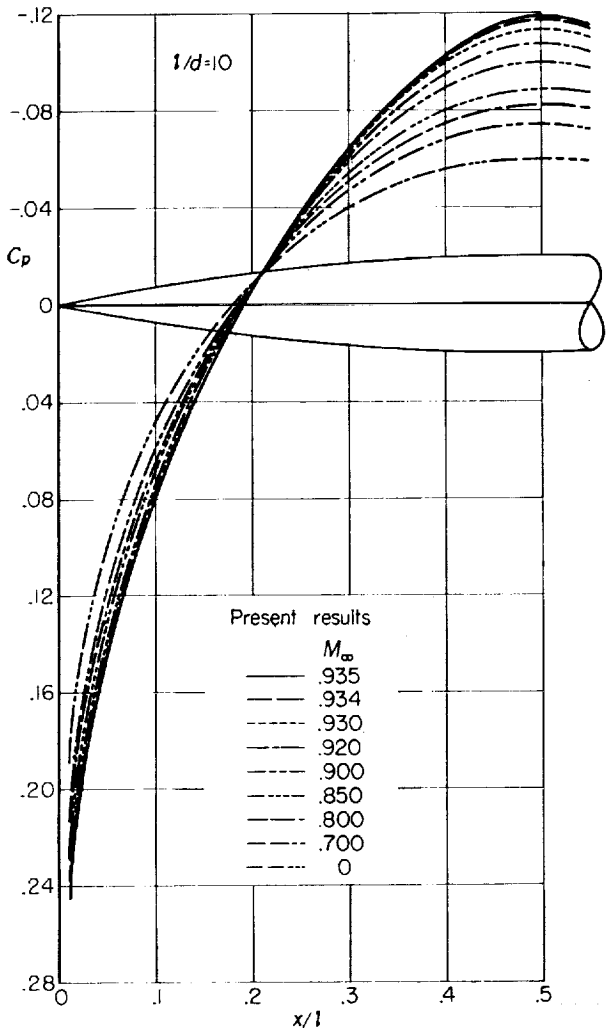

FIGURE 2.—Pressure distributions on a parabolic-arc body of revolution of fineness ratio 10 at subcritical Mach numbers as indicated by present theory.

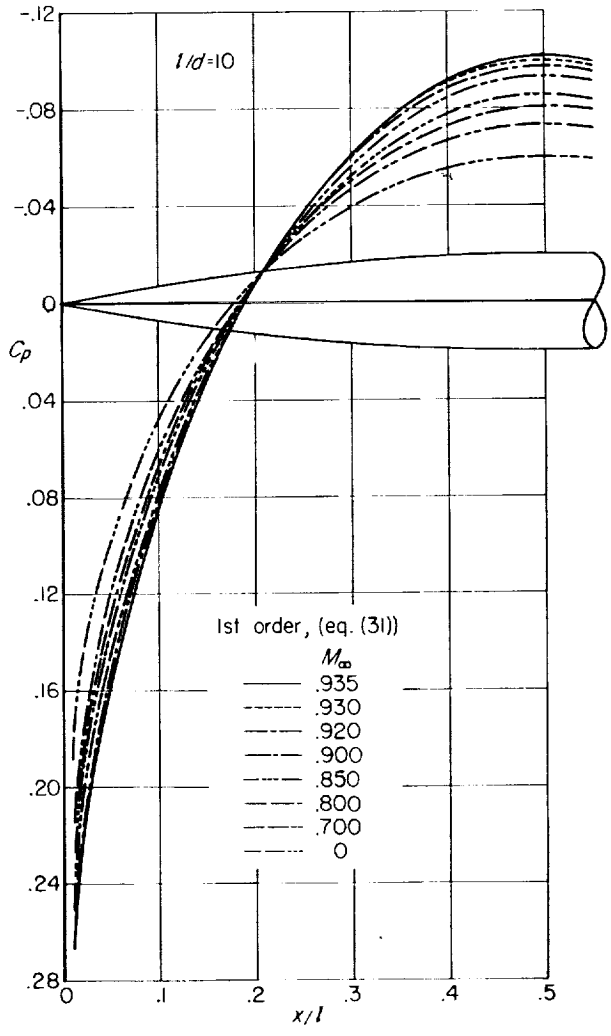

FIGURE 3.—Pressure distributions on a parabolic-arc body of revolution of fineness ratio 10 at subcritical Mach numbers as indicated by linear theory.

501377—59——2

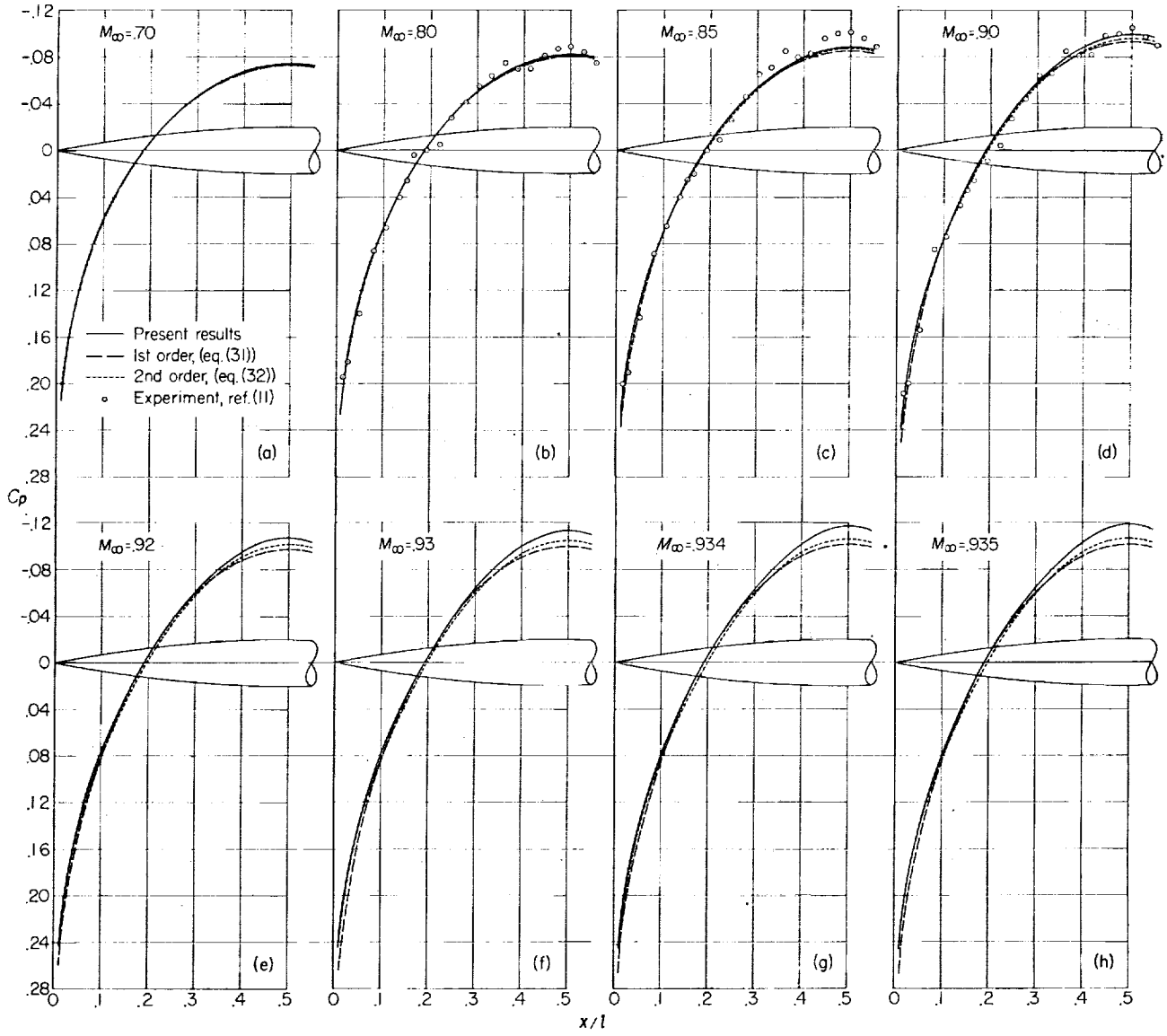

(a) $M_\infty=0.70$ (b) $M_\infty=0.80$ (c) $M_\infty=0.85$ (d) $M_\infty=0.90$
(e) $M_\infty=0.92$ (f) $M_\infty=0.93$ (g) $M_\infty=0.934$ (h) $M_\infty=0.935$

FIGURE 4.—Pressure distributions on a parabolic-arc body of revolution of fineness ratio 10 at subcritical Mach numbers as indicated by present theory, by other theoretical results, and by experiment.

latter results are calculated by use of the expression

$$C_{p_2}=C_{p_1}-\frac{M_\infty^2(\gamma+1)}{1-M_\infty^2}\tau^4\left[3-\frac{17}{2}\left(\frac{R'}{\tau}\right)^2+\frac{47}{16}\left(\frac{R'}{\tau}\right)^4\right] \tag{32}$$

which is obtained from a corresponding result given by Van Dyke in reference 10. The expression given in reference 10 differs from equation (32) in that the quantity $M_\infty^2(\gamma+1)$ is replaced by $\gamma+1$. This change, which is associated with a corresponding difference in the coefficient k of the nonlinear term of equation (4), has very little effect on the values for C_p calculated by means of equation (32) since the quantity involved is absent in the first-order term and first appears in the much smaller contribution of the second-order term. The consequences of such a change in the quantity represented by k become of con-

siderably greater significance in the calculation of transonic flows and in the determination of the critical Mach number, however, because the magnitude of u/U_∞ associated with the occurrence of sonic velocity is inversely proportional to k. As an example, the critical value for the pressure coefficient $C_{p_{cr}}$ associated with the free-stream Mach number of 0.85 and zero φ_r is -0.320 if $M_\infty^2(\gamma+1)$ is used for kU_∞, and -0.231 if $\gamma+1$ is used. Since the exact value indicated by isentropic flow theory is -0.302, it follows that the formulation of transonic flow theory in which kU_∞ is equal to $M_\infty^2(\gamma+1)$ is about four times as accurate in this respect as the formulation in which kU_∞ is equal to $\gamma+1$.

Experimental data from reference 11 by Taylor and McDevitt are also included in this figure for all subcritical Mach numbers for which results were measured. The tests were conducted in the Ames 14-foot transonic wind tunnel with a model that consists of approximately the forward 85 percent of a parabolic-arc body of revolution of fineness ratio 10 and length 6.67 feet. The model was supported from the rear by a circular cylinder having a diameter somewhat smaller than that of the base of the body. No corrections have been applied to the data to take account of either wind-tunnel wall interference or the abbreviated length of the body.

It can be seen from the foregoing comparisons that the principal differences between the pressure distribution indicated by linear theory and by higher approximations occur near the middle of the body at Mach numbers near the critical. Insight into the magnitude of these effects can be had by examination of figure 5 which shows the variation of C_p with M_∞ at the midpoint of a

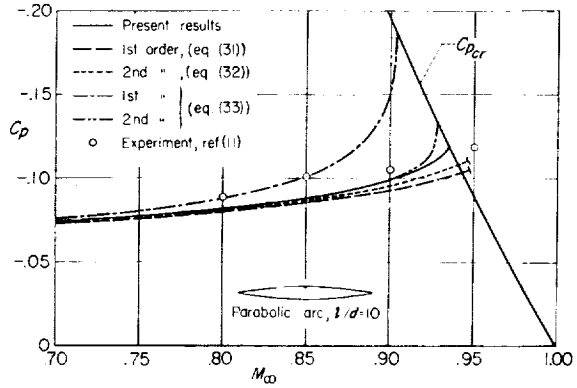

FIGURE 5.—Variation of pressure coefficient with Mach number at the midpoint of a parabolic-arc body as indicated by present theory, by experiment, and by two different methods of successive approximation to the transonic equation.

parabolic-arc body of revolution of fineness ratio 10. Also included in this figure is a line indicating the variation of the critical pressure coefficient associated with the occurrence of sonic velocity at a point, such as the midpoint of a parabolic-arc body, at which dR/dx is zero. The present results are included in this figure together with experimental results from reference 11, theoretical results indicated by equations (31) and (32), and by the first two steps of an alternative method of successive approximation described in the appendix of reference 12 that involves the solution of quadratic rather than linear equations at each step of the iteration process. The latter values for C_p on the surface of a body of revolution are calculated by application of the following expression in which the subscript N refers to the results indicated by the quadratic method and n refers to the nth approximation using the classical method of successive approximation:

$$C_{p_N}+\left(\frac{dR}{dx}\right)^2=\frac{-2(1-M_\infty^2)}{M_\infty^2(\gamma+1)}\left(1-\sqrt{\left\{1+\frac{M_\infty^2(\gamma+1)}{2(1-M_\infty^2)}\left[C_{p_{n-1}}+\left(\frac{dR}{dx}\right)^2\right]\right\}}^2+\frac{M_\infty^2(\gamma+1)}{1-M_\infty^2}\left(C_{p_n}-C_{p_{n-1}}\right)\right) \tag{33}$$

in which

$$C_{p_{n-1=0}}=-\left(\frac{dR}{dx}\right)^2$$

Values for $C_{p_{n=1}}$ and $C_{p_{n=2}}$ can be calculated for parabolic-arc bodies by application of equations (31) and (32). It is evident from the form of equation (33) that the values for C_{p_N} approach those for C_{p_n} in the limit of an infinite number of iteration steps, provided, of course, that the series expression for C_{p_n} converges. If only a finite number of terms are considered, as must be done in any practical application of the method of successive approximation, the approximate values for the pressure indicated by C_{p_n} and C_{p_N} are different. The utility of considering the two sets of results simultaneously resides in the fact that the values indicated by C_{p_n} tend to underestimate the true variation of the peak negative pressure with Mach

number, whereas those indicated by C_{p_N} tend to overestimate the true variation. The true variation is thus bounded within well defined limits. It can be seen from examination of figure 5 that the results of the present numerical calculations fall within or very close to these limits. Similar applications of the quadratic method of successive approximations to two-dimensional flows can be found in references 4 and 13.

The problem described by equations (26), (29), and (30) has also been solved numerically for several subcritical Mach numbers for a parabolic-arc body of revolution of fineness ratio 6. The resulting values for u/U_∞, $\Delta/29$, and C_p are tabulated in Table II. The pressure distributions are also illustrated graphically in figure 6. The corresponding results indicated by linearized compressible flow theory are shown in figure 7. These results are repeated in figure 8 together with the corresponding theoretical results indicated by the second-order approximation given by equation (32), and the experimental results of Drougge from reference 14. The latter results were obtained from tests with a model that consists of the forward 5/6 of a parabolic-arc body of revolution of fineness ratio 6. It was supported in the wind tunnel by a circular cylinder of the same diameter as the base of the body. Although no corrections have been applied for the effects of the abbreviated length of the body, it is clear that the values for C_p on a complete body should be somewhat more negative than those on the partial body tested by Drougge. Theoretical considerations indicate that the magnitude of this effect is about 0.007 at the

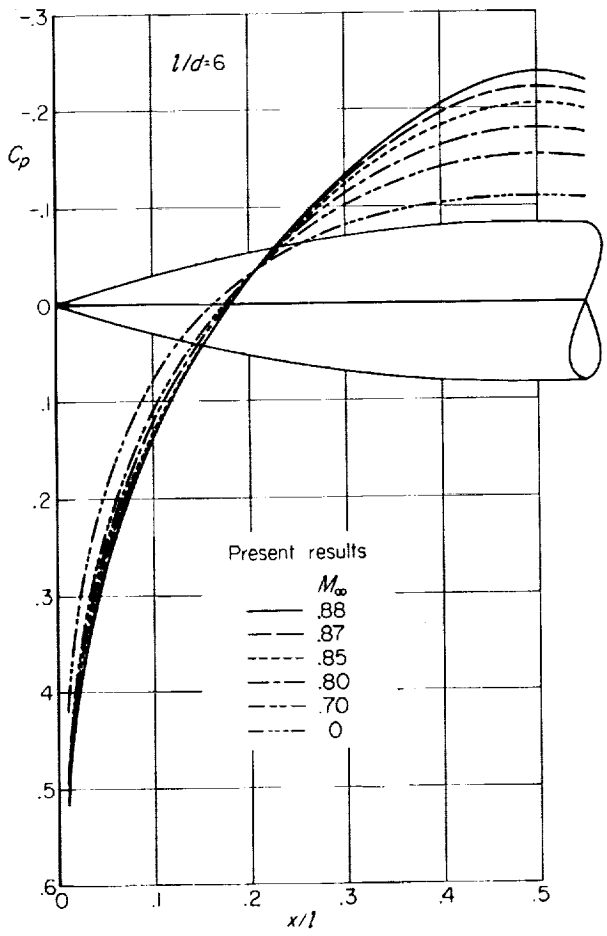

FIGURE 6.—Pressure distributions on a parabolic-arc body of revolution of fineness ratio 6 at subcritical Mach numbers as indicated by present theory.

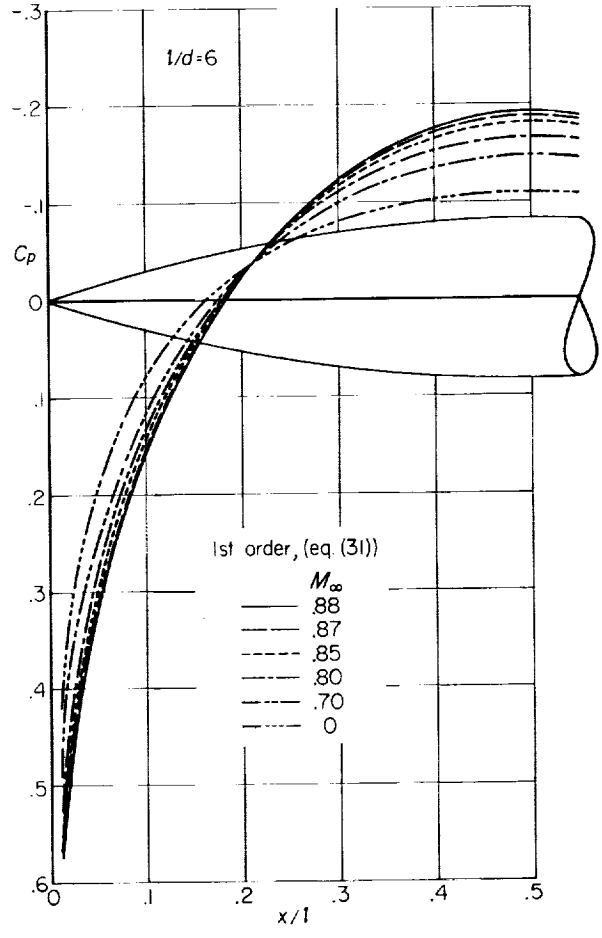

FIGURE 7.—Pressure distributions on a parabolic-arc body of revolution of fineness ratio 6 at subcritical Mach numbers as indicated by linear theory.

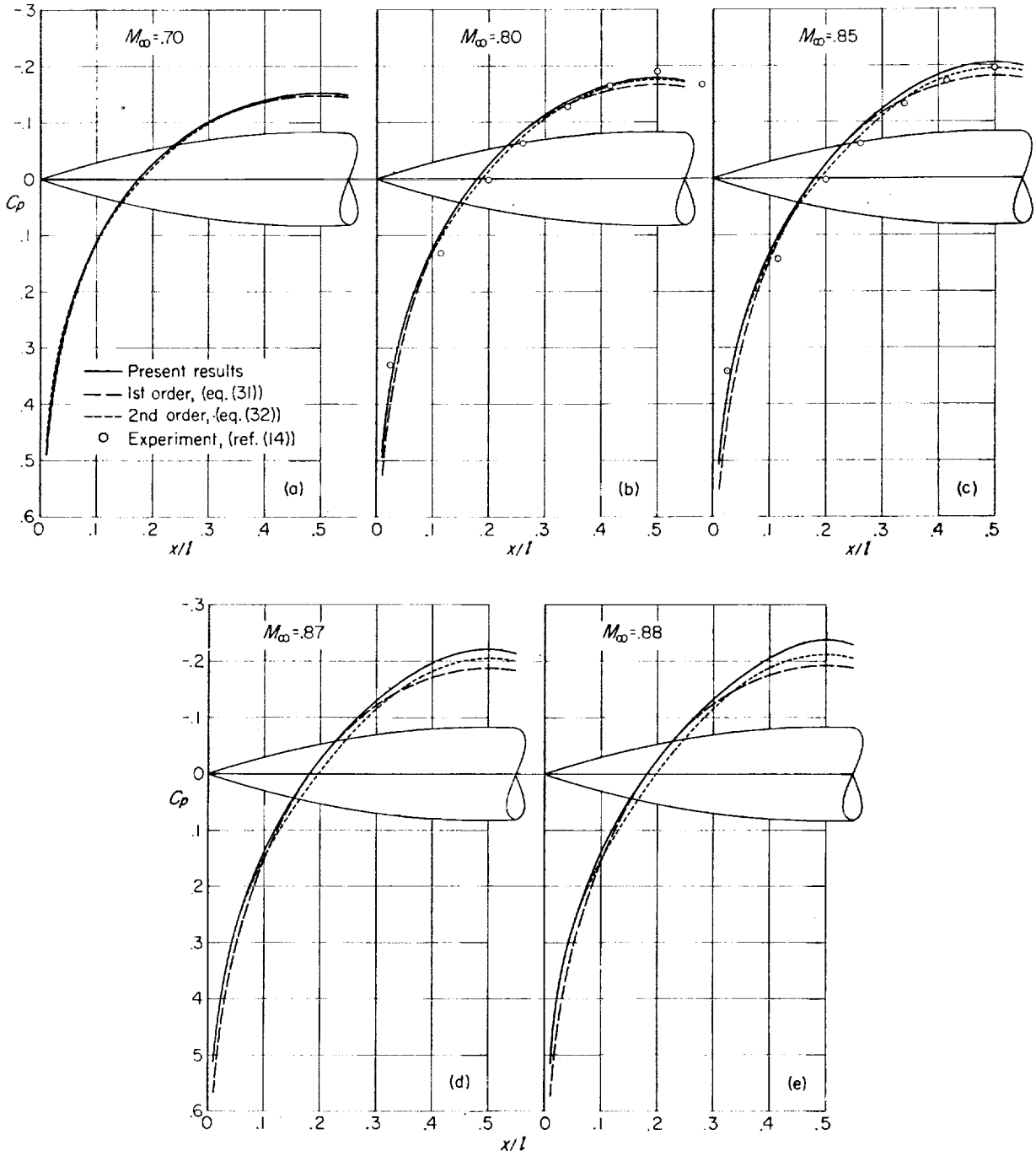

(a) $M_\infty = 0.70$ (b) $M_\infty = 0.80$ (c) $M_\infty = 0.85$ (d) $M_\infty = 0.87$ (e) $M_\infty = 0.88$

FIGURE 8.—Pressure distributions on a parabolic-arc body of revolution of fineness ratio 6 at subcritical Mach numbers as indicated by present theory, by other theoretical results, and by experiment.

middle of the body, and about 0.001 at the nose of the body. A more detailed investigation of this matter can be found in reference 10 by Van Dyke.

Two conclusions emerge from a comparison of the theoretical and experimental results illustrated in figure 8. They are that slender-body theory is capable of yielding reliable results for subsonic flow past a parabolic-arc body of revolution of fineness ratio 6, and that the simple result provided by linearized compressible flow theory remains a useful approximation for all Mach numbers up to the immediate vicinity of the critical

Theoretical pressure distributions for a parabolic-arc body of revolution of fineness ratio 6 could also have been calculated, and with less effort, by application of the similarity rule given by equations (9) and (12) to the results already calculated for the parabolic-arc body of fineness ratio 10. As noted in the course of the preceding discussion of the similarity rule, the results obtained by application of equations (9) and (12) do not agree perfectly with those obtained by direct calculations. It is the purpose of the present discussion to illustrate the magnitude of these differences by an examination of the specific case mentioned above. Figure 9 shows

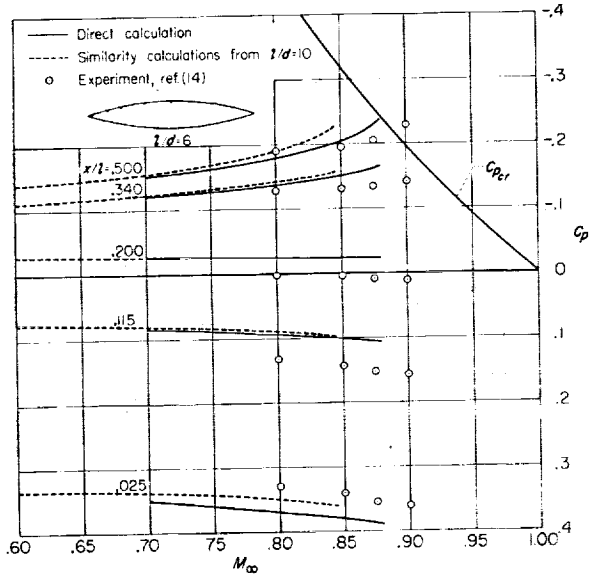

FIGURE 9.—Variation of pressure coefficient with Mach number at various stations on a parabolic-arc body of fineness ratio 6 as obtained by direct calculations using the present theory, by use of the similarity rule, and by experiment.

the variation of C_p with free-stream Mach number at several stations along the length of the body as indicated by the direct calculations for the body of fineness ratio 6, by application of the similarity rules together with the results calculated for the body of fineness ratio 10, and by the experimental results of Drougge (ref. 14) for a body of fineness ratio 6. The stations for which results are included on this graph are selected so as to coincide with the location of the orifices in the model tested by Drougge. It can be seen that the results obtained by application of the similarity rule are very close to those obtained by direct calculation over substantial portions of the body, but that important differences occur in the vicinity of the middle of the body as the free-stream Mach number approaches the critical and the local velocities approach the speed of sound. Perhaps the most striking difference concerns the free-stream Mach numbers at which the two sets of theoretical results terminate. In the direct calculation, the results terminate with the attainment of the critical Mach number, whereas the results obtained by application of the similarity rule terminate at Mach numbers well below the critical. If it is presumed that results appropriate for supercritical Mach numbers would contain shock waves, and that the bodies would experience a pressure drag, it is clear that the results obtained by application of the similarity rules would be in serious error since, in the present example, such effects would begin to appear at a Mach number of about 0.845 rather than about 0.88. It is evident, furthermore, that the magnitude of these effects would be less if the fineness ratios of the two bodies were more nearly the same, but greater if the fineness ratios were more different, and of opposite sign if the similarity rule were applied to calculate the pressure distribution on a thin body using known results for a thicker body.

SUPERSONIC FLOWS

APPROXIMATE SOLUTION OF EQUATIONS

The procedure described in the preceding section will now be applied to the analysis of supersonic flows. Thus, introduce the symbol λ_H as an abbreviation for the coefficient of φ_{xx}

$$\lambda_H=M_\infty{}^2-1+M_\infty{}^2\frac{\gamma+1}{U_\infty}\varphi_x=M_\infty{}^2-1+ku>0 \tag{34}$$

and rewrite equation (4) as follows:

$$\lambda_H\varphi_{xx}-\frac{1}{r}\varphi_r-\varphi_{rr}=0 \tag{35}$$

If it is again assumed that λ_H is neither zero nor infinite and that it varies sufficiently slowly that its derivatives can be disregarded, the problem is equivalent to that encountered in linearized supersonic slender-body theory. The solution for φ for points on the surface of a smooth slender pointed body of revolution is given by (see, e.g., ref. 8, p. 190)

$$\varphi_H=-\frac{U_\infty}{2\pi}\int_0^{x-\sqrt{\lambda_H}r}\frac{S'(\xi)d\xi}{\sqrt{(x-\xi)^2-\lambda_H r^2}} \tag{36}$$

where the subscript H denotes that the solution refers to equation (35) of hyperbolic type with λ_H constant. The corresponding expression for u_H can be approximated for points on the surface of a smooth slender body by

$$\frac{u_H}{U_\infty}=\frac{S''(x)}{4\pi}\ln\frac{\lambda_H S}{4\pi x^2}+\frac{1}{2\pi}\int_0^x\frac{S''(x)-S''(\xi)}{x-\xi}d\xi$$
$$=\frac{S''(x)}{4\pi}\ln\lambda_H+f_H(x) \tag{37}$$

where $f_H(x)$ can be interpreted as the expression for u/U_∞ indicated by linear theory for a free-stream Mach number of $\sqrt{2}$. Differentiation yields

$$\frac{d(u_H/U_\infty)}{dx}=\frac{S'''(x)}{4\pi}\ln\lambda_H+\frac{df_H(x)}{dx} \tag{38}$$

If, in the same manner as described for the subsonic case, M_∞^2-1+ku is restored in place of λ_H so that, in effect, the local value for λ_H is used at each point and the subscript H on u is dropped, equation (38) becomes

$$\frac{d(u/U_\infty)}{dx}=\frac{S'''(x)}{4\pi}\ln(M_\infty^2-1+ku)+\frac{df_H(x)}{dx} \tag{39}$$

As in the previous discussion of subsonic flows, the resulting relation for u on the body surface is a nonlinear ordinary differential equation of the first order, and it is necessary to supply a value for u at some point along the body in order to evaluate the constant of integration. Perhaps the most logical method for the evaluation of this constant for flows that are supersonic everywhere is to use the value for u at $x=0$ that is provided by the solution of the equations of transonic flow theory for flow around a cone tangent to the nose of the body. Practical difficulties arise in the application of this procedure, however, because first, the solution for the cone cannot be written in a simple form, and second, the numerical tables and charts in which the results of numerous specific cases are summarized are generally inadequate for the present purposes because of the lack of sufficient calculated results for slender bodies for low supersonic Mach numbers. These comments apply not only to the fairly recent results of Oswatitsch and Sjodin (ref. 15) and Shen (ref. 16) based on the simplified equations of transonic flow theory, but also to the older and more extensive results based on the complete equations of compressible flow theory and presented in references 17 and 18. An alternative method that avoids this difficulty and parallels the procedures employed for the approximate solutions of other problems in this paper and in reference 4 is to evaluate the constant by assuming that u equals u_H at the point on the forebody where $S''(x)$ vanishes, since u_H is independent of λ_H and hence of Mach number at this point; thus

$$\frac{u}{U_\infty}=f_H \quad \text{where} \quad S''(x)=0 \tag{40}$$

The calculation of u on the surface of a body of revolution of specified shape in supersonic flow is thus reduced to the solution of an ordinary differential equation of the form

$$\frac{du}{dx}=F(x,u) \tag{41}$$

subject to the additional condition given by equation (40). This problem is identical in form to that encountered at the corresponding point in the discussion of subsonic flows, and can be solved numerically in a similar manner. Once the values for u on the surface of the body are determined, the corresponding values of C_p follow directly upon insertion of the results into equation (3).

APPLICATION TO PARABOLIC-ARC BODY

As an application of the foregoing theory, consider supersonic flow past a parabolic-arc body of revolution of length l and maximum diameter d.

The expressions for the ordinates R, the cross-section area S, and the location of the points at which $S''(x)$ vanishes are given by equations (25), (26), and (27). Substitution of these relations into equations (37) and (39) leads directly to the following differential equation for u on the surface of a parabolic-arc body of revolution in supersonic flow:

$$\frac{d(u/U_\infty)}{dx}=\frac{S'''(x)}{4\pi}\ln(M_\infty^2-1+ku)+\frac{d}{dx}\left\{\frac{S''}{2\pi}\ln\left[\tau\left(1-\frac{x}{l}\right)\right]-12\tau^2\frac{x}{l}\left(2-3\frac{x}{l}\right)\right\} \quad (42)$$

The constant of integration is evaluated by imposing the condition derived from equations (26), (27), and (40) that

$$\frac{u}{U_\infty}=-2\sqrt{3}\,\tau^2 \quad \text{at} \quad x=\frac{l}{2}\left(1-\frac{\sqrt{3}}{3}\right) \quad (43)$$

The problem described by equations (26), (42), and (43) has been solved numerically, by application of Milne's method described in the preceding section on subsonic flows, for several supersonic Mach numbers for a body of fineness ratio l/d of 10. The resulting values for u, $\Delta/29$, and C_p are tabulated in table III. The results for C_p are also shown graphically in figure 10. The corresponding results indicated by linearized compressible flow theory are shown in figure 11. The latter results are calculated by use of the following expression derived from equations (3), (26), and (37) with λ_H replaced by M_∞^2-1.

$$C_{p_1}=-\frac{S''}{\pi}\ln\left[\sqrt{M_\infty^2-1}\,\tau\left(1-\frac{x}{l}\right)\right]+24\tau^2\frac{x}{l}\left(2-3\frac{x}{l}\right)-R'^2 \quad (44)$$

The results presented in table III and figures 10 and 11 are repeated in figure 12 together with the corresponding results indicated by the following expression given by Van Dyke in reference 10 for the second-order approximation to the solution of the equations of transonic flow theory for slender parabolic-arc bodies of revolution:

$$C_{p_2}=C_{p_1}+\frac{M_\infty^2(\gamma+1)}{M_\infty^2-1}\tau^4\left[3-\frac{17}{2}\left(\frac{R'}{\tau}\right)^2+\frac{47}{4}\left(\frac{R'}{\tau}\right)^4\right] \quad (45)$$

As noted previously in the discussion of subsonic flows, the quantity $\gamma+1$ that appears in the result given by Van Dyke has been replaced by $M_\infty^2(\gamma+1)$ to conform with the present formulation of the equations of transonic flow theory.

It can be seen upon examination of figures 10, 11, and 12 that the results obtained by application of the present theory are again qualitatively similar to those indicated by first- and second-order theories and that the main differences occur

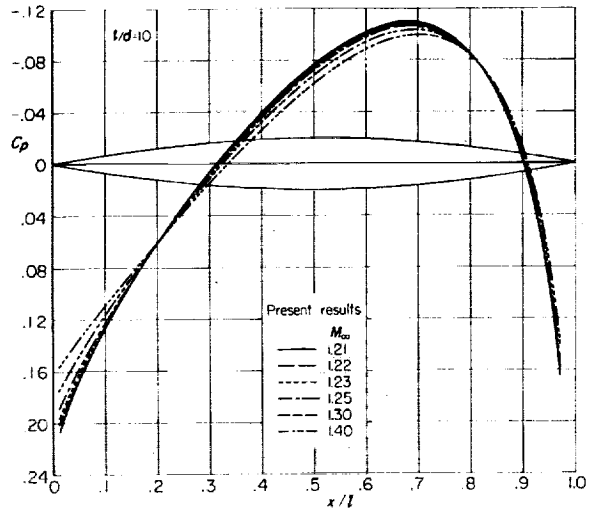

FIGURE 10.—Pressure distributions on a parabolic-arc body of revolution of fineness ratio 10 at Mach numbers above the upper critical as indicated by present theory.

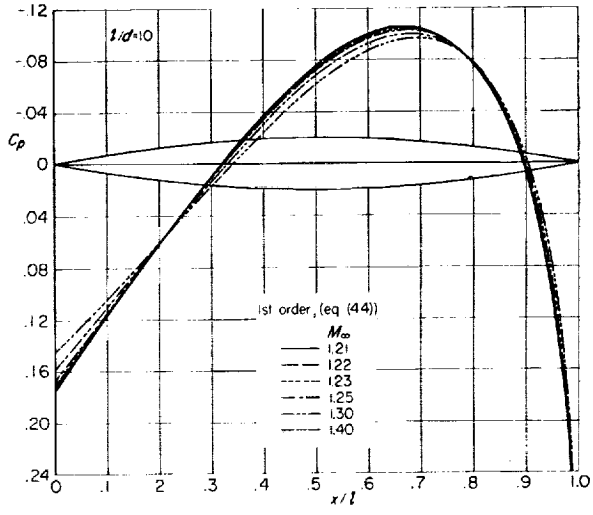

FIGURE 11.—Pressure distributions on a parabolic-arc body of revolution of fineness ratio 10 at Mach numbers above the upper critical as indicated by linear theory.

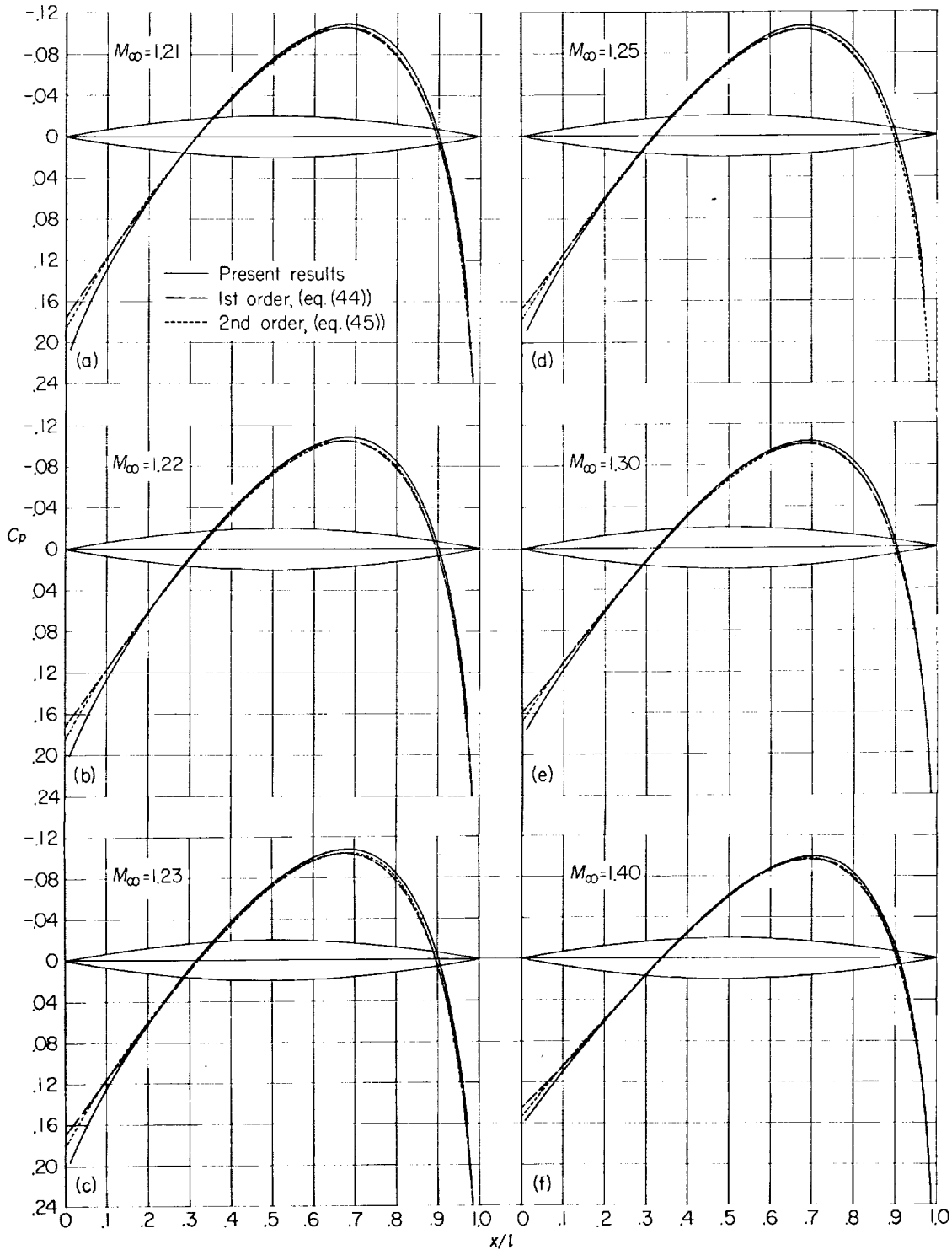

(a) $M_\infty = 1.21$ (b) $M_\infty = 1.22$ (c) $M_\infty = 1.23$
(d) $M_\infty = 1.25$ (e) $M_\infty = 1.30$ (f) $M_\infty = 1.40$

FIGURE 12.—Pressure distributions on a parabolic-arc body of revolution of fineness ratio 10 at Mach numbers above the upper critical as indicated by present theory and by other theoretical results.

501377—59——3

in the regions where the local Mach number approaches unity. The most prominent difference occurs near the tail of the bodies where the first- and second-order theories indicate that the flow is subsonic.

This result is contradictory to the basic assumption that the flow is supersonic, but it is nevertheless qualitatively correct, since more exact investigations also indicate that the flow is subsonic at the tail of a body of revolution that terminates like a cone. There is no assurance that the smooth deceleration through sonic velocity indicated by the first- and second-order theories is correct, however, and further investigation appears necessary for the clarification of this detail. On the other hand, the results indicated by the present theory terminate when u reaches the value $(M_\infty^2-1)/k$ associated with the occurrence of sonic velocity. When this situation occurs, the inequality specified by equation (34) is no longer satisfied, the argument of the logarithmic term of equation (39) vanishes, and du/dx increases logarithmically to infinity. If the solution for the remainder of the body is required, it is necessary to consider the nature of the shock wave that must be present in the vicinity of the rear of the body and to use equations that are not restricted in application to supersonic flows. As a result, further discussion of this matter is deferred to the subsequent section on flows with free-stream Mach number near 1. In any case, the entire question is of rather an academic nature for parabolic-arc bodies in the Mach number range considered in the preceding discussion because (a) the region involved is only a small fraction of the body length, (b) significant viscous effects are generally present in this region, and (c) the information is frequently not needed because the bodies used in practice or investigated in the wind tunnel are cut off forward of this region.

No experimental pressure distributions for a parabolic-arc body of revolution of fineness ratio 10 are available for comparison with the theoretical results shown in figure 12. The maximum test Mach number of the investigation reported in reference 11 is 1.20, whereas the lowest Mach number for which the present theoretical results indicate supersonic flow at the nose is 1.21, The comparison with first- and second-order theory should suffice, however, for an estimate of the accuracy of the present results for supersonic flows.

FLOWS WITH FREE-STREAM MACH NUMBER NEAR 1

APPROXIMATE SOLUTION OF EQUATIONS

The analyses of subsonic and supersonic flows given in the preceding sections have started by introduction of a symbol λ for the coefficient of φ_{xx} and the assumptions that λ is neither zero nor infinite and that it varies sufficiently slowly that it can be regarded as a constant in the early stages of the analysis. Since the results so obtained terminate if $\lambda=0$, or physically if a point is approached at which the velocity is sonic, it is evident that additional considerations are necessary to permit the study of flows with free-stream Mach number near 1 in which the acceleration from subsonic to supersonic velocities is an essential feature.

The technique adopted is to introduce the symbol λ_P as an abbreviation for the coefficient of φ_x rather than φ_{xx}, thus

$$\lambda_P=M_\infty^2\frac{\gamma+1}{U_\infty}\varphi_{xx}\equiv k\frac{\partial u}{\partial x}>0 \tag{46}$$

whence equation (4) may be written as follows:

$$\frac{1}{r}\varphi_r+\varphi_{rr}-\lambda_P\varphi_x=(M_\infty^2-1)\varphi_{xx}\equiv f_P \tag{47}$$

It is assumed, once again, that λ_P is nonsingular and that it varies sufficiently slowly that it can be considered as a constant in the initial stages of the analysis. The resulting differential equation is linear and is of elliptic or hyperbolic type depending on whether the free-stream Mach number, rather than the local Mach number, is less than or greater than unity. At free-stream Mach number 1, the term f_P vanishes and equation (47) reduces to a partial differential equation of parabolic type that is familiar from the study of heat conduction. This appears to be reasonable inasmuch as properties of equations of parabolic type are intermediate, in a certain sense, between those of equations of elliptic and hyperbolic type. At free-stream Mach numbers slightly different from 1, the term f_P remains, but is small. The present analysis of such flows is therefore also based on considerations that are normally applied to equations of parabolic type.

The starting point is the following relation for φ_P derived from equation (47) with λ_P positive and constant, the boundary conditions stated in

equation (1), and the form of Green's theorem associated with the left side of equation (47):

$$\varphi_P=-\frac{U_\infty}{4\pi}\int_0^x \frac{S'(\xi)}{x-\xi}\, e^{\frac{-\lambda_P r^2}{4(x-\xi)}}\, d\xi$$

$$-\frac{1}{\lambda_P}\int_0^{2\pi} d\theta \int_0^\infty \rho d\rho \int_{-\infty}^x \sigma_P f_P d\xi \qquad (48)$$

where

$$\sigma_P=\frac{\lambda_P}{4\pi(x-\xi)}\, e^{-\frac{\lambda_P[r^2+\rho^2-2r\rho\cos(\theta-\Theta)]}{4(x-\xi)}}$$

The corresponding expression for u_P follows by differentiation. It can be approximated for points on the surface of a smooth slender body by

$$\frac{u_P}{U_\infty}=\frac{S''(x)}{4\pi}\ln\frac{\lambda_P S e^C}{4\pi x}-\frac{1}{4\pi}\int_0^x \frac{S''(\xi)-S''(x)}{x-\xi}\, d\xi$$

$$-\frac{1}{\lambda_P}\frac{\partial}{\partial x}\int_0^{2\pi} d\theta \int_0^\infty \rho d\rho \int_{-\infty}^x f_P \sigma_P d\xi \qquad (49)$$

where

$$C=\text{Euler's constant}\approx 0.577215665\ \ldots$$

If the free-stream Mach number is unity, f_P vanishes and u_p can be calculated directly. The resulting expression is precisely that proposed by Oswatitsch and Keune in references 19 and 20 for the calculation of u on the surface of the forepart of an arbitrary slender, pointed body of revolution at free-stream Mach number 1. They have shown that the results are in remarkably good agreement with those measured on the front half of a parabolic-arc body having a thickness ratio τ of 1/6. In this comparison, the parameter λ_P was arbitrarily equated to

$$\lambda_P=\frac{1}{a^2}(\gamma+1)\frac{\pi\tau^2}{l/2};\qquad \frac{1}{a^2}=2 \qquad (50)$$

in the notation of the present paper. In the investigations mentioned above as well as further studies reported in references 21 through 26, the parameter λ_P is regarded throughout as a constant, and various means are proposed for the selection of an appropriate value. It appears, in general, that the results obtained in this way are remarkably accurate if the resulting values for $\partial u/\partial x$ are indeed reasonably constant. If, on the other hand, $\partial u/\partial x$ varies sufficiently along the body, no choice of a single value for λ_P will lead to a useful result. This point, which has already been discussed in some detail for two-dimensional flows in reference 5, is developed further in the course of the following discussions. Some criticisms of the above procedure, although principally from a different point of view, have appeared in a note by Miles (ref. 27).

If the free-stream Mach number is not unity, equation (49) is an integral equation, and it might appear that little progress toward a solution has been made. If attention is confined to Mach numbers near unity, however, it is only necessary to approximate $\varphi_{\xi\xi}$ well locally and it is sufficient to substitute λ_P/k for $\varphi_{\xi\xi}$ or $\partial u/\partial\xi$ in the triple integral. The integral can then be evaluated and the following relationship results:

$$\frac{u_P}{U_\infty}=\frac{1-M_\infty^2}{M_\infty^2(\gamma+1)}+\frac{S''(x)}{4\pi}\ln\frac{\lambda_P S e^C}{4\pi x}$$

$$+\frac{1}{4\pi}\int_0^x \frac{S''(x)-S''(\xi)}{x-\xi}\, d\xi \qquad (51)$$

If, once again, $k(\partial u/\partial x)$ is restored in place of λ_P, the subscript P is dropped, and use is made of the following relation between $\partial u/\partial x$ and du/dx along the surface of the body

$$\frac{d}{dx}\left(\frac{u}{U_\infty}\right)_R=\left[\frac{\partial}{\partial x}\left(\frac{u}{U_\infty}\right)\right]_R+\left[\frac{\partial}{\partial r}\left(\frac{u}{U_\infty}\right)\right]_R\frac{dR}{dx}$$

$$=\left[\frac{\partial}{\partial x}\left(\frac{u}{U_\infty}\right)\right]_R+\frac{S'S''}{4\pi S} \qquad (52)$$

a nonlinear ordinary differential equation is obtained for u on the body surface. It is

$$\frac{u}{U_\infty}=\frac{1-M_\infty^2}{M_\infty^2(\gamma+1)}+\frac{S''(x)}{4\pi}\ln\left\{\left[\frac{d}{dx}\left(\frac{u}{U_\infty}\right)-\frac{S'S''}{4\pi S}\right]\left[\frac{M_\infty^2(\gamma+1)Se^C}{4\pi x}\right]\right\}$$

$$+\frac{1}{4\pi}\int_0^x \frac{S''(x)-S''(\xi)}{x-\xi}\, d\xi \qquad (53a)$$

or

$$\frac{d}{dx}\left(\frac{u}{U_\infty}\right)=\frac{d}{dx}\left[\frac{u}{U_\infty}+\frac{M_\infty^2-1}{M_\infty^2(\gamma+1)}\right]=\frac{S'S''}{4\pi S}$$

$$+\exp\left\{\frac{4\pi}{S''(x)}\left[\frac{u}{U_\infty}+\frac{M_\infty^2-1}{M_\infty^2(\gamma+1)}-\frac{S''(x)}{4\pi}\ln\frac{M_\infty^2(\gamma+1)Se^C}{4\pi x}-\frac{1}{4\pi}\int_0^x \frac{S''(x)-S''(\xi)}{x-\xi}\, d\xi\right]\right\} \qquad (53b)$$

This equation is of the first order and the same general form

$$\frac{du}{dx}=F(x,u) \tag{54}$$

as encountered in the analysis of subsonic and supersonic flows in the preceding sections, and it is again necessary to specify some condition for the evaluation of the constant of integration. Two classes of cases are to be distinguished. One class includes the foreparts of bodies with a convex corner, such as a cone-cylinder, for which the necessary condition is supplied by the fact that the velocity must be sonic, that is,

$$\frac{u}{U_\infty}=\frac{1-M_\infty^2}{M_\infty^2(\gamma+1)} \tag{55}$$

at the shoulder. The other includes smooth bodies along which the velocity accelerates smoothly through sonic velocity and for which there is no point for which a value for u can be specified by a priori considerations. The procedures followed in the preceding sections and in reference 5 suggest that u be equated to u_P at the point on the forepart of the body where $S''(x)$ is zero, since, for Mach numbers near unity, u_P is independent of λ_P at this point. This point has the additional property, evident from equations (53) and (55), of corresponding to the station toward which the sonic point approaches as the thickness ratio of the body becomes vanishingly small.

This procedure does not suffice to determine a solution in the present case, however, because equation (53) is singular at this point and an infinity of integral curves pass through the value $u=u_P$ at the point where $S''(x)$ vanishes. Of all these curves, however, only one is analytic (all derivatives finite) at this point, and selection of it suffices to determine a unique solution. That this is so can be seen by consideration of the series of expressions obtained by successive differentiation of equation (53a) with respect to x. After an arbitrary number n of differentiations, an expression is obtained for d^nu/dx^n that involves derivatives of u with respect to x up to the order $n+1$. The $n+1$ derivative is, of course, unknown, but it is multiplied by $S''(x)$ and the product vanishes at the point where $S''(x)$ is zero, provided always that $d^{n+1}u/dx^{n+1}$ is finite. It thus follows that all of the coefficients of a Taylor series expansion for u at the point where $S''(x)$ is zero can be determined, the only requirement being that, at each step, the derivative of next higher order is finite. The Taylor series suffices for the determination of the solution of equation (53) in the neighborhood of the point where $S''(x)$ vanishes. The remainder of the solution can be determined by application of standard methods such as that of Milne described in the preceding section on subsonic flows.

APPLICATION TO CONE-CYLINDER

A simple application of the foregoing theory is provided by consideration of flow with free-stream Mach number near 1 past a slender circular cone-cylinder of maximum diameter d and cone length

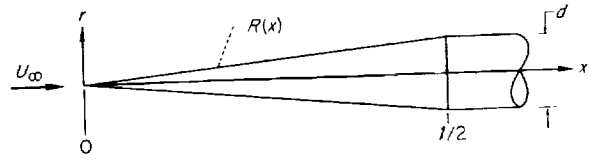

FIGURE 13.—View of cone and principal dimensions.

$l/2$ as illustrated in figure 13. The ordinates R of this body are given by

$$\left.\begin{aligned} R=d\frac{x}{l}=\tau x \quad &\text{for} \quad 0<x<l/2 \\ R=\frac{d}{2}=\tau\frac{l}{2} \quad &\text{for} \quad x>l/2 \end{aligned}\right\} \tag{56}$$

The variation of cross-section area S with x along the conical part of the body is thus

$$S=\pi R^2=\pi\tau^2x^2 \tag{57}$$

Details of the solution.—Substitution of the expression for $S(x)$ given in equation (57) into equation (53b) leads to the following differential equation for u along the surface of the cone:

$$\frac{d}{dx}\left[\frac{u}{U_\infty}+\frac{M_\infty^2-1}{M_\infty^2(\gamma+1)}\right]=\frac{\tau^2}{x}+\exp\left\{\frac{2}{\tau^2}\left[\frac{u}{U_\infty}+\frac{M_\infty^2-1}{M_\infty^2(\gamma+1)}-\tau^2\ln x-\frac{\tau^2}{2}\ln\frac{M_\infty^2(\gamma+1)\tau^2e^C}{4x}\right]\right\} \tag{58}$$

Introduction of the new variable $G(x)$ defined by

$$G(x)=\frac{u}{U_\infty}+\frac{M_\infty^2-1}{M_\infty^2(\gamma+1)}-\tau^2\ln x \tag{59}$$

leads to an equivalent differential equation

$$\frac{dG}{dx}=\left[\frac{4x}{M_\infty^2(\gamma+1)\tau^2e^C}\right]\exp\frac{2G}{\tau^2} \tag{60}$$

which can be solved by separation of variables. The result is

$$G=-\frac{\tau^2}{2}\ln\left[C_I-\frac{4x^2}{M_\infty^2(\gamma+1)\tau^4e^C}\right] \tag{61}$$

The corresponding expression for u along the surface of the cone follows from equation (59) and is

$$\frac{u}{U_\infty}=-\frac{M_\infty^2-1}{M_\infty^2(\gamma+1)}+\tau^2\ln x -\frac{\tau^2}{2}\ln\left[C_I-\frac{4x^2}{M_\infty^2(\gamma+1)\tau^4e^C}\right] \tag{62}$$

The constant of integration C_I that appears in equations (61) and (62) is evaluated by use of the condition mentioned in the preceding section that the local velocity must be sonic at the shoulder; that is, the relation given by equation (55) holds at $x=l/2$. This procedure leads to the following result:

$$C_I=\left(\frac{l}{2}\right)^2\left[1+\frac{4}{M_\infty^2(\gamma+1)\tau^4e^C}\right] \tag{63}$$

Substitution of this result for C_I in equation (62) and a slight rearrangement of terms yields the following expression:

$$\frac{u}{U_\infty}=-\frac{M_\infty^2-1}{M_\infty^2(\gamma+1)}+\tau^2\ln\left(\frac{\tau x}{l/2}\right) -\frac{\tau^2}{2}\ln\left\{\tau^2+\frac{4\left[1-\frac{x^2}{(l/2)^2}\right]}{M_\infty^2(\gamma+1)\tau^2e^C}\right\} \tag{64}$$

The corresponding expression for the pressure coefficient C_p on the surface of the cone follows from equation (3) and is

$$C_p=\frac{2(M_\infty^2-1)}{M_\infty^2(\gamma+1)}-2\tau^2\ln\frac{\tau x}{l/2} +\tau^2\ln\left\{\tau^2+\frac{4\left[1-\frac{x^2}{(l/2)^2}\right]}{M_\infty^2(\gamma+1)\tau^2e^C}\right\}-\tau^2 \tag{65}$$

A plot of the values for C_p that result upon application of equation (65) to the special case of a cone-cylinder of semiapex angle τ of 1/10 in a flow with free-stream Mach number 1 is shown in figure 14.

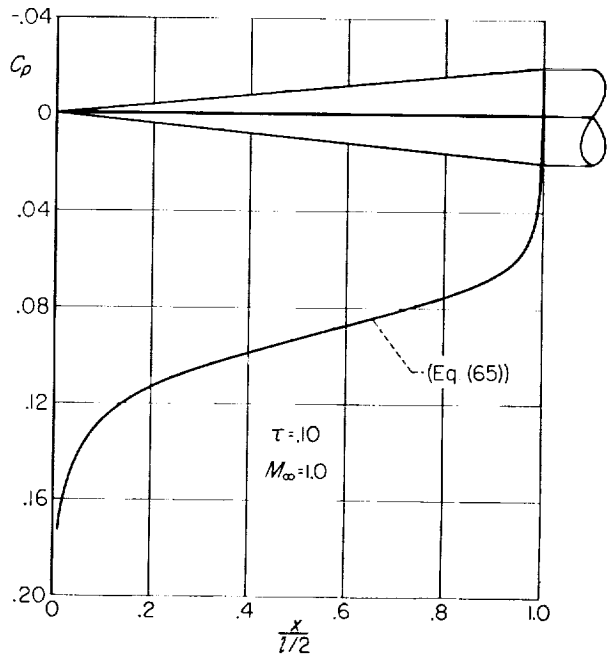

FIGURE 14.—Pressure distribution on a cone-cylinder at Mach number 1, as indicated by equation (65).

Examination of the result given by equation (65) reveals that the similarity rule for the surface pressures given by equations (9) and (12) is not satisfied exactly. It is evident, however, that perfect agreement would be attained if the following approximation were introduced:

$$\tau^2+\frac{4\left[1-\left(\frac{x}{l/2}\right)^2\right]}{M_\infty^2(\gamma+1)\tau^2e^C}\approx\frac{4\left[1-\left(\frac{x}{l/2}\right)^2\right]}{M_\infty^2(\gamma+1)\tau^2e^C} \tag{66}$$

It follows, therefore, that the similarity rule is very nearly satisfied over most of the length of the cone, and that the anticipated failure of the similarity rule in the vicinity of the shoulder is effectively confined to a very small region.

Further examination of the result given by equation (64) reveals that the condition that $\partial u/\partial x$ is greater than zero specified by equation (46) at the outset of the analysis is not satisfied at the apex. This is evident from the following ex-

pression derived from equations (52), (57), and (64)

$$\left[\frac{\partial}{\partial x}\left(\frac{u}{U_\infty}\right)\right]_R=\frac{d}{dx}\left(\frac{u}{U_\infty}\right)_R-\frac{S'S''}{4\pi S}$$

$$=\frac{4\tau^2\left(\frac{x}{l/2}\right)}{\frac{l}{2}\left\{M_\infty^2(\gamma+1)\tau^4 e^C+4\left[1-\left(\frac{x}{l/2}\right)^2\right]\right\}} \quad (67)$$

from which it can be seen that $\partial u/\partial x$ vanishes at $x=0$. This result suggests that the range of usefulness of equation (65) has probably been exceeded in the vicinity of the apex, and recalls an example in two-dimensional flow presented in reference 4 in which $\partial u/\partial x$ vanishes and then becomes negative along the rear part of a particular airfoil.

Determination of correction for the vicinity of the nose.—The calculation of the pressure distribution at a Mach number near 1 on a body of such a shape that $\partial u/\partial x$ is positive along part of body and negative along the remainder cannot be accomplished by direct application of any one of the relations developed in the preceding sections. On the one hand, the considerations based on a differential equation of parabolic type that lead to equation (53) permit the analysis of flows that pass through sonic velocity, but fail when $\partial u/\partial x$ is zero. On the other hand, the considerations based on a differential equation of elliptic or hyperbolic type that lead to equations (20) and (39) permit the analysis of flows in which $\partial u/\partial x$ passes through zero even though the free-stream Mach number may be unity, but fail if the local velocity is sonic. The breakdown is associated in each case with the fact that the basic partial differential equation, that is equation (16), (35), or (47), assumes a degenerate form when λ is zero. The pressure distribution along a body having the properties described above can, nevertheless, be calculated by considering the solution in sections and joining together the various results in such a way that the failings associated with vanishing λ are avoided. This procedure, which is much simpler than a complete re-analysis of the problem from a sufficiently general point of view to encompass the entire problem in a single sweep, is exactly the same as that already employed in reference 4 in the analysis of the related problem in two-dimensional flow mentioned above.

The flow in the vicinity of the apex of a slender cone-cylinder is subsonic in nature, hence the further investigation of the pressure distribution on this part of the body is based essentially on equation (20). It is necessary, however, to add some qualifying remarks about the expression to be used for u_i, the solution for zero Mach number, since the discontinuity in the slope of the surface at the shoulder violates the conditions imposed in the derivation that the body be smooth. The particular case of a slender cone-cylinder in incomprehensible flow, or in linearized subsonic flow, has been investigated by several authors and approximate solutions involving various degrees of refinement and complexity are presently available. It is not necessary to employ the more refined approximations in the present application, however, since only the part of the result that pertains to the forward part of the cone is to be used. A simple expression that is adequate for the present purposes is one that follows from equation (17) upon carrying out the indicated operations, expanding the terms containing τ in a power series, and disregarding terms proportional to the third or higher power of τ. The resulting expression has been given by Laitone in reference 28, and can also be obtained directly from somewhat more general expressions given in references 29 and 30, or on page 311 of reference 6. It is

$$\left(\frac{u}{U_\infty}\right)_E=\tau^2\ln\left(\frac{\tau x}{l/2}\right)-\frac{\tau^2}{2}\ln\left[4\left(\frac{x}{l/2}\right)\left(1-\frac{x}{l/2}\right)\right]$$

$$+\frac{\tau^2}{2}\frac{1}{\left(1-\frac{x}{l/2}\right)}+\frac{\tau^2}{2}\ln\lambda_E \quad (68)$$

The corresponding expression for the pressure coefficient C_p can be determined by substitution of this relation into equation (3). A measure of the accuracy of this approximation can be had by comparison with the results of a much more refined analysis of incompressible flow past a slender cone-cylinder given by Fraenkel in reference 31. The results of such a comparison are illustrated in figure 15 for the special case of a cone-cylinder having a semiapex angle τ of 1/10. It can be seen that the two theories are in very good agreement over the forward portion of the cone.

Differentiation of equation (68) in accordance with the procedure associated with equations (18)

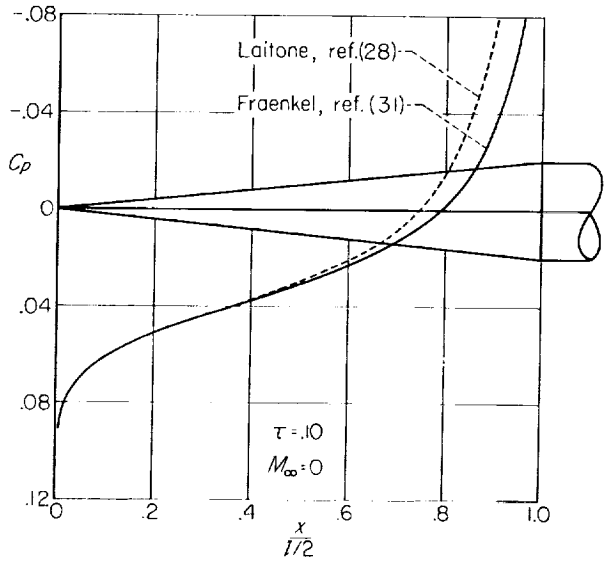

FIGURE 15.—Pressure distribution on a cone-cylinder in incompressible flow.

and (19) results in the complete loss of λ_E in the analysis. The subsequent integration is immediately possible, therefore, and the resulting expression differs from equation (68) only in that the term involving λ_E is replaced by an arbitrary constant of integration, thus

$$\frac{u}{U_\infty}=\tau^2\ln\left(\frac{\tau x}{l/2}\right)-\frac{\tau^2}{2}\ln\left[4\left(\frac{x}{l/2}\right)\left(1-\frac{x}{l/2}\right)\right]+\frac{\tau^2}{2}\frac{1}{\left(1-\frac{x}{l/2}\right)}+C_I \quad (69)$$

The value for the constant of integration C_I is to be selected so that the value for u given by equation (69) is equal to that given by equation (64) at the point where the two results are joined. The latter point is determined by selecting the point at which the two values for du/dx obtained by differentiating equations (64) and (69) are equal. It is found, upon following these procedures and using the approximate relation stated in equation (66), that the point at which the two results are to be joined is situated at

$$\frac{x}{l/2}=\frac{1}{3} \quad (70)$$

and that the expression for the constant of integration is given by

$$C_I=-\frac{M_\infty^2-1}{M_\infty^2(\gamma+1)}-\frac{3}{4}\tau^2-\frac{\tau^2}{2}\ln\left[\frac{4}{M_\infty^2(\gamma+1)\tau^2 e^C}\right] \quad (71)$$

These results lead to the following expression for C_p upon assembly and insertion into equation (3):

$$C_p=\frac{2(M_\infty^2-1)}{M_\infty^2(\gamma+1)}-2\tau^2\ln\left(\frac{\tau x}{l/2}\right)+\tau^2\ln\left\{\left[\frac{16}{M_\infty^2(\gamma+1)\tau^2 e^C}\right]\left[\left(\frac{x}{l/2}\right)\left(1-\frac{x}{l/2}\right)\right]\right\}+\frac{\tau^2}{2}\left(\frac{1-3\frac{x}{l/2}}{1-\frac{x}{l/2}}\right)-\tau^2 \quad (72)$$

It follows furthermore that equation (72) is to be used to calculate the pressure distribution for the forward third of the cone, and equation (65) is to be used for the remainder of the length of the cone.

The magnitude of the difference between the two results and the manner in which they join together are illustrated in figure 16 for the special case of a cone-cylinder of semiapex angle τ of 1/10 in a flow with free-stream Mach number 1. This figure shows the values for C_p indicated by equation (72) for the front portion of the cone together with those indicated by equation (65) for the entire length of the cone. It is evident from this comparison that the two results can be joined together in a manner that is acceptable for most practical purposes. Although the difference between the two results is not large over most of the forward third of the cone, the result indicated by equation (72) confirms the general motivation for the determination of a correction for this region since the values for $\partial u/\partial x$ are negative in the vicinity of the apex. It may be noted, furthermore, that the results indicated by equation (72) are in perfect agreement with the similarity rule indicated by equations (9) and (12). This is a consequence of the systematic use of the approximate relation given in equation (66).

Comparison with experimental and other theoretical results.—Experimental results for C_p on the surface of a cone-cylinder having a semiapex

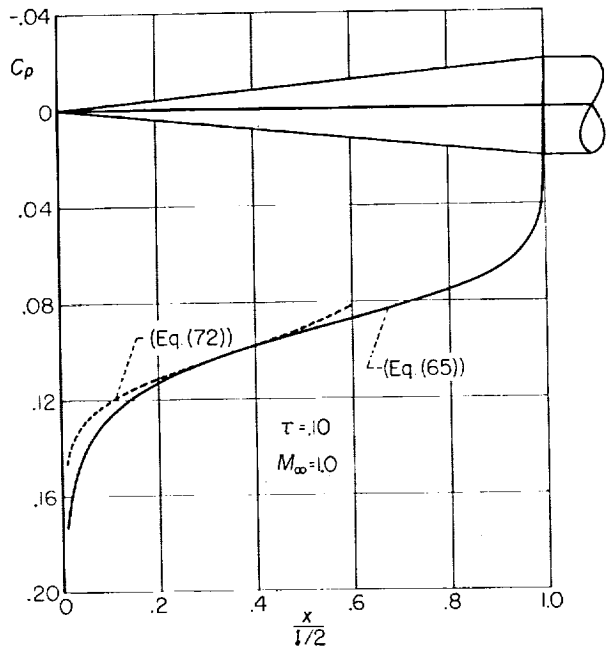

FIGURE 16.—Illustration of nose correction to pressure distribution on a cone-cylinder at Mach number 1.

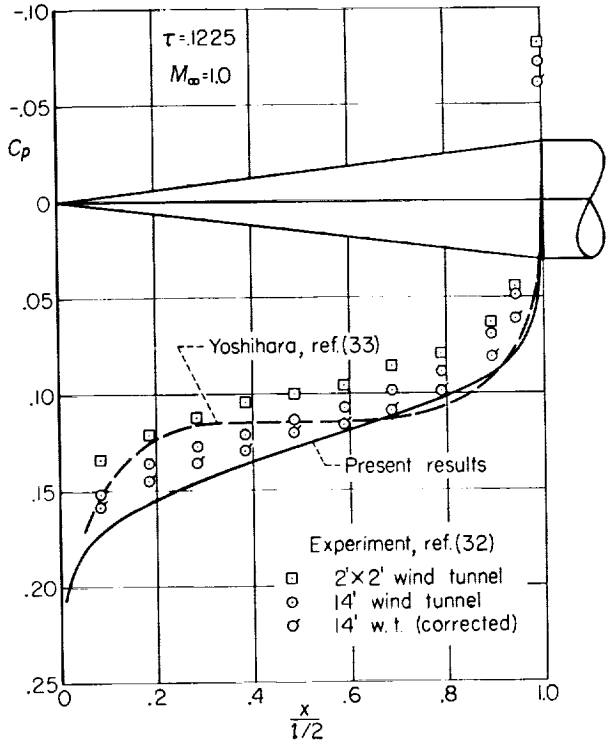

FIGURE 17.—Pressure distribution on a cone-cylinder at Mach number 1, as indicated by present theory, by other theoretical results, and by experiment.

angle of approximately 7° ($\tau=0.1225$) have been given for a range of Mach numbers around unity by Page in reference 32. Since it was considered particularly important in Page's investigation to both minimize and ascertain the degree to which the results are influenced by wind-tunnel wall interference, the tests were conducted in two wind tunnels of different size, one having a test section 14 feet square, the other 2 feet square, using a small model, the conical part of which was 5.50 inches in length. The results for free-stream Mach number 1 are presented in figure 17. The difference between the two sets of experimental results is attributed by Page to wind-tunnel wall interference. Page goes on to show that substantial interference effects remain even in the data obtained in the larger wind tunnel, and finally determines, by both theoretical and experimental considerations, a curve for the pressure distribution corrected for interference. The latter results are indicated in figure 17 by the flagged symbols. The corresponding theoretical pressure distribution calculated by use of equations (65) and (72) is indicated by a solid line. Also included in this figure is a plot of the pressure distribution indicated by the numerical approximate solution of Yoshihara (ref. 33) [1] for a cone-cylinder having a semiapex angle of 1/10 radian transformed so as to be appropriate for a 7° cone by application of the similarity rule given by equation (12). It can be seen that the pressure distribution given by the present theory is distinctly different from that given by Yoshihara, but is similar in form to the experimental pressure distributions, although displaced somewhat. The displacement is considerably less for the tests conducted in the large wind tunnel than in the small wind tunnel, and nearly disappears when the results of the tests in the large wind tunnel are corrected for interference.

The foregoing results may be compared with those obtained by application of the simple linearized theory of Oswatitsch and Keune (refs. 19 and 20) for sonic flow past a slender body of revolution. In this theory, λ_P is replaced by a constant, such as that indicated by equation (50), and the corresponding expression for the pressure

[1] A correction has been applied to Yoshihara's results to allow for a sign error in the quadratic term of the expression for C_p.

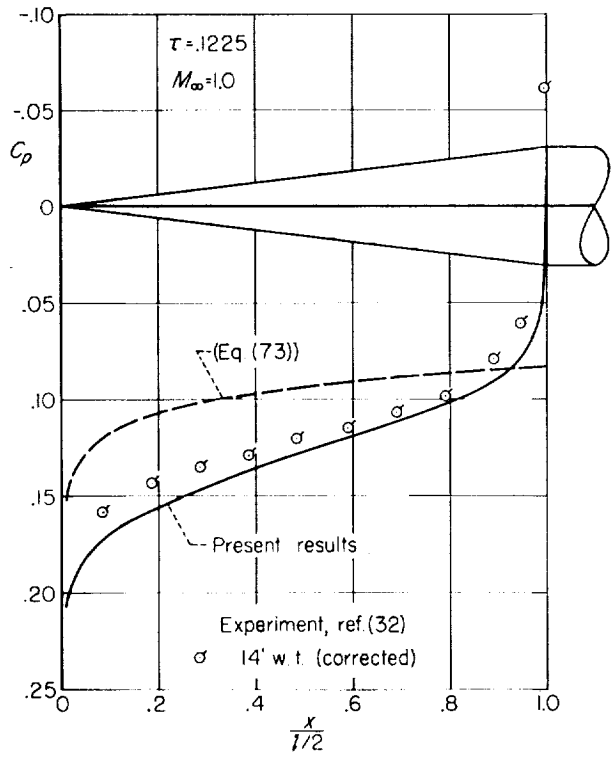

FIGURE 18. Comparison of results indicated by equation (73) with those indicated by the present theory for the pressure distribution on a cone-cylinder at Mach number 1.

distribution on the conical part of a slender cone-cylinder follows directly from equations (51) and (3). It is

$$C_p=-\tau^2 \ln\left[\frac{\pi(\gamma+1)\tau^4 e^C}{2}\left(\frac{x}{l/2}\right)\right]-\tau^2 \qquad (73)$$

if equation (50) is used to evaluate λ_p. Figure 18 shows a plot of the numerical results for a cone-cylinder having a semiapex angle of 7° together with the present theoretical results and the experimental results of Page, as corrected for wall interference. It can be seen that the results indicated by equation (73) are of more or less the correct order of magnitude, but fail to predict, even qualitatively, the proper behavior in the vicinity of the shoulder. It should be observed, furthermore, that no essential improvement would result if λ_p were replaced by some other constant that than indicated by equation (50) since such a change leads only to a uniform change in C_p along the entire length of the cone. This difficulty of the linearized theory for sonic flow is to be expected because the region of dependence for the solution at an arbitrary point is confined to the part of space situated upstream of this point. As a result, the influence of the part of the cone-cylinder situated between the arbitrary point and the shoulder is not included in the solution, although it should be since the flow in this region is subsonic. The present theory, on the other hand, includes the influence of this region in the final result since the constant of integration associated with the differential equation that results upon replacement of λ_p by $k(\partial u/\partial x)$ is specified at the shoulder and the integration proceeds in the upstream direction. In this way, the approximate expression for C_p indicated by equation (65), and therefore also that indicated by equation (72), depends on conditions along the entire conical part of the cone-cylinder, and the influence of regions situated both upstream and downstream from an arbitrary point are included in the result.

Theoretical results for the pressure distribution on a slender cone-cylinder in flows with high subsonic or sonic free-stream velocity have also been given recently by Kusukawa in reference 34. These results were obtained by application of an approximate relation between axisymmetric and two-dimensional flows given previously by the same author in reference 35. In this way, the solution for a cone-cylinder is related to that for an airfoil having ordinates proportional to x^2 followed by a straight section extending downstream to infinity. Kusukawa obtains an approximate solution for the latter problem by considering a flow that separates from the shoulder of the airfoil and calculates the pressure distribution on the airfoil surface with the aid of a pressure correction formula. This formula, which was given in a third paper by the same author (ref. 36), relates the pressure at a given point in a compressible flow to that at the same point in an incompressible flow past the same airfoil. This procedure has been applied to calculate the pressure distribution on a cone-cylinder having a semiapex angle of 7° and the results are presented in figure 19 together with the present theoretical results and the experimental results of Page. The latter results are again corrected for wall interference, as noted in the discussion associated with figure 17. It appears from this comparison that the values for C_p calculated by the method of Kusukawa are too

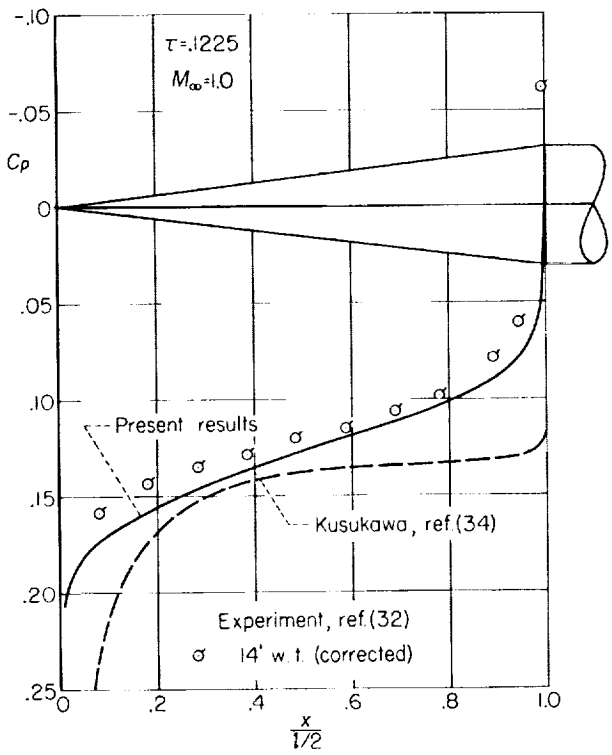

FIGURE 19.—Comparison of results indicated by Kusukawa (ref. 34) with those indicated by the present theory for the pressure distribution on a cone-cylinder at Mach number 1.

large at all points along the length of the cone. Of the three principal steps in the derivation of Kusukawa's results, the only one that has not been checked by a number of comparisons with experimental or other theoretical results, and is thus the most likely source of the discrepancy, is the approximate relation between axisymmetric and two-dimensional flows. It is not likely that a significant part of the discrepancy is a consequence of the use of the assumption that the flow separates from the shoulder instead of performing a Prandtl-Meyer expansion around the corner, since it has been shown in references 36, 37, and 5 for the case of a wedge profile that the nature of the flow behind the shoulder has very little effect on the pressure distribution on the part of the airfoil ahead of the shoulder. Neither is it likely that a significant part of the discrepancy can be traced to the use of the pressure-correction formula. This formula, which was derived by Kusukawa by application of the WKB method of approximation to the equations of transonic flow theory expressed in terms of hodograph variables, has also been found independently (except for replacement of $\gamma+1$ by $M_\infty^2(\gamma+1)$ as a result of a corresponding change in the fundamental equations of transonic flow theory) by application of much different considerations and is presented as equation (28) in reference 4. This result is evaluated in references 4, 5, and 36 by numerous comparisons with other theoretical and experimental results. Of the various examples, the one that is most closely associated with the present discussion is a comparison given in reference 5 with the results indicated by the exact solution of the equations of transonic flow theory for separated flow past a wedge profile published recently by Helliwell and Mackie in reference 37. This comparison shows that the numerical values for the pressure distribution on the surface of the wedge are hardly distinguishable, whether calculated by use of the exact or approximate formulas.

Some insight into the range of Mach numbers surrounding unity for which the present theory might be expected to give useful results can be gained by noting that the indicated variation of C_p with M_∞ is essentially proportional to $M_\infty-1$ and that the constant of proportionality is very nearly equal to that associated with the known invariance of local Mach number M with changes in free-stream Mach number M_∞ at $M_\infty=1$, that is, with the relation

$$\left(\frac{dM}{dM_\infty}\right)_{M_\infty=1}=0 \tag{74}$$

The exact relation for dC_p/dM_∞ for $M_\infty=1$ for isentropic flow that corresponds to equation (74) is

$$\left(\frac{dC_p}{dM_\infty}\right)_{M_\infty=1}=\frac{4}{\gamma+1}-\frac{2}{\gamma+1}(C_p)_{M_\infty=1} \tag{75}$$

The approximate relation indicated by the present theory is

$$\left(\frac{dC_p}{dM_\infty}\right)_{M_\infty=1}=\frac{4}{\gamma+1}-2\tau^2 \tag{76}$$

except at the shoulder where it is

$$\left(\frac{dC_p}{dM_\infty}\right)_{M_\infty=1}=\frac{4}{\gamma+1} \tag{77}$$

All three relations are nearly equivalent, since $2C_p/(\gamma+1)$ and $2\tau^2$ are very small in comparison

with $4/(\gamma+1)$ for slender bodies. It follows, therefore, that the variation of C_p with M_∞ indicated by the present theory is sufficiently accurate for all engineering purposes within at least a small range of Mach numbers surrounding $M_\infty=1$. It should be noted that the range of Mach numbers for which the above results may be expected to apply is much smaller than in two-dimensional flows, since Guderley has indicated (ref. 38, p. 296) that the leading term in the expansion of the deviation of M from its value for $M_\infty=1$ is proportional to $(M_\infty-1)^3$ for planar flows and $(M_\infty-1)^{5/3}$ for axisymmetric flows.

Pressure drag.—The pressure drag of a slender cone-cylinder at free-stream Mach number 1 and vicinity can be found by integration of the general relation given by equation (13) with the expressions given by equations (57), (65), and (72) substituted for S and C_p. This procedure leads to the following expression for the drag coefficient referred to maximum cross-section area if equation (65) is used for C_p along the entire length of the cone:

$$C_D=\frac{D}{\left(\frac{\rho_\infty}{2}U_\infty^2\right)[\pi\tau^2(l/2)^2]}=2\,\frac{M_\infty^2-1}{M_\infty^2(\gamma+1)}+\tau^2\left[-1+\ln\frac{4}{M_\infty^2(\gamma+1)\tau^4e^C}\right] \quad (78)$$

If equation (72) is used instead of equation (65) to calculate C_p along the forward third of the cone, the value for C_D is smaller by an amount given by

$$\Delta C_D=\tau^2\left(\frac{1}{2}+\ln\frac{16}{27}\right) \quad (79)$$

so that

$$C_D=2\,\frac{M_\infty^2-1}{M_\infty^2(\gamma+1)}+\tau^2\left[-\frac{1}{2}+\ln\frac{64}{27M_\infty^2(\gamma+1)\tau^4e^C}\right] \quad (80)$$

Comparison with equations (9) and (14) reveals that both of these results for C_D satisfy the similarity rule exactly.

The variation of C_D with τ for free-stream Mach number 1 indicated by equation (80), which reduces to the following simple form for $M_\infty=1$ and $\gamma=1.4$,

$$C_D=-\tau^2(1.08965+4\ln\tau) \quad (81)$$

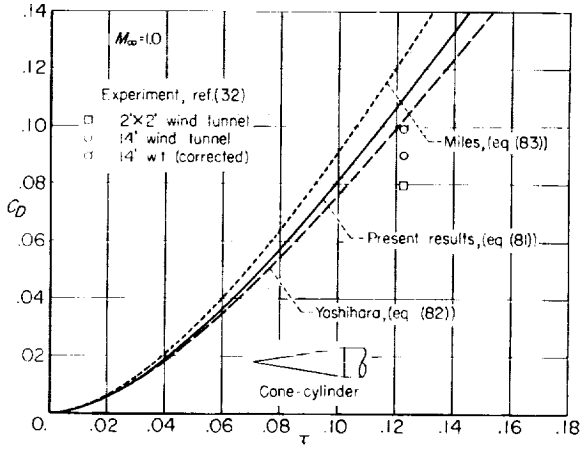

FIGURE 20.—Variation of pressure-drag coefficient with thickness ratio for a cone-cylinder at Mach number 1, as indicated by present theory, by other theoretical results, and by experiment.

is shown graphically in figure 20. Also included in this figure are the corresponding theoretical results indicated by the following equation determined by combination of the similarity rule and Yoshihara's result for a cone-cylinder having a semiapex angle of 1/10 radian:

$$C_D=-\tau^2(1.55+4\ln\tau) \quad (82)$$

and by the following equation given by Miles in reference 39.

$$C_D=-\tau^2(0.091+4\ln\tau) \quad (83)$$

The latter formula is derived by an approximate procedure based on matching a solution of Laplace's equation in two dimensions for points near the axis with the asymptotic solution of Guderley and Yoshihara (refs. 40 and 41) for points at great distances from the axis. The solutions are joined at the sonic line, and the drag is determined by application of momentum methods without an intermediate calculation of the pressure distribution. Three data points for a cone-cylinder having a semiapex angle of 7° are also included in figure 20. They represent the values obtained from the experimental investigation of Page reported in reference 32. In accordance with the notation already employed in the display of Page's results in figure 17, the square symbol represents the result obtained from tests in a 2-foot wind tunnel, the plain circle represents the result obtained in a 14-foot wind tunnel, and the flagged symbol

represents the latter result corrected for wall interference. It can be seen that the latter result is very close to the theoretical curves computed by means of either equation (81) or (82), but is noticeably less than that indicated by equation (83).

Comparison with results for subsonic and supersonic flow.—The remainder of the discussion of the aerodynamic properties of cone-cylinders is concerned with an examination of the relation between the results given in the preceding section for Mach number 1 and vicinity and those available from other sources for subsonic and supersonic flows. The discussion is of particular interest because possession of knowledge of the results for Mach numbers near unity greatly facilitates an understanding of the process by which the pressure distribution changes from the form shown in figure 15 for incompressible flow to the familiar constant pressure associated with supersonic flow.

In order to be more specific, consider the special case of a cone-cylinder having a semiapex angle of 1/10 radian. Figure 21 shows the pressure distribution on the conical part of such a body for the highest Mach number for purely subsonic flow (namely $M_\infty=0$), for Mach number 1, and for the lowest Mach number for purely supersonic flow. The latter Mach number is very nearly 1.055. The results for zero Mach number are those given by Fraenkel in reference 31 and shown previously herein in figure 15. The results for Mach number 1 are those indicated by equation (72) for the forward third of the cone and by equation (65) for the remainder of the cone. The results for the upper critical Mach number are determined from the numerical results given by Oswatitsch and Sjodin in reference 15 and by Shen in reference 16 reinterpreted so as to conform with the formulation of the equations of transonic flow theory given in equations (1) through (5). Although the differences in the numerical results are small, such a change is necessary because the basic equations used by Oswatitsch and Sjodin and by Shen are not only slightly different from those used herein, but are slightly different from each other. The difference is concerned entirely with the quantity $M_\infty^2(\gamma+1)$ that appears in equations (4) and (5). This quantity is replaced by $\gamma+1$ in the investigation of Shen and by $(M_\infty^2-1)U_\infty/(U_\infty-a^*)$, where a^* is the critical speed of sound, in the investigation of Oswatitsch and Sjodin.

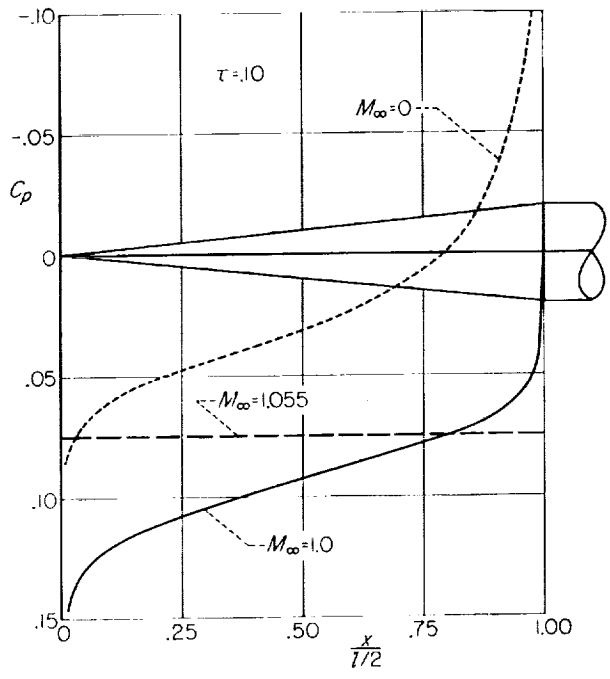

FIGURE 21.—Pressure distributions on a cone-cylinder at the upper and lower critical Mach numbers and at Mach number 1.

A plot of the variation of pressure coefficient C_p with free-stream Mach number M_∞ on the surface of an infinite cone having a semiapex angle of 1/10 radian, as indicated by the theoretical analyses of references 15 and 16 reinterpreted in the manner described in the preceding paragraph, is shown in figure 22. A second curve labeled $C_{p_{cr}}$ is included on this plot to illustrate the variation with free-stream Mach number of the critical pressure coefficient associated with the occurrence of sonic velocity (i.e., $u/U_\infty=(1-M_\infty^2)/[M_\infty^2(\gamma+1)]$) on the surface of the cone. This curve, which is computed by use of the expression

$$C_{p_{cr}}=2\frac{M_\infty^2-1}{M_\infty^2(\gamma+1)}-\tau^2 \tag{84}$$

does not pass through 0 at free-stream Mach number 1 because of the particular manner in which the sonic velocity is expressed in the approximate equations of transonic flow theory. The point of intersection of the two curves determines the upper critical Mach number and the associated value for the surface pressure coefficient that are shown in figure 21.

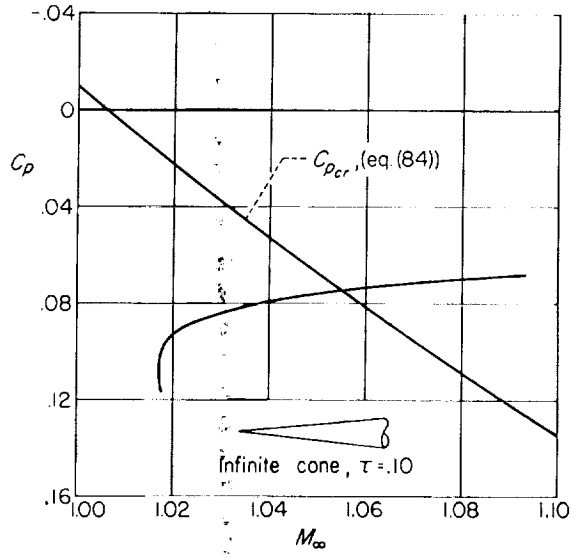

FIGURE 22.—Variation of pressure coefficient with Mach number on the surface of an infinite cone.

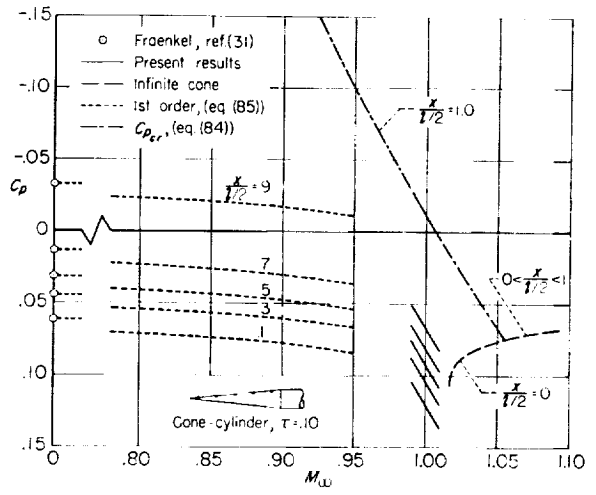

FIGURE 23.—Variation of pressure coefficient with Mach number at various stations along the length of a cone-cylinder of thickness ratio 1/10, as indicated by theory.

If the free-stream Mach number is greater than the upper critical, the flow is supersonic everywhere and the results summarized in the preceding paragraph apply equally to a cone of infinite or finite length. If the free-stream Mach number is less than the upper critical, but greater than unity, the flow adjacent to the surface of the cone is subsonic and the flow field as a whole is transonic. In this case, the result summarized in the preceding paragraph may be expected to apply only to a cone of infinite length, or to points near the apex of a cone of finite length, as in the case of a cone-cylinder. It is known, in particular, that the velocity must be sonic at the sohulder of a cone-cylinder if the flow is subsonic along the surface of the cone. Since intermediate pressures would be anticipated at intermediate points along the surface of the conical part of a cone-cylinder, the two curves shown in figure 22 represent the variation with Mach number of the upper and lower bounds for the values for the pressure coefficient along the conical part of a cone-cylinder having a semiapex angle of 1/10 radian. The smallest Mach number for which a value for the surface pressure is indicated in figure 22 represents the limit of conical flow past an infinite cone and is the lowest Mach number for which the bow wave is attached to either an infinite or finite cone having a semiapex angle of 1/10 radian. At still smaller Mach numbers, the bow wave is detached, or nonexistent if the free-stream Mach number is less than unity, and a stagnation point occurs at the apex. The approximations of slender-body theory are not sufficient to provide a solution that exhibits the proper behavior at the apex, however, and a logarithmic infinity appears at this point instead of the proper value associated with a stagnation point.

Further details of the transition from subsonic to supersonic flow are illustrated by the curves shown in figure 23 in which the results shown in figure 22 are repeated together with additional curves for smaller Mach numbers. Several curves are shown, each of which represents the variation of the pressure coefficient with Mach number at a certain station along the length of a cone-cylinder having a semiapex angle of 1/10 radian. The additional results shown in figure 23 are from three different sources. The small circles at zero Mach number represent the values indicated by the solution given in reference 31 by Fraenkel for incompressible flow. The short lines at Mach number 1 represent the values indicated by equations (65) and (72) of the present theory. The dashed lines at subsonic Mach numbers represent the variation of pressure coefficient with Mach number calculated by use of the following expression derived by combination of the results of Fraenkel $C_{p_{i_F}}$ for incompressible flow and the

influence of Mach number indicated by equation (18) with λ_E replaced by $1-M_\infty^2$:

$$C_p=-2\tau^2 \ln \sqrt{1-M_\infty^2}+C_{p_{i_F}} \tag{85}$$

It should be noted that results calculated in this way are not of the same quality as the remainder of the results shown in figure 23, since they represent a solution of the linearized equations of subsonic flow rather than the nonlinear equations of transonic flow theory. One important consequence of this fact that is not apparent from this plot is that the value indicated for the pressure coefficient at the shoulder is infinite rather than the finite value associated with the occurrence of sonic velocity. The subsonic results indicated on this plot for points removed from the shoulder are probably in at least qualitative agreement with those that would be indicated by the solution of the nonlinear equations of transonic flow theory, provided the free-stream Mach number does not approach too closely to unity. It may be noted, in particular, that the effect of Mach number indicated by equation (85) is simply to shift the entire curve representing the pressure distribution. A similar result would also occur if the present method of approximation were applied to equation (18) to determine an approximate solution of the equations of transonic flow theory. The reason is that the entire term containing λ is lost in the initial differentiation and is, in effect, replaced by an unknown constant upon integration of the differential equation. It would be necessary, however, to include some additional refinement in the details of the solution at the shoulder before a result would be obtained that exhibits the proper behavior in the vicinity of this point.

Additional insight into the nature of the variation with Mach number of the pressure distribution on a cone-cylinder can be gained by examination of the experimental data of Page for a cone-cylinder having a semiapex angle of 7°. Figure 24 has been included, accordingly, to summarize the theoretical and experimental results for three representative stations along the length of the cone. The plain data points represent the values measured in a 2-foot wind tunnel. The flagged data points represent the values measured on the same model in a 14-foot wind tunnel. It can be seen that the two sets of results are in good agreement at Mach numbers well removed from unity, but that substantial differences occur at Mach numbers near unity. As noted previously in the discussion of these same data, Page attributes these differences to wind-tunnel wall interference, and proceeds to determine a theoretical estimate of the necessary corrections that must be applied in order to simulate free-air conditions with free-stream Mach number 1. The solid data points represent the results from the 14-foot wind tunnel corrected in this way for wall interference. Also included in this sketch are a number of solid and dashed curves representing theoretical results calculated in the same manner as described in connection with figure 23. It can be seen that the experimental data support the remarks of the preceding paragraph concerning the general nature of the transition from subsonic to supersonic flow indicated by the various theoretical results. These data also indicate some of the difficulties encountered in the determination of experimental data for free-stream Mach number 1 that are essentially free of wind-tunnel wall interference.

Although substantial gaps remain for which the drag of a cone-cylinder cannot be computed at the present time, it is possible to sketch the variation of drag with Mach number from the results and discussion of the preceding paragraphs. The basic framework is provided by three classes of results; namely, those for zero Mach number, those for Mach numbers near unity, and those for Mach numbers greater than the upper critical. At zero Mach number the drag is zero in accordance with D'Alembert's paradox. At Mach numbers near unity the drag is given by equation (81). At Mach numbers greater than the upper critical, the drag coefficient is the same as for an infinite cone, and is equal numerically to the value for C_p shown in figure 22. These results are illustrated in figure 25 by solid lines and a small circle. The dashed line at Mach numbers less than the upper critical, but greater than the Mach number for shock attachment, represents the values for the drag coefficient of an infinite cone. It follows from the discussion of the pressure distribution given in the preceding pages that the drag coefficient for a cone-cylinder is less than that for an infinite cone. The dashed line at subsonic Mach numbers represents the values for the drag coefficient that are associated with the pressure distribution indicated by equation (85). These values are given by the

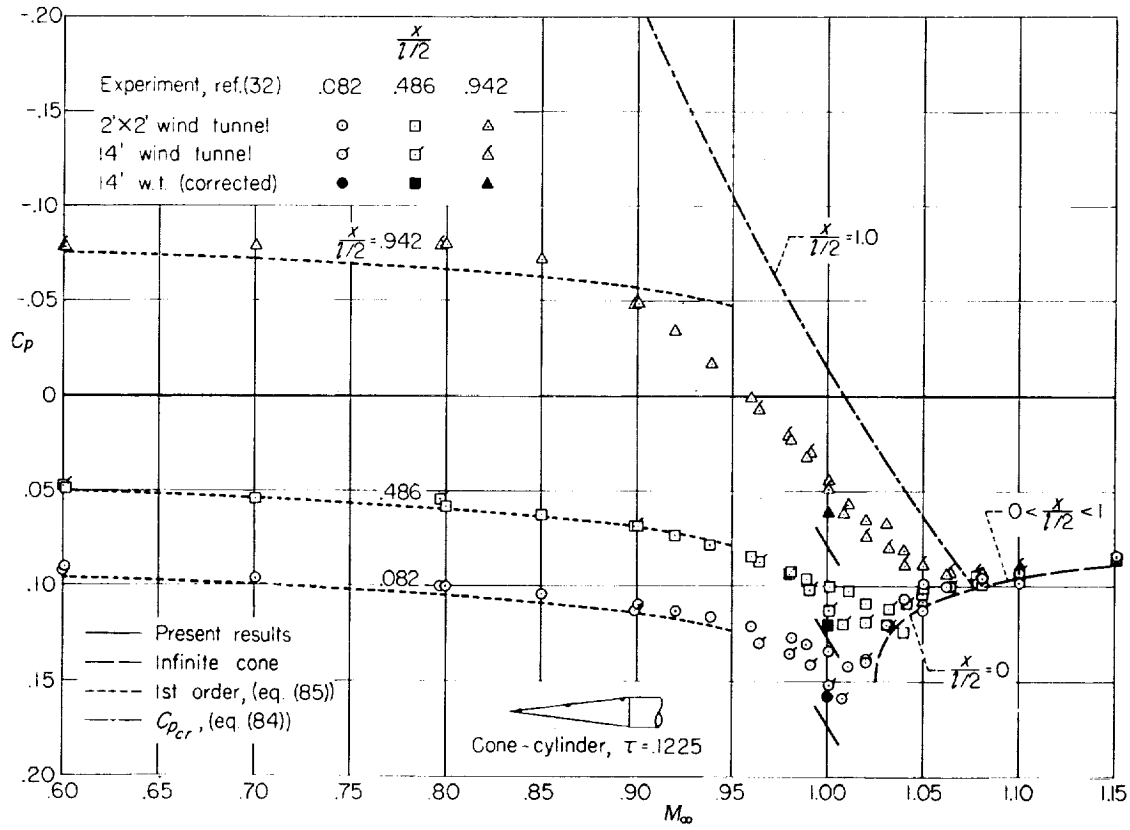

FIGURE 24. Variation of pressure coefficient with Mach number at various stations along the length of a cone-cylinder of thickness ratio 0.1225, as indicated by theory and by experiment.

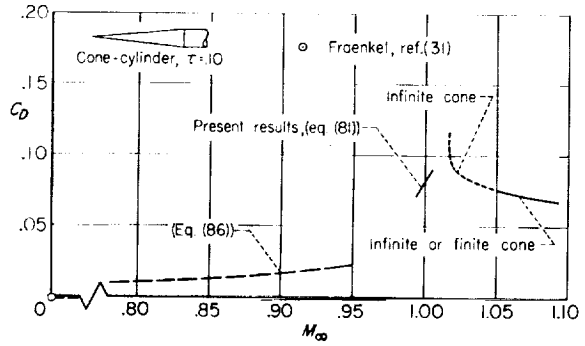

FIGURE 25. Variation of pressure-drag coefficient with Mach number for a cone-cylinder of thickness ratio 1/10, as indicated by theory.

following relation obtained when equations (13) and (85) are combined

$$C_D = -2\tau^2 \ln \sqrt{1-M_\infty^2} \tag{86}$$

Although it is apparent from the discussion in the preceding paragraphs that the latter results are not as reliable as the remainder of the results shown in figure 25, they are included because they display the proper qualitative trend until the Mach number approaches very near to unity. There is considerable likelihood that the quantitative values are too small at Mach numbers much less than unity, however, since the pressure distributions on which the calculations are based indicate a value for C_p of negative infinity at the shoulder rather than the proper finite value associated with the occurrence of sonic velocity.

APPLICATION TO THE FRONT HALF OF A PARABOLIC-ARC BODY

As a first application of the present theory for flow with free-stream Mach number near 1 around a smooth body, consider the case of the front half of a parabolic-arc body of revolution of length l and diameter d. The expressions for the ordinates R, the cross-section area S, and the location of the points at which $S''(x)$ vanishes are given by equations (25), (26), and (27). Attention is confined in this section, however, to the part of the body

situated between $x=0$ and $x=l/2$. The pressure distribution for this part of the body is independent within wide limits, of the shape of the rear and is appropriate, in particular, for either the case in which the rear part of the body continues as a parabolic-arc body or in which it continues as a cylinder extending downstream from $x=l/2$. For the special case described above, the ordinary differential equation for u on the surface of an arbitrary body of revolution given by equation (53b) reduces to the following form:

$$\frac{d}{dx}\left[\frac{u}{U_\infty}+\frac{M_\infty^2-1}{M_\infty^2(\gamma+1)}\right]=\frac{S'S''}{4\pi S}+\exp\left\{\frac{4\pi}{S''}\left[\frac{u}{U_\infty}+\frac{M_\infty^2-1}{M_\infty^2(\gamma+1)}-\frac{S''}{4\pi}\ln\frac{M_\infty^2(\gamma+1)Se^C}{4\pi x}+6\tau^2\left(2\frac{x}{l}-3\frac{x^2}{l^2}\right)\right]\right\} \quad (87)$$

As described in connection with the discussion of the properties of equation (53) for smooth bodies, the calculation of the solution of equation (87) is started by use of the assumption that u is analytic at the singular point where $S''(x)$ vanishes. The solution can thus be expanded in a Taylor's series from which the values for u can be readily calculated for points slightly removed from the singular point. Once these values are known, the solution for the remainder of the body can be calculated numerically by Milne's method. The corresponding values for the pressure coefficient can be calculated directly therefrom with the aid of equation (3).

Comparison with experimental and other theoretical results.—Experimental results for the pressure distribution at free-stream Mach number 1 on the front half of parabolic-arc body of fineness ratio 6 followed by a cylindrical section have been given in reference 19 by Oswatitsch and Keune. These results are presented graphically in figure 26 together with the theoretical pressure distribution calculated in the manner described above. It can be seen that the agreement between the theoretical and experimental results is satisfactory for most purposes.

Attention is called, however, to the fact mentioned previously that the simpler approximation of references 19 and 20 in which λ_P is replaced by the constant indicated by equation (50) also leads to theoretical results that agree well with the

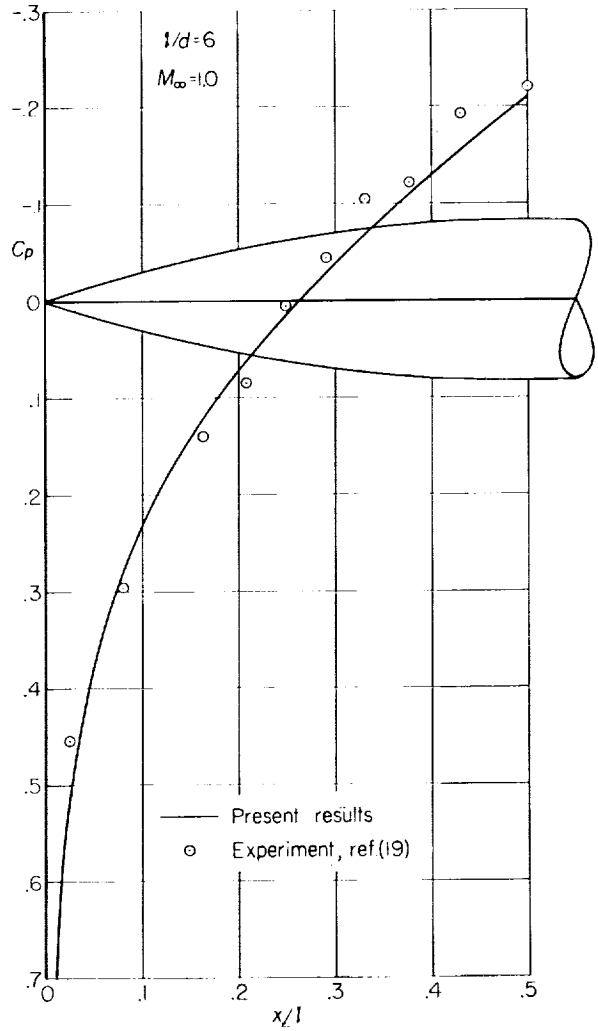

FIGURE 26. Pressure distribution on the front half of a parabolic-arc body of fineness ratio 6 at Mach number 1, as indicated by present theory and by experiment.

experimental pressure distribution shown in figure 26. The results of such a calculation are shown in figure 26 together with the theoretical and experimental results from figure 26. Also included is another curve calculated with constant λ_P evaluated using equation (50) with $a^2=1$ rather than ½. These two values for a^2 are those considered originally in references 19 and 20. It is shown in these references that both have merit, but the value of $a^2=0.50$ is recommended because it is superior in the treatment of certain important details of the flow field. It is also stated that according to the similarity rule, the parameter

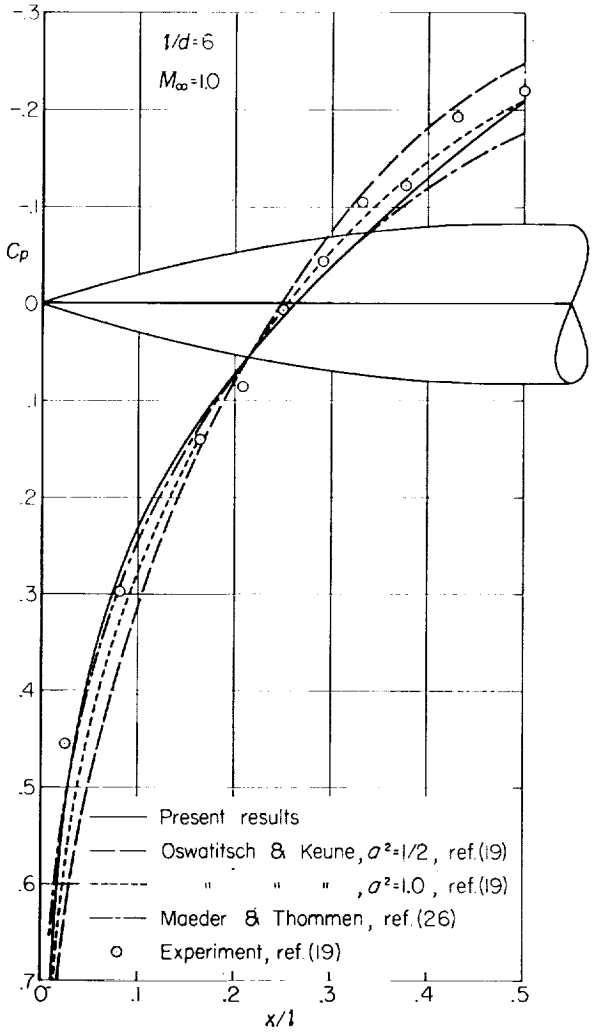

FIGURE 27.—Pressure distribution on the front half of a parabolic-arc body of fineness ratio 6 at Mach number 1, as indicated by present theory, by experiment, and by other theoretical results.

a^2 depends on the shape, but not the thickness ratio of the body.

Keune has modified these conclusions in more recent publications (refs. 21, 22, and 23), and has suggested, on the basis of considerations relating to the mass flow, the selection of such a value for a^2 that the value for λ_P agrees with half the value for $(\gamma+1)\varphi_{xx}/U_\infty$ at the sonic point. It is further shown that this procedure leads to values for a^2 of 0.455 and 0.28 for parabolic-arc bodies having thickness ratios τ of 0.146 and 0.073.

Maeder and Thommen have independently proposed a similar procedure, but without the factor ½, and have presented a curve in reference 26 from which the resulting values for a^2 can be readily determined for any parabolic-arc body having a thickness ratio less than 0.25. This curve leads to the following values for a^2, 0.274, 0.248, and 0.135, for parabolic-arc bodies having thickness ratios of ⅛, 0.146, and 0.073. Although these values should be exactly half those indicated by Keune for a body of the same thickness ratio, it may be observed that the values are actually related in a slightly different manner. The present authors have not sought the source of this discrepancy since the differences are much smaller than those associated with the factor ½ that exists between the intended values. The pressure distribution on the front half of a parabolic-arc body of fineness ratio 6 has been computed using the value for a^2 given by Maeder and Thommen, and is presented in figure 27. It is evident from examination of the various results shown in this figure that the procedure adopted for the selection of a suitable value for a^2 has a significant effect on the resulting pressure distribution. Although certain of these procedures lead to results of good quality for the pressure distributions on the front half of a parabolic-arc body, it should be recalled that no selection of a constant for λ_P can lead to a reasonable pressure distribution on a cone-cylinder.

Theoretical pressure distributions for the front halves of parabolic-arc bodies of revolution of fineness ratio 6 $\sqrt{2}$, 10, 12, and 14 in flows with free-stream Mach number 1 have also been calculated by means of the present theory. These results, together with those given above for the body of fineness ratio 6, are presented in graphical form in figure 28. The numerical values for all five cases are given in table IV. It should be observed that only the values for x/l between 0 and 0.50 are to be considered in the present discussion. This particular family of bodies has been selected because experimental pressure distributions are available from the investigations of references 14 and 11. In both cases, tests were conducted on bodies that more nearly approximate complete bodies than half bodies, but the results should be suitable for comparison with the present theoretical results because the pressures on the front part of such a body do not depend, at free-stream Mach number 1, on the shape of the rear. The results of such a comparison are shown in figure 29. Although it is evident from the scatter of the experimental data that the relative accuracy

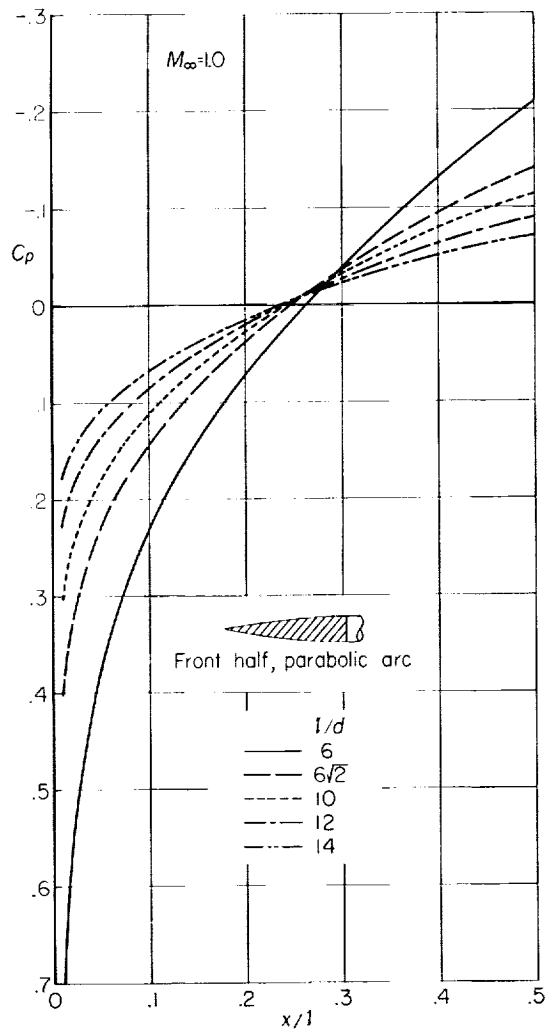

FIGURE 28.—Pressure distributions on the front halves of a series of parabolic-arc bodies of various fineness ratios at Mach number 1, as indicated by present theory.

of the experimental results diminishes with increasing fineness ratio, these comparisons show that the theoretical and experimental results are in essential agreement.

The results presented in the preceding paragraph indicate that the magnitudes of the values for C_p are strongly influenced by the fineness ratio. The similarity rule given by equation (12) indicates the existence of such an effect, and figure 30 is included to illustrate quantitatively the degree to which the present results conform to the similarity rule. In this figure the values for C_p for each of the bodies are converted to the corresponding values for a body of fineness ratio 10 by use of equation (12). If the present results conformed perfectly to the similarity rule, the results for all five bodies would define a single curve. It can be seen that the present results when so presented do not quite define a single curve, but the differences between the various curves are small. This indicates that the present results for the pressure distributions on the front halves of a series of parabolic-arc bodies of different fineness ratios are related, at free-stream Mach number 1, in a manner that very nearly conforms with the similarity rule. This conclusion is similar to that for the cone-cylinder at free-stream Mach number 1, but quite different from that for the parabolic-arc body at Mach numbers in the vicinity of the critical.

Pressure drag.—Once the pressure distribution on the front half of a slender parabolic-arc body has been calculated, the corresponding value for the pressure drag can be found immediately by numerical integration of the general relations given by equation (13). The necessary calculations have been carried out for each of the five cases considered in this section, and the resulting values for $C_D=D/[(\rho_\infty/2)U_\infty^2 S_m]$ at Mach number 1 are

l/d	6	$6\sqrt{2}$	10	12	14
C_D	0. 05988	0. 02903	0. 02063	0. 01416	0. 01031

These values are plotted as a function of τ in figure 31 to illustrate the effect of thickness ratio on C_D. It can be seen from examination of these values, or by inspection of figure 32 in which C_D/τ_2 is plotted as a function of τ, that C_D is very nearly proportional to the square of τ as indicated by the similarity rule given in equation (14).

Experimental values for the pressure drag can be obtained by a similar integration of equation (13) using the measured values for C_p given in references 11, 14, and 19, and repeated here in figures 29 and 26. Oswatitsch and Keune have already given the results of such a calculation in reference 19 for the case of the front half of a parabolic-arc body of fineness ratio 6 followed by a cylindrical body. Their result that C_D equals 0.058 compares very favorably with the corresponding value of 0.05988 indicated by the present theory. Experimental values for C_D have

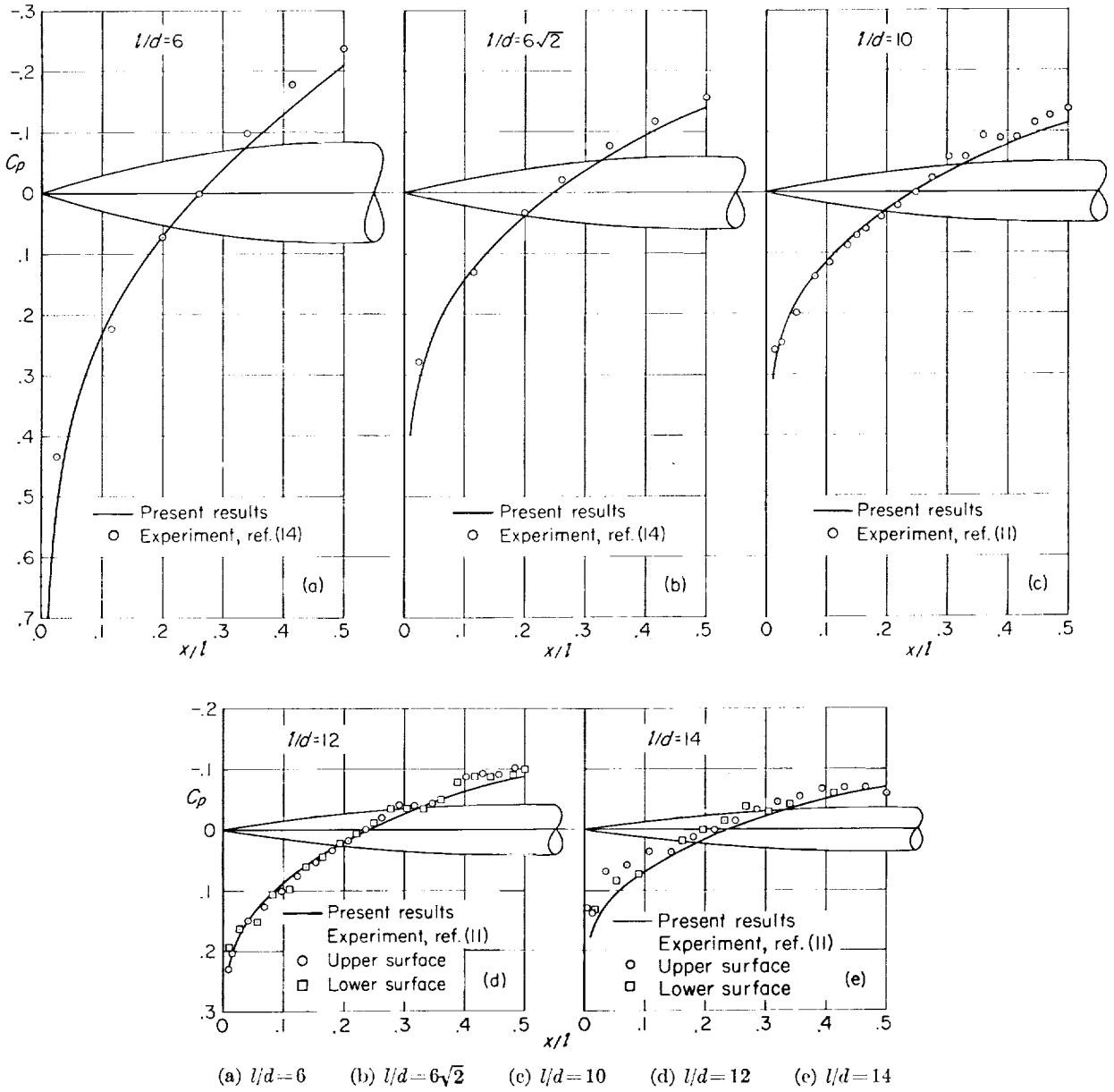

(a) $l/d=6$ (b) $l/d=6\sqrt{2}$ (c) $l/d=10$ (d) $l/d=12$ (e) $l/d=14$

FIGURE 29.—Pressure distributions on the front halves of parabolic-arc bodies of various fineness ratios at Mach number 1, as indicated by present theory and by experiment.

also been determined for each of the other five bodies for which measured pressure distributions are presented in figure 29. The results are included in figures 31 and 32. Attention is directed, however, to the fact that the scatter in the measured values for C_p for the bodies of fineness ratio 10, 12, and particularly 14 is such that considerable uncertainty exists in the values for C_D. An indication of the estimated magnitude of the uncertainty due to this cause is provided by the vertical lines attached to the symbols. It can be seen that the uncertainties associated with scatter in the pressure-distribution data are not sufficiently great to account for the result, obviously incorrect, that the drag of the body of fineness ratio 14 is negative. It appears quite possible, on the basis of the results for the cone-cylinder presented in reference 32 and shown here in

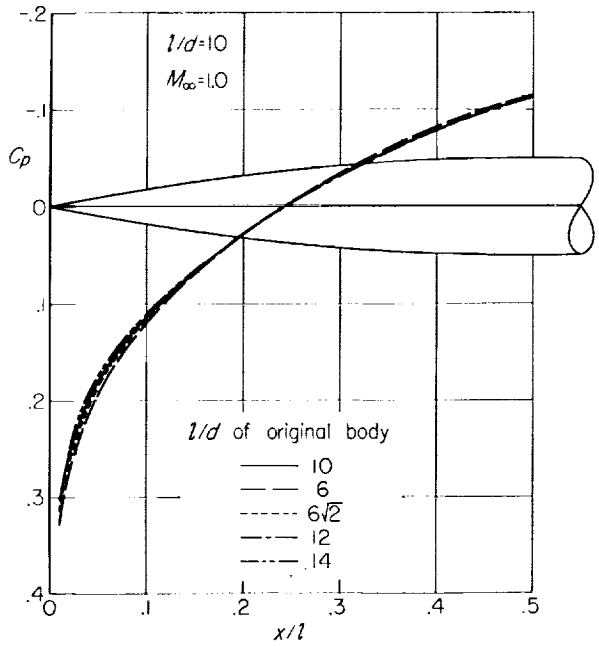

FIGURE 30.—Pressure distribution on the front half of a parabolic-arc body of fineness ratio 10, as obtained by direct calculation using the present theory and by use of the similarity rule.

figures 17 and 24, that this property of the experimental data may be associated with the effects of wind-tunnel wall interference. The results in figures 31 and 32 are in agreement with the fact that the effects of wind-tunnel wall interference at free-stream Mach number 1 are of greater importance, relative to the quantities measured, for thin bodies than for thick bodies.

It is of interest at this point to compare the experimental and theoretical values for C_D given in the preceding paragraph with those indicated by the linearized theory of sonic flow given in references 19 and 20. This theory leads to a simple rule for the calculation of the drag of half bodies that states that the drag does not depend on the value selected for a^2 in equation (50) and is equal to exactly half of the value indicated by linearized supersonic theory. This rule, when applied to the front half of a parabolic-arc body of thickness ratio τ, results in the following simple expression for C_D:

$$C_D=(7/3)\tau^2 \tag{88}$$

Curves illustrating the variation of C_D with τ indicated by this result have been included in figures 31 and 32, from which it can be seen that

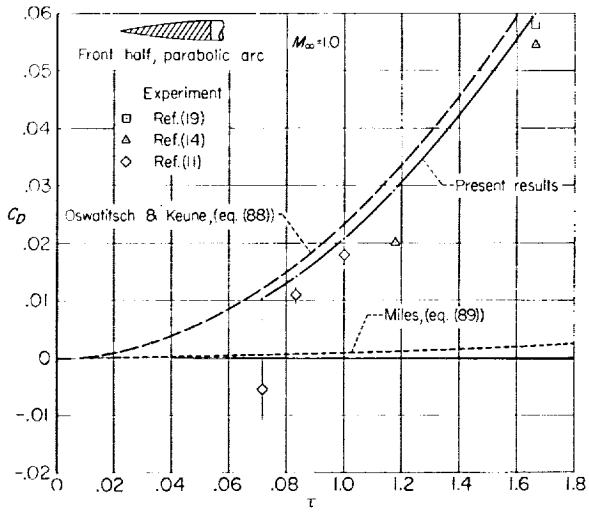

FIGURE 31.—Variation of pressure-drag coefficient with thickness ratio for the front half of a parabolic-arc body at Mach number 1, as indicated by present theory, by other theoretical results, and by experiment.

the values indicated by equation (88) are somewhat larger than either the experimental values or the calculated values indicated by the present theory. Before leaving this topic, it should be mentioned that Keune states briefly (ref. 23) that a more elaborate analysis of this case in which the quantity a^2 is replaced by a function of x, rather than by a constant, leads to a value for C_D that is about 10 percent smaller than indicated by equation (88). This result corresponds very closely with the results of the present calculations.

The approximate theory of Miles (ref. 39) described briefly here in the section on cone-

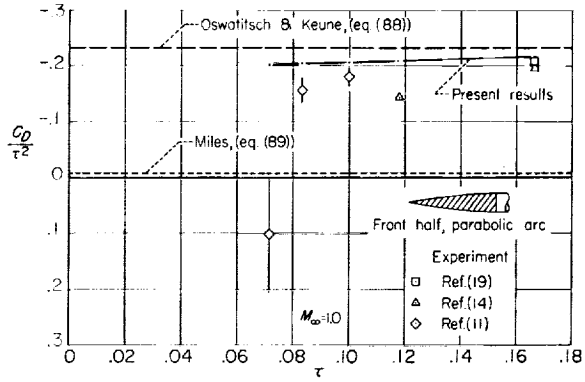

FIGURE 32.—Variation of C_D/τ^2 with thickness ratio for the front half of a parabolic-arc body at Mach number 1, as indicated by present theory, by other theoretical results, and by experiment.

cylinders also contains a general expression for the calculation of the pressure drag of the forepart of a smooth slender body of revolution in a flow with free-stream Mach number 1. Miles' expression, which appears to lead, in general, to very small values for the drag of smooth bodies, reduces to the following expression when applied to the front half of a parabolic-arc body:

$$C_D = 0.0735\tau^2 \tag{89}$$

This result is also plotted in figures 31 and 32 from which it is immediately apparent that these values for C_D are much smaller than either the experimental values or the calculated values indicated by the present theory or by the theory of Oswatitsch and Keune.

APPLICATION TO COMPLETE PARABOLIC-ARC BODY

The calculation of the pressure distribution along the entire length of a complete parabolic-arc body for free-stream Mach number 1 represents an interesting application of the procedures described in the preceding pages. The pressure distribution on the front half of such a body is, of course, the same as discussed at length in the preceding section. Although the procedures can be used to calculate the pressures at points somewhat rearward of the middle of the body, they cannot be used to calculate the pressures along the entire length of the body. The reason is that the velocity reaches a maximum at a point somewhat rearward of the middle, and then decreases continuously along the remainder of the body, thereby violating the condition imposed by equation (46) that $\partial u/\partial x$ or λ_P be positive. The flow, moreover, is subsonic in the vicinity of the rear tip.

The pressure distribution along the entire length of a parabolic-arc body can, nevertheless, be calculated by considering the solution in sections and joining together the various results in the same manner as described for the cone-cylinder. This procedure is quite analogous to the procedures commonly employed in many other theoretical investigations of transonic flows in which the conditions in the subsonic region and a restricted part of the adjacent supersonic region are computed using hodograph or relaxation methods and the solution for the remainder of the supersonic region is computed by the method of characteristics. The following discussion is organized accordingly into three parts concerned, respectively, with transition through sonic velocity on the forebody, supersonic flow on the afterbody, and subsonic flow in the vicinity of the rear tip.

Transition through sonic velocity on the forebody.—A principal feature of the flow on the forward part of a body is the smooth transition from subsonic velocities at the nose to supersonic velocities near the middle of the body. It is amply demonstrated in the preceding section that equation (87) can be used together with equation (3) to calculate the pressure distribution on the front half of a parabolic-arc body of revolution. The same procedures can also be applied to calculate the pressures at points somewhat rearward of the middle. Such calculations have been made for each of the five parabolic-arc bodies of fineness ratio 6, $6\sqrt{2}$, 10, 12, and 14 for which experimental results are available from references 11 and 14. The calculated results are summarized in table IV. The pressure distribution cannot be calculated in this way for points along the entire rear half of the body since, as can be observed by examination of equation (87), a discontinuity in du/dx, and hence the slope of the pressure distribution curve, occurs at the point on the rear of the body where $S''(x)$ vanishes. This equation shows, moreover, that du/dx is zero just upstream and infinite just downstream of this point. The property is symptomatic of the breakdown of the approximation furnished by equation (87) and signals that the use of this relation should be terminated at some point more forward along the length of the body. As a consequence, the results enumerated in table IV for four of the five bodies considered are terminated well forward of the point on the rear of the body where $S''(x)$ vanishes. The results for the fifth body, namely that of fineness ratio 10, are given for all points back to that at which $S''(x)$ vanishes in order to illustrate certain features in the discussion of the supersonic flow on the afterbody. The results for the body of fineness ratio 10 are shown graphically in figure 33.

Supersonic flow on the afterbody.—The calculation of the pressure distribution on the portion of the remainder of the body along which the local velocity is supersonic can be continued by application of equation (42) rather than equation (87). Inasmuch as these two equations are based on somewhat different approximations, the two sets of results cannot be expected to continue analyti-

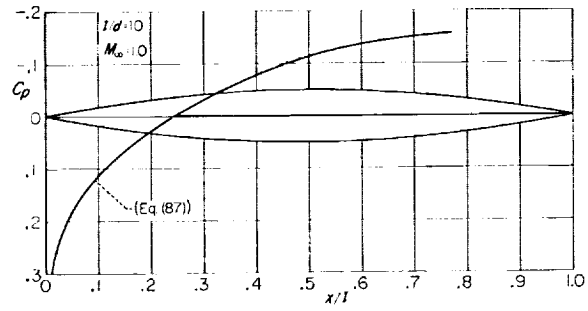

FIGURE 33.—Pressure distribution on the forward part of a parabolic-arc body of revolution at Mach number 1, as indicated by equation (87).

cally into each other at the point at which the two sets of results are joined. The determination of the point at which both C_p and dC_p/dx match can be accomplished in a simple manner once a series of values for u for various stations along the length of the body has been calculated by numerical integration of equation (87). Substitution of these values into equations (42) and (87) leads to two sets of values for du/dx, each of which defines a single curve when plotted as a function of x/l as illustrated in figure 34 for the special case of the

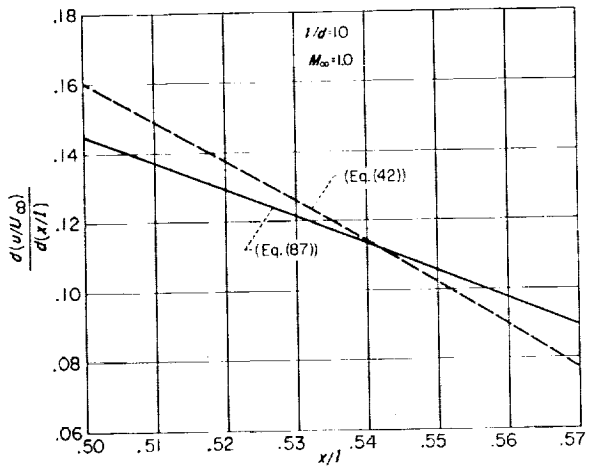

FIGURE 34.—Illustration of graphical technique for selecting the point at which the solution obtained by equation (42) is to be joined to that obtained by equation (87).

parabolic-arc body of fineness ratio 10. As can be seen, the two curves intersect at a certain point, in this case situated at a value for x/l of about 0.542. Since the two values for u and du/dx and hence C_p and dC_p/dx are the same at the point of intersection whether calculated using equations (42) or (87), this point determines the desired location of the point at which the two solutions are to be joined. The procedure has been followed in the present calculations except for the slight simplification introduced by joining the solutions at the nearest point for which values for C_p are given in table IV. This simplification results in a slight mismatching of the values for dC_p/dx, but the effects are small since it follows from the fact that these values for C_p are given for every 2 percent of the body length that the point at which the two solutions are joined is at most only 1 percent of the body length from the point at which the two values for dC_p/dx are exactly the same.

Once the point at which the solutions are to be joined and the associated value for u at this point are determined, the calculation of the pressure distribution on the remainder of the region of supersonic flow on the afterbody can proceed in a straightforward manner by application of any of the many standard methods available for the numerical integration of equation (42). Table V presents the results of such calculations performed by the method of Milne (ref. 9) described in a previous section of this report, for each of the five parabolic-arc bodies of fineness ratio 6, 6 $\sqrt{2}$, 10, 12, and 14. The calculations for the body of fineness ratio 10 were carried out for points situated upstream as well as downstream of the point at 54.2 percent of the body length at which the solutions were joined in order to investigate the degree to which the two approximate solutions overlap. The results are shown graphically in figure 35. It

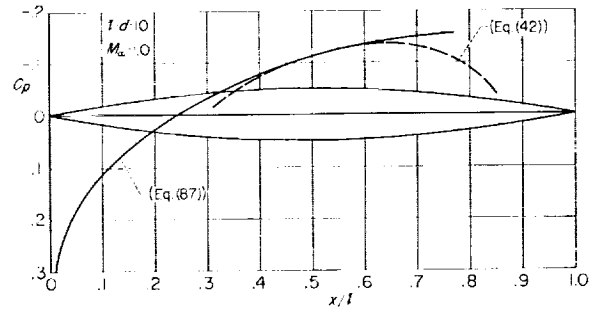

FIGURE 35.—Pressure distribution on a parabolic-arc body of revolution at Mach number 1 as indicated by equation (87) and by equation (42).

can be seen that the two sets of results agree very well over a substantial fraction of the length of the body. They indicate that the selection of the point at which the solutions are joined is not criti-

cal, and that the approximation afforded by use of either equation (42) or (87) is very nearly the same provided the values for neither u nor $\partial u/\partial x$ approach too close to zero.

It can be seen from the results presented above that the region of supersonic flow does not extend all the way to the rear tip of the body. Instead, the flow decelerates and reaches sonic velocity at a point somewhat forward of the rear tip, for example at 86.3 percent of the body length. The procedures described above terminate at this point since u is zero and the quantity $\ln(M_\infty^2-1+ku)$ in equation (42) leads, at $M_\infty=1$, to a logarithmic infinity in du/dx.

The termination of the supersonic region forward of the rear tip of a parabolic-arc body and the great increase in the value of du/dx as the sonic point is approached are similar to the behavior indicated both by the present calculations for Mach numbers greater than unity and by results calculated by the method of characteristics in reference 42. Most of the examples presented are for Mach numbers considerably greater than unity, but one example is included in this reference in which an approximate solution is determined for a parabolic-arc body of fineness ratio 6 in a flow with free-stream Mach number 1. Inasmuch as the method of characteristics is appropriate only in a region where the flow is supersonic, it is necessary in this particular example to introduce some other procedure for the determination of the solution for the region of subsonic flow that exists in the vicinity of the forward part of the body. It is important that a good approximation be used since the results not only determine the values for the subsonic region, but also affect the values calculated by the supersonic region as well. The reason is that the initial values required to start the calculations with the method of characteristics at the upstream boundary of the supersonic region must be provided by the solution for the subsonic region. The particular method used by Oswatitsch was the linearized theory for sonic flow described in references 19 and 20 which follows from the equations given herein upon replacing λ_P in equation (47) by the constant value indicated by equation (50). The results given by Oswatitsch are shown in figure 36 together with the corresponding results indicated by the present calculations for the same body. It can be seen that the two theoretical results are

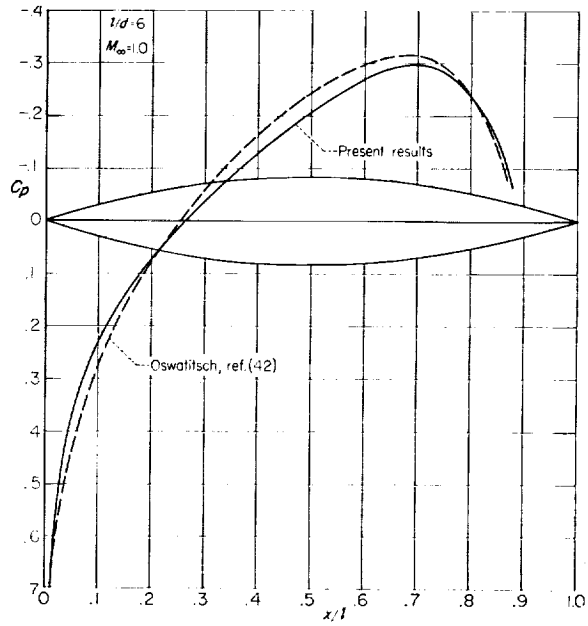

FIGURE 36.—Pressure distribution on a parabolic-arc body of revolution at Mach number 1 as indicated by present theory and by other theoretical results.

in essential agreement with regard to the details of the behavior of the solution in the vicinity of the rear sonic point. The slight discrepancies between the two results over the forward and middle portions of the body are associated with the selection of an appropriate value for λ_P, and would be less if the calculations were repeated using a smaller value for λ_P as advocated by Keune in references 21, 22, and 23 and by Maeder and Thommen in reference 26, as discussed in connection with figures 26 and 27.

Subsonic flow near rear tip.—The results presented in the preceding section clearly indicate that the flow along the surface of a parabolic-arc body of revolution decelerates smoothly and continuously from a maximum supersonic velocity at about two-thirds of the body length to sonic velocity at a point definitely forward of the rear tip. It is known, furthermore, that the flow in the immediate vicinity of the rear tip must be subsonic. Little more has been established previously regarding the nature of the solution in this region. It is evident, however, that two possibilities exist regarding the nature of the transition from supersonic to subsonic flow along the body surface. The transition may be accomplished in a discontinuous manner involving one or more

shock waves that extend to the body surface, as is familiar in two-dimensional flows at Mach numbers somewhat greater than the critical (see ref. 13 for a theoretical analysis of such cases); or it may be accomplished in a continuous manner with a smooth deceleration through sonic velocity, as is indicated by the first- and second-order approximations for supersonic flow past a parabolic-arc body illustrated in figures 11 and 12. It should be understood that shock waves are present in the flow field in both cases, but do not extend to the surface of the body in the case of smooth deceleration through sonic velocity.

It is assumed in the present investigation that the transition from supersonic to subsonic flow along the surface of the body is of a continuous nature and that the results calculated in the preceding section are applicable right up to the sonic point. It is assumed, furthermore, that the results for the subsonic flow along the remainder of the body can be calculated by means of equation (29). This equation is useful for the analysis of subsonic flows, but cannot be applied to supersonic flows because of the presence of the term $\ln(1-M_\infty^2-ku)$. This term leads, moreover, to a logarithmically infinite value of du/dx at the sonic point. It follows from these properties that the two sets of values for the ordinate u and the slope du/dx calculated by use of equations (29) and (42) match when joined at the sonic point. The two sets of results do not overlap, as in the cases described in the preceding section, since the regions of applicability of equations (29) and (42) both terminate abruptly at the sonic point. It should be remarked before proceeding to the discussion of the detailed results of the flow at the rear of the body that the logarithmically infinite deceleration at the sonic point is not altogether unreasonable physically since it may be that such a behavior represents the vanishing influence of a shock wave that exists in the flow field but does not quite extend to the body surface. The experimental investigation of such a detail would be a difficult task because the presence of the boundary layer would probably modify the phenomenon to such an extent that considerable uncertainty would be introduced into the interpretation of the results.

The pressure distribution on the rear of each of the five parabolic-arc bodies considered in the preceding sections has been calculated by use of equation (29) in the manner described above. The results were determined again by application of Milne's method. The only part of the calculation that remains to be described is the detail by which the starting value was determined so that the solution of equation (29) would indicate the same sonic point as the solution of equation (49). It is immediately evident that a special treatment of some sort is necessary because the occurrence of infinite values for du/dx at the sonic point imposes a definite limit on the radius of convergence of a power series expansion of the solution such as employed herein in the previous applications of Milne's method.

The first step in the procedures that were used in the present calculations is to increase the precision with which the sonic point is located. This is desirable because the results for the supersonic region summarized in table V were calculated for intervals of 2 percent of the body length, and thereby leave a possible uncertainty of nearly equal magnitude in the precise location of the sonic point. The desired increase in precision could, of course, be attainable by introducing smaller intervals in the application of Milne's method, but this is rather inconvenient because it is necessary to repeat the starting procedure or to use interpolation formulas every time a smaller interval is introduced. Although such a reduction in interval size can be more readily accomplished with certain alternative numerical methods such as the Runge-Kutta method, the desired increase in detail near the sonic point was achieved in the present calculations by a careful application of the numerical and graphical method of isoclines. This procedure has special merit in the present application since it is not only capable of locating the sonic point when proceeding in the downstream direction from the last point in the supersonic region for which the results have been calculated by Milne's method, but is also very convenient for the continuation of the calculation into the subsonic region for a sufficient distance downstream from the sonic point that the remainder of the calculation can again be accomplished with the numerical method of Milne.

The nature of the singularity at the sonic point, and the details of the manner in which the solutions of equations (29) and (42) match when joined at this point are illustrated in the series of

successive enlargements of the isocline plots shown in figure 37 for the body of fineness ratio 10. It can be seen that there is an extremely small region in which the values for du/dx are large and that the values for du/dx are remarkably similar at short distances upstream and downstream from the sonic point. The method of isoclines was used to calculate the solution for the portion of the body that extends from about 85 to 89 percent of the body length. The results for the remainder of the body were calculated using the method of Milne with intervals of 1 percent of the body length. The numerical results are summarized in table VI, and a plot of the pressure distribution for the complete parabolic-arc body of fineness ratio 10 is shown in figure 38. It can be seen from this plot that the local effects associated with the infinite deceleration at the sonic point are of such small magnitude and extent that they cannot be represented on a plot of this scale. The corresponding results for the rear parts of the other parabolic-arc bodies of fineness ratio 6, $6\sqrt{2}$, 12, and 14 have also been computed in the same way. The results of these calculations are also summarized in table VI.

Summary and discussion of results.—The calculations described in the preceding sections provide a set of values for the pressure coefficient C_p at free-stream Mach number 1 for points spaced at intervals no greater than 2 percent of the body length along the surface of each of five parabolic-arc bodies having fineness ratios of 6, $6\sqrt{2}$, 10, 12, and 14. These results are shown graphically in figure 39 together with the experimental results from references 11 and 14 for parabolic-arc bodies truncated at about 5/6 of the length, as indicated by the dashed lines. It can be seen that the theoretical and experimental results are in essential agreement, and that the principal discrepancies are confined in each case to a small region in the immediate vicinity of the base of the body. This discrepancy is undoubtedly associated, for the bodies of fineness ratio 6 and $6\sqrt{2}$, with the occurrence of a shock wave that must be detached from the corner because the local Mach number is too small. The situation is not so clear for the other bodies, although it would appear from inspection of the data shown in figure 5 that the phenomena involved are not too different from those for the bodies of fineness ratio 6 and $6\sqrt{2}$.

Comparison of the calculated results for the parabolic-arc bodies of different fineness ratio reveals that the values for the pressure coefficient C_p vary with thickness ratio τ in a manner that is very nearly in accordance with the similarity rule given by equation (12). This fact is illustrated in figure 40 in which are plotted the pressure distribution for a parabolic-arc body of fineness ratio 10 as determined by direct calculation, and by use of the similarity rule together with the calculations for the bodies of fineness ratio 6, $6\sqrt{2}$, 12, and 14. The five curves would coalesce to form a single curve if the results of the present calculations were in perfect agreement with the similarity rule. It can be seen that the five curves do not coalesce perfectly onto one line, but the deviations therefrom are small for the range of thickness ratios considered. This result is very similar to that stated previously in the discussion of the cone-cylinder at free-stream Mach number 1, but quite different from the behavior of the present results for Mach numbers in the vicinity of the critical.

Pressure drag.—A value for the pressure drag for each of the five parabolic-arc bodies for which the pressure distribution is given in the preceding section has been calculated by numerical integration of equation (13). The resulting values for $C_D=D/[(\rho_\infty/2)U_\infty^2 S_m]$ at Mach number 1 are

l/d	6	$6\sqrt{2}$	10	12	14
C_D	0. 2485	0. 1288	0. 09343	0. 06534	0. 04675

These values are plotted as a function of τ in figure 41. The corresponding values of C_D/τ^2 are plotted as a function of τ in figure 42 to illustrate that C_D is very nearly proportional to the square of τ as indicated by the similarity rule given by equation (14).

Two additional sets of values for C_D for complete parabolic-arc bodies are also included in figures 41 and 42 for purposes of comparison. Both of these should be considered as more approximate than the present results since they are derived through considerations involving the linearized theory for sonic flow given by Oswatitsch and Keune in references 19 and 20. Straightforward application of that theory to a body that is pointed at the nose and is either pointed or cylindrical at the stern leads to the simple con-

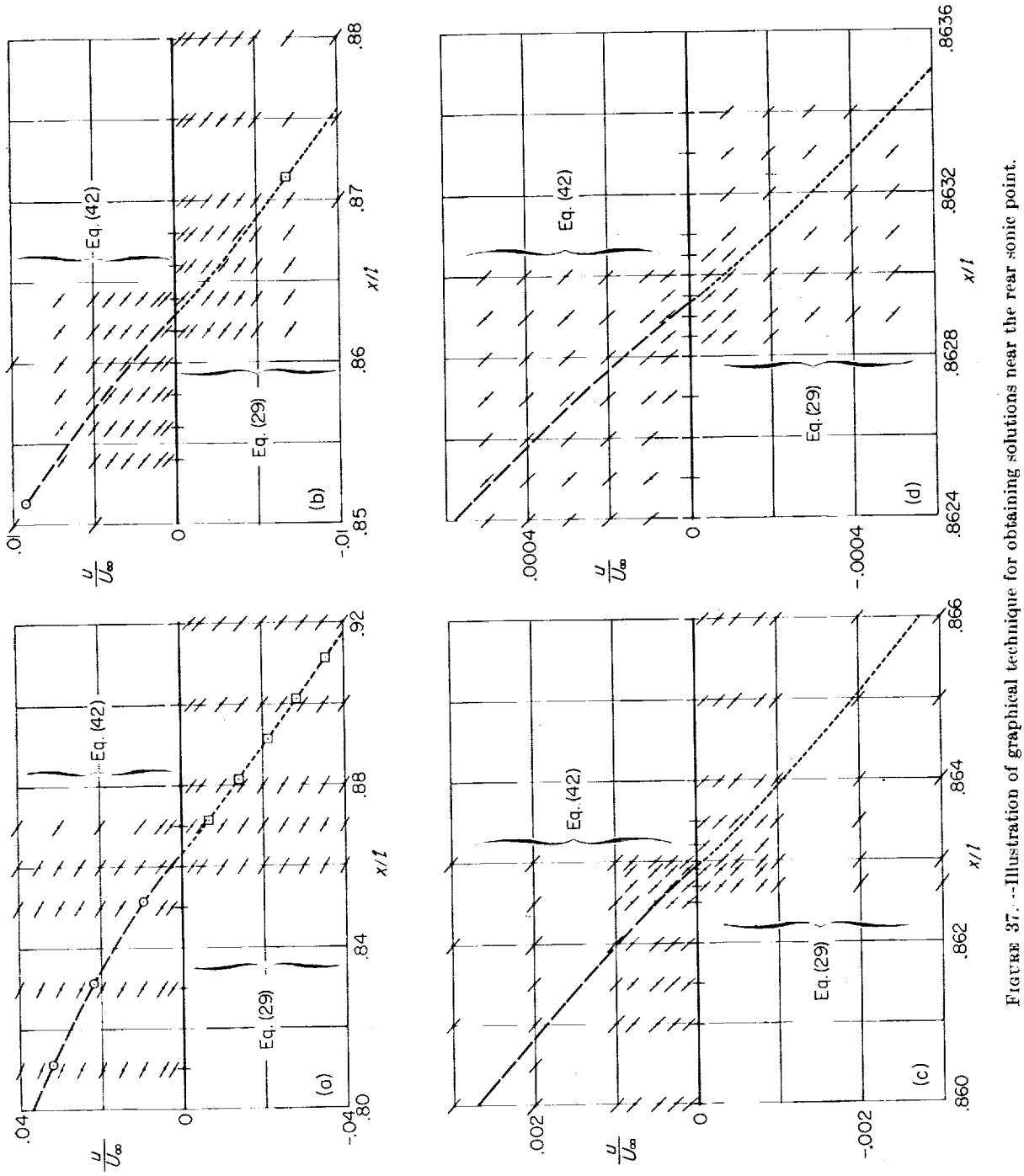

FIGURE 37.—Illustration of graphical technique for obtaining solutions near the rear sonic point.

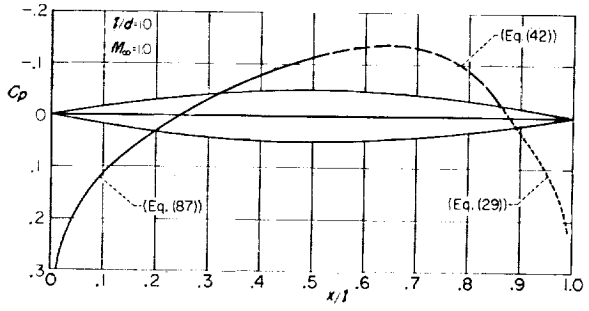

FIGURE 38.—Pressure distribution on a parabolic-arc body of revolution at Mach number 1 as indicated by present theory.

clusion that the value for C_D at free-stream Mach number 1 is exactly half that indicated for supersonic Mach numbers by linearized compressible flow theory. This result holds, independently of the particular value selected for a^2 in equation (50), and leads to the following expression for C_D for a complete parabolic-arc body in a flow with free-stream Mach number 1.

$$C_D=(16/3)\tau^2 \tag{90}$$

Oswatitsch and Keune mention the general conclusion stated above as a purely formal conse-

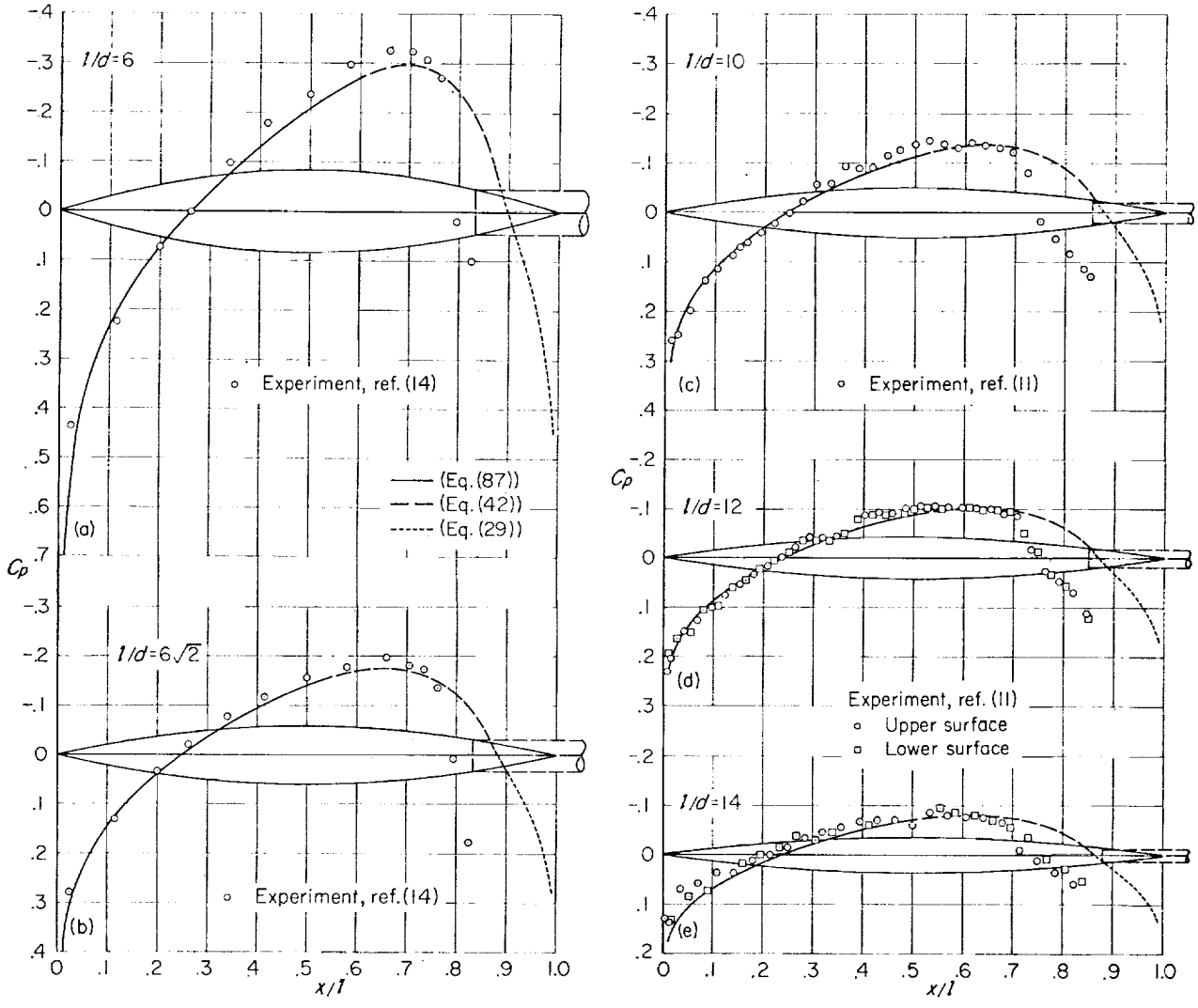

(a) $l/d=6$ (b) $l/d=6\sqrt{2}$ (c) $l/d=10$ (d) $l/d=12$ (e) $l/d=14$

FIGURE 39.—Pressure distributions on parabolic-arc bodies of various fineness ratios at Mach number 1 as indicated by present theory and by experiment.

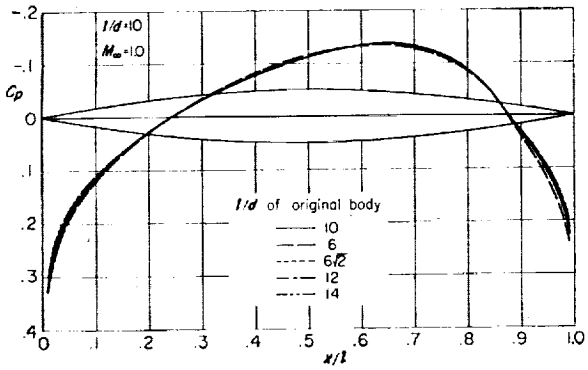

FIGURE 40.—Pressure distribution on a parabolic-arc body of fineness ratio 10, as obtained by direct calculation using the present theory and by use of the similarity rule.

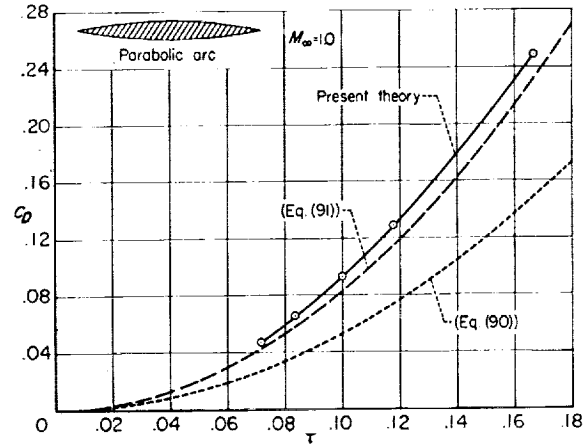

FIGURE 41.—Variation of pressure-drag coefficient with thickness ratio for a parabolic-arc body at Mach number 1, as indicated by present theory and by other theoretical results.

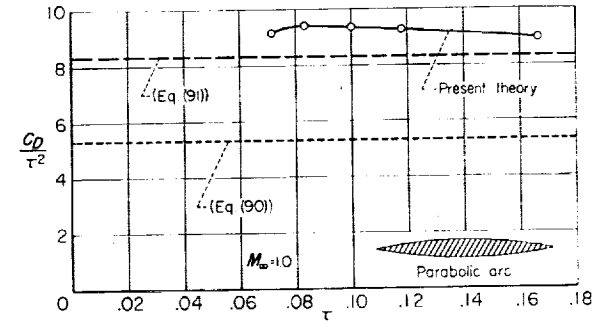

FIGURE 42.—Variation of C_D/τ^2 with thickness ratio for a parabolic-arc body at Mach number 1, as indicated by present theory and by other theoretical results.

quence of the theory, but suggest that approval of the result be withheld for bodies with a pointed stern until a check is made to ascertain whether the assumption of approximately constant acceleration would hold near the rear of such bodies. It is evident from inspection of the theoretical or experimental pressure distributions summarized in figure 5 that this condition is not approached, even in a qualitative sense, since $\partial u/\partial x$ is positive along the forward part of the body, but negative along the rear part. The same property is exhibited by the related results calculated by the method of characteristics that are shown in figure 36, as well as by similar results given in reference 43 for additional examples. It is shown, furthermore (refs. 25 and 26), that even the results calculated by use of the linearized theory for sonic flow display negative values for $\partial u/\partial x$ over the rear of a parabolic-arc body in spite of the fact that $\partial u/\partial x$ is replaced by a positive constant in the derivation. Maeder and Thommen have nevertheless advocated in references 25 and 26, that equation (88) be used to calculate the pressure drag of a parabolic-arc body of revolution in a flow with free-stream Mach number 1. It can be seen that the values for C_D indicated by equation (90) are much smaller than those indicated by the present calculations.

The second additional set of values for C_D included in figures 41 and 42 has been calculated by a simple rule proposed in reference 43. It states that the value for C_D for a body of revolution in a flow with free-stream Mach number 1 is equal to the sum of half the supersonic drag of the forebody plus the full value of the supersonic drag of the afterbody. The values for the supersonic drag are to be calculated in both instances by means of the linearized theory of compressible flow, and the line of demarcation between the forebody and afterbody is taken to be the station of maximum diameter. This rule is not established by a deductive process, but is proposed as a generalization, approximate in nature, of observations of specific results calculated for three different bodies. Application of this rule to the specific case of a parabolic-arc body of revolution leads to the following expression for C_D:

$$C_D=(25/3)\tau^2 \tag{91}$$

It can be seen upon inspection of figures 41 and 42 that the values for C_D indicated by equation (91) are somewhat smaller than those indicated by the more elaborate calculations of the present investigation. It should be pointed out that this comparison does not fully represent an additional test of the rule, however, since the parabolic-arc body considered here is one of the three cases used by Keune and Oswatitsch in the establishment of the rule. It appears to the present authors, in spite of the moderate success of this rule in the three cases considered to date, that the final decision regarding the general applicability of this rule should be withheld until either similar comparisons are made for a much larger class of bodies or a better understanding of the fundamental basis for the rule is discovered.

Comparison with results for subsonic and supersonic flow.—The remainder of this report is concerned with a discussion of the relation between the results calculated for a parabolic-arc body of revolution for Mach number 1 and those calculated for other Mach numbers. The results for both pressure distribution and drag will be considered, but attention is confined to the case of a body of fineness ratio 10. Although all of the results required to make similar comparisons for bodies of other fineness ratios have not been determined, it is presumed that the relations among the results for various Mach numbers will remain qualitatively the same. Figure 43 shows a comparison of the pressure distribution calculated for Mach number 1 and those calculated for the upper and lower critical Mach numbers. It can be seen that the results for Mach number 1 are qualitatively similar to those for the lower critical Mach number along the forward part of the body, and qualitatively similar to those for the upper critical Mach number along the rear part of the body. The results for various Mach numbers are displayed in a second manner in figure 44 which shows the variation of the pressure coefficient with Mach number for several selected points along the surface of the body. Two additional curves are included on this plot to show the variation with Mach number of the pressure coefficients corresponding to the occurrence of sonic velocity $\left(\text{i.e., } u/U_\infty=\frac{1-M_\infty^2}{M_\infty^2(\gamma+1)}\right)$ at the midpoint and at the nose of the body. It can be seen that the line segments for the surface pressures could be connected by reasonably smooth curves for points along the front part of the body, but not for points along the rear part. This situation is similar to that encountered in the analysis of transonic flow around airfoils (see, e.g., ref. 13) and it is known that the necessary adjustment is achieved, in an inviscid flow, in a discontinuous manner involving a shock wave that extends to the surface of the body. The presence of the boundary layer in a viscous flow softens the discontinuous change indicated by the inviscid theory, but the general behavior is otherwise much the same. The actual existence of such effects for the special case of a parabolic-arc body of revolution is clearly demonstrated experimentally by the data reported in references 11 and 14.

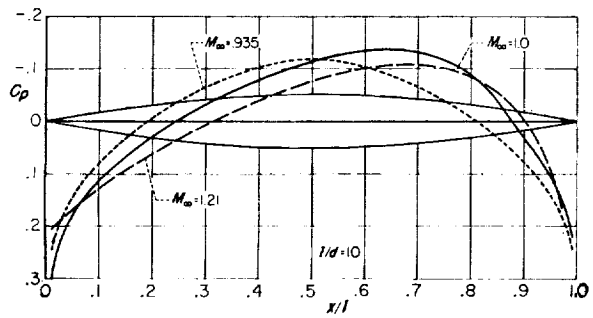

FIGURE 43.—Pressure distributions on a parabolic-arc body of revolution at the upper and lower critical Mach numbers and at Mach number 1.

The variation with Mach number of the pressure drag coefficient for a parabolic-arc body of fineness ratio 10 is shown in figure 45. The small circles represent the values for the drag coefficient of the complete body as indicated by the present theory. The numerical values are

M_∞	1.21	1.22	1.23	1.25	1.30	1.40
C_D	0.1153	0.1149	0.1146	0.1142	0.1133	0.1122

The dashed line of figure 45 that is adjacent to the small circles represents the values calculated by use of the following expression that results from both first- and second-order supersonic slender-body theory.

$$C_D=(32/3)\tau^2 \qquad (92)$$

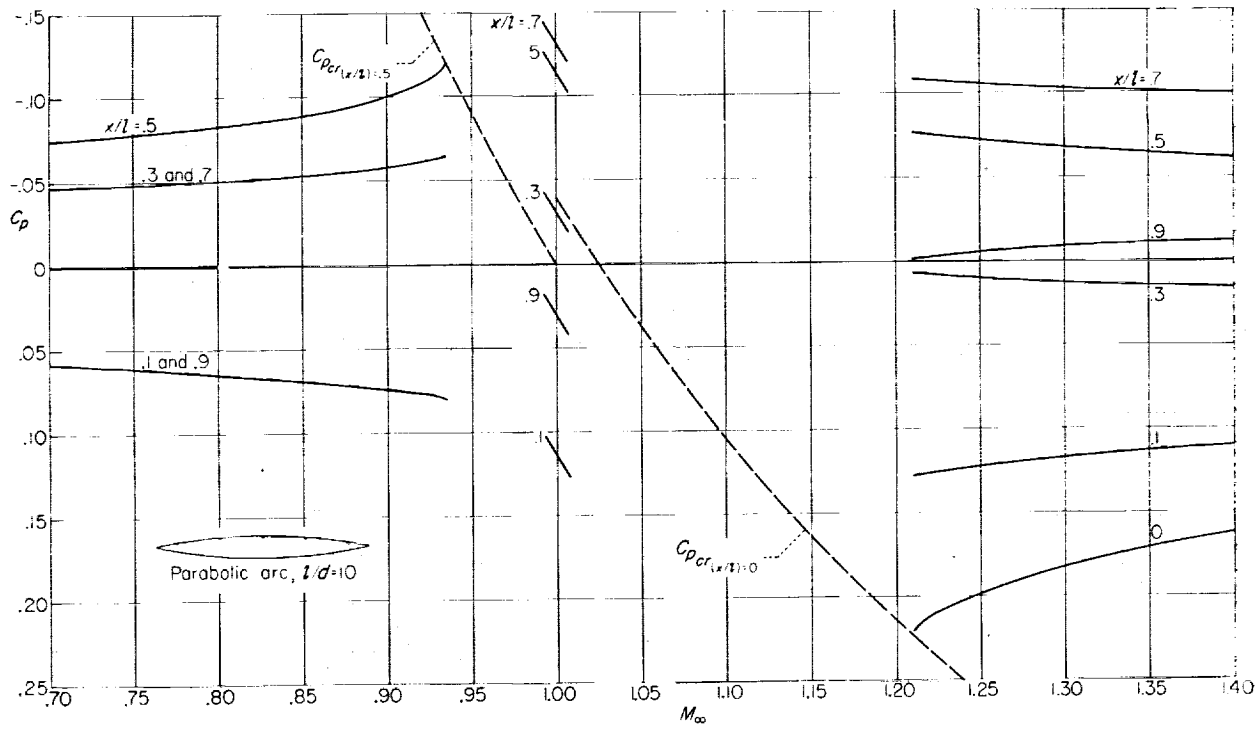

FIGURE 44.—Variation of pressure coefficient with Mach number at various stations along the length of a parabolic-arc body of fineness ratio 10, as indicated by present theory.

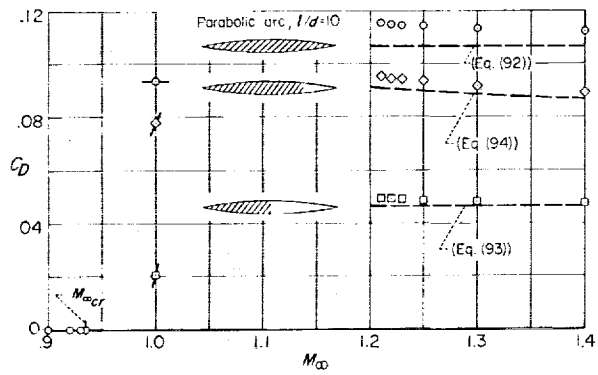

FIGURE 45.—Variation of the pressure-drag coefficient with Mach number for a parabolic-arc body of fineness ratio 10, as indicated by present theory and by other theoretical results.

It can be seen that the values indicated by the present theory are slightly greater than those indicated by equation (92).

A second set of calculated results, indicated by small squares, is included in figure 45 to represent the contribution to the drag that arises from the forces on the front half of the complete body. The numerical values are

M_∞	1.21	1.22	1.23	1.25	1.30	1.40
C_D	0.04943	0.04922	0.04904	0.04878	0.04832	0.04783

The adjacent dashed line in this figure represents the values calculated by means of the following relation provided by first-order slender-body theory

$$C_D=(14/3)\tau^2 \tag{93}$$

This result shows once again that only about half of the drag rise of a half body occurs at Mach numbers less than unity; whereas the previous result shows that nearly all of the drag rise of a complete parabolic-arc body occurs in the same range of Mach numbers.

A third set of calculated results, indicated by small diamonds, is also included in this figure to represent the contribution to the drag coefficient that arises from the forces on the front three-fourths of a parabolic-arc body. The numerical results are

M_∞	1. 21	1. 22	1. 23	1. 25	1. 30	1. 40
C_D	0. 09508	0. 09455	0. 09406	0. 09320	0. 09147	0. 08898

The adjacent dashed line represents the values indicated by the first-order slender-body theory which have been calculated with the aid of the following expression:

$$C_D=\frac{9}{2}\tau^2\left(1-\frac{1}{4}\ln\frac{\sqrt{M_\infty^2-1}\,\tau}{4}\right) \qquad (94)$$

Although it is clear from this expression that the drag is not independent of the free-stream Mach number, as in the case of the complete body and also the half body, it can be seen from figure 45 that the effect is very small.

CONCLUDING REMARKS

It has been amply demonstrated in the preceding pages that the approximate method for the solution of the nonlinear equations of transonic flow theory described in reference 4 can also be applied to axisymmetric flows. As in the case of two-dimensional flows, the results are shown, by comparison with experimental and other theoretical results, to be of almost surprising accuracy considering both the small perturbation and slender-body approximations inherent in the fundamental equations of the theory and the novel nature of the procedures used to obtain a simple approximate solution of these equations.

The results of this investigation are of interest not only because of the frequent use of a body of revolution in aeronautical design, but also because of the central role of the body of revolution in applications of the transonic area and equivalence rules. The best known of these rules is probably that for wave drag discovered experimentally by Whitcomb and announced in reference 1; but recent developments (ref. 3 for a résumé) enable the ready calculation of not only the drag, but also the pressure distribution and other aerodynamic properties of slender wings, bodies, wing-body combinations, etc., provided that the pressure distribution is known for the equivalent nonlifting body of revolution having the same longitudinal distribution of cross-section area. Thus the utility of these rules is greatly increased by the availability of the methods described in this paper for the calculation of the pressure distribution on the equivalent body. Although no examples of such an application are given in the present paper, the results for a simple case involving a thin elliptic cone that resembles a delta wing are given in reference 5.

While the development of a reliable theory for the prediction of the aerodynamic properties of bodies of revolution in transonic flow is a subject primarily of interest to aerodynamicists, it would seem to the authors that the method of approximation and some of the results for specific applications might also be of interest to mathematicians concerned with the solution of nonlinear partial differential equations. It should be remarked in this connection, that the method of approximation is only described briefly and from a simple heuristic point of view, in the present paper. Those interested in a further discussion of the method from a number of alternative points of view are referred to the appendix of reference 4. The latter discussion is for two-dimensional flow, but the necessary extension to axisymmetric flow can be accomplished directly without the introduction of any new concepts. While it is hoped that the discussion of the method of approximation presented in reference 4 is illuminating and helps to make the procedure more plausible than does the brief account presented herein, the underlying reason for the success of the method remains only incompletely understood from a mathematical point of view. On the other hand, the demonstrated ability of the method to nearly reproduce the results of available, but far more complicated, theories and of experiments should be sufficient to warrant further mathematical study.

AMES RESEARCH CENTER
NATIONAL AERONAUTICS AND SPACE ADMINISTRATION
MOFFETT FIELD, CALIF., *Nov. 26, 1958*

REFERENCES

1. Whitcomb, Richard T.: A Study of the Zero-Lift Drag-Rise Charateristics of Wing-Body Combinations Near the Speed of Sound. NACA Rep. 1273, 1956. (Supersedes NACA RM L52H08)
2. Oswatitsch, Klaus, and Keune, Friedrich: Ein Äquivalensatz für nichtangestellte Flügel kleiner Spannweitte in schallnaher Strömung. Zeitschrift für Flugwissenschaften, 3 Jahrgang, Heft 2, Feb. 1955, S. 29–46.

3. Heaslet, Max. A., and Spreiter, John R.: Three-Dimensional Transonic Flow Theory Applied to Slender Wings and Bodies. NACA Rep. 1318, 1957. (Supersedes NACA TN 3717)
4. Spreiter, John R., and Alksne, Alberta Y.: Thin Airfoil Theory Based on Approximate Solution of the Transonic Flow Equation. NACA TN 3970, 1957.
5. Spreiter, John R., and Alksne, Alberta Y.: Aerodynamics of Wings and Bodies at Mach Number One. Proc. Third U.S. National Congress of Applied Mechanics, ASME, 1958, pp. 827–835.
6. Oswatitsch, Klaus: Gas Dynamics (English Version). Academic Press, Inc., 1956.
7. Oswatitsch, Klaus, and Berndt, Sune B.: Aerodynamic Similarity at Axisymmetric Transonic Flow Around Slender Bodies. KTH-Aero TN 15, Roy. Inst. Tech., Division of Aeronautics, Stockholm, Sweden, 1950.
8. Ward, G. N.: Linearized Theory of Steady High-Speed Flow. Cambridge Univ. Press, 1955.
9. Milne, William Edmund: Numerical Calculus. Princeton Univ. Press, 1949.
10. Van Dyke, Milton D.: Second-Order Slender-Body Theory—Axisymmetric Flow. NACA TN 4281, 1958.
11. Taylor, Robert A., and McDevitt, John B.: Pressure Distributions at Transonic Speeds for Parabolic-Arc Bodies of Revolution Having Fineness Ratios of 10, 12, and 14. NACA TN 4234, 1958.
12. Spreiter, John R., and Alksne, Alberta: Theoretical Prediction of Pressure Distributions on Nonlifting Airfoils at High Subsonic Speeds. NACA Rep. 1217, 1955. (Supersedes NACA TN 3096)
13. Spreiter, John R., Alksne, Alberta Y., and Hyett, B. Jeanne: Theoretical Pressure Distributions for Several Related Nonlifting Airfoils at High Subsonic Speeds. NACA TN 4148, 1958.
14. Drougge, Georg: Some Measurements on Bodies of Revolution at Transonic Speeds. Ninth International Congress of Applied Mechanics, Univ. of Brussels, 1957, pp. 70–77.
15. Oswatitsch, K., and Sjödin, L.: Kegelige Überschallströmung in Schallnähe. Österr. Ing.-Archiv., vol. 8, no. 4, 1954, pp. 284–292.
16. Shen, Yung-chung: Similarity Solution for Transonic Flow Past a Cone. OSR TN 56–121, Mar. 1956.
17. Taylor, G. I., and Maccoll, J. W.: The Air Pressure on a Cone Moving at High Speeds. Proc. Roy. Soc. of London, ser. A., vol. 139, 1933, p. 278.
18. Staff of the Computing Section (under the direction of Zdenek Kopal): Tables of Supersonic Flow Around Cones. Tech. Rep. no. 1, Center of Analysis, Mass. Inst. of Tech., Cambridge, Mass., 1947.
19. Oswatitsch, K., and Keune, F.: The Flow Around Bodies of Revolution at Mach Number 1. Proc. Conf. on High-Speed Aeronautics, Polytechnic Institute of Brooklyn, Brooklyn, N.Y., June 20–22, 1955, pp. 113–131.
20. Keune, F.: Bericht über eine Näherungstheorie der Strömung um Rotationskörper ohne Anstellung bei Machzahl Eins. DVL Bericht Nr. 3 Westdeutscher Verlag, Köln und Opladen, 1955.
21. Keune, F.: Über den Kompressibilitätseinfluss bei und nahr Machzahl Eins für Körper kleiner Streckung und schlanke Rotationskörper. Zs. f. Flugwiss. 4 Jahr., Heft 1/2, Jan/Feb. 1956, pp. 47–53.
22. Keune, Friedrich: Über eine Näherungstheorie zur Berechnung der auftriebslosen Strömung um Schlanke Körper bei Schallanströmung. Jahrbuch der Wissenschaft lichen Gesellschaft für Luftfahrt E.V. (WGL), 1955, pp. 176–186.
23. Keune, Friedrich: A Contribution to an Approximate Calculation of the Flow on Pointed Halfbodies of Revolution in the Lower Transonic Range. Ninth International Congress of Applied Mechanics, Univ. of Brussels, 1957, pp. 25–33.
24. Maeder, P. F., and Thommen, H. U.: Some Results of Linearized Transonic Flow About Slender Airfoils and Bodies of Revolution. Jour. Aero. Sci., vol. 23, no. 2, Feb. 1956, pp. 187–188.
25. Maeder, Paul F.: Solutions to the Linearized Equation for Transonic Flows and Their Comparison with Experiment. Ninth International Congress of Applied Mechanics, Univ. of Brussels, 1957, pp. 15–24.
26. Maeder, P. F., and Thommen, H. U.: Linearized Transonic Flow About Slender Bodies of Revolution at Zero Incidence. Technical Rep. WT–25, Brown University, July 1957.
27. Miles, John W.: On Linearized Transonic Flow Theory for Slender Bodies. Jour. Aero. Sci., vol. 23, no. 7, July 1956, pp. 704–705.
28. Laitone, E. V.: Experimental Measurement of Incompressible Flow Along a Cylinder with a Conical Nose. Jour. Appl. Phys., vol. 22, no. 1, Jan. 1951, pp. 63–64.
29. Laitone, E. V.: The Subsonic Flow About a Body of Revolution. Quart. Appl. Math., vol. 5, 1947, pp. 227–231.
30. Laitone, E. V.: The Linearized Subsonic and Supersonic Flow About Inclined Slender Bodies of Revolution. Jour. Aero. Sci., vol. 14, 1947, pp. 631–642.
31. Fraenkel, L. E.: Incompressible Flow Past Quasi-Cylindrical Bodies and Some Associated Problems. Quart. Jour. Mech. and Appl. Math., vol. XI, pt. 2, May 1958, pp. 212–222.
32. Page, William A.: Experimental Study of the Equivalence of Transonic Flow About Slender Cone-Cylinders of Circular and Elliptic Cross Section. NACA TN 4233, 1958.
33. Yoshihara, Hideo: On the Flow Over a Cone-Cylinder at Mach Number One. WADC Tech. Rep. 52–295, Nov. 1952.
34. Kusukawa, Ken-Ichi: On the Compressible Flow Over a Slender Body of Revolution with a Flat Base Placed in an Unbounded Fluid and in a Choked Wind Tunnel. Jour. Phys. Soc. Japan, vol. 12, no. 9, Sept. 1957, pp. 1042–1048.

35. Kusukawa, Ken-Ichi: On the Transonic Flow of a Compressible Fluid Past an Axisymmetric Slender Body at Zero Incidence. Jour. Phys. Soc. Japan, vol. 12, no. 4, April 1957, pp. 401–410.

36. Kusukawa, Ken-Ichi: On the Two-Dimensional Compressible Flow Over a Thin Symmetric Obstacle with Sharp Shoulders Placed in an Unbounded Fluid and in a Choked Wind Tunnel. Jour. Phys. Soc. Japan, vol. 12, no. 9, Sept. 1957, pp. 1031–1041.

37. Helliwell, J. B., and Mackie, A. G.: Two Dimensional Subsonic and Sonic Flow Past Thin Bodies. Jour. Fluid Mech., vol. 3, pt. 1, Oct. 1957, pp. 93–109.

38. Guderley, K. G.: Theorie schallnaher Strömungen. Springer-Verlag, 1957.

39. Miles, John W.: On the Sonic Drag of a Slender Body. Jour. Aero. Sci., vol. 23, no. 2, Feb. 1956, pp. 146–154.

40. Guderley, G., and Yoshihara, H.: An Axial-Symmetric Transonic Flow Pattern. Quart. Appl. Math., vol. 4, no. 4, April 1951, pp. 333–339.

41. Guderley, G., and Yoshihara, H.: Axial-Symmetric Transonic Flow Patterns. AF Tech. Rep. 5797, USAF AMC, Dayton, Ohio, 1949.

42. Oswatitsch, K.: Die Berechnung wirbelfreier achsensymmetrischer Überschallfelder. Österr. Ing.-Archiv., vol. 10, no. 4, 1956, pp. 359–382.

43. Keune, F., and Oswatitsch, K.: On the Influence of the Geometry of Slender Bodies of Revolution and Delta Wings on Their Drag and Pressure Distribution at Transonic Speeds. KTH–Aero TN 42, 1956.

TABLE I.—RESULTS OF CALCULATIONS FOR PARABOLIC-ARC BODY OF FINENESS RATIO 10 AT SUBCRITICAL MACH NUMBERS (PURELY SUBSONIC FLOWS)

x/l	(a) $M_\infty = 0.70$			(b) $M_\infty = 0.80$			(c) $M_\infty = 0.85$			(d) $M_\infty = 0.90$		
	u/U_∞	$\Delta/29$	C_p	u/U_∞	$\Delta/29$	C_p	u/U_∞	$\Delta/29$	C_p	u/U_∞	$\Delta/29$	C_p
0.0113249	−0.125623	−0.0001566	0.213038	−0.130509	−0.0001565	0.222809	−0.133829	−0.0001565	0.229450	−0.138118	−0.0001565	0.238027
.0313249	−.093099	−.0000166	.151054	−.097572	−.0000165	.159998	−.100641	−.0000165	.166136	−.104643	−.0000165	.174141
.0513249	−.074023	−.0000041	.115836	−.078039	−.0000041	.123868	−.080822	−.0000041	.129434	−.084490	−.0000041	.136770
.0713249	−.059443	−.0000014	.089485	−.062978	−.0000014	.096554	−.065451	−.0000014	.101500	−.068746	−.0000014	.108091
.0913249	−.047376	−.0000006	.068030	−.050412	−.0000006	.074102	−.052557	−.0000006	.078392	−.055449	−.0000006	.084175
.1113249	−.037000	−.0000003	.049830	−.039528	−.0000003	.054884	−.041331	−.0000003	.058490	−.043790	−.0000003	.063409
.1313249	−.027886	−.0000002	.034024	−.029900	−.0000002	.038052	−.031350	−.0000002	.040953	−.033353	−.0000002	.044959
.1513249	−.019773	−.0000001	.020095	−.021274	−.0000001	.023096	−.022365	−.0000001	.025278	−.023891	−.0000001	.028330
.1713249	−.012495	−.0000001	.007705	−.013486	−.0000001	.009688	−.014213	−.0000001	.011142	−.015244	−.0000001	.013204
.1913249	−.005932		−.003380	−.006422		−.002401	−.006785		−.001676	−.007305		−.000634
.2113249	0		−.013333	0		−.013333	0		−.013333	0		−.013333
.2313249	.005366		−.022282	.005841		−.023231	.006198		−.023947	.006726		−.025002
.2513249	.010216	.0000000	−.030327	.011147	.0000000	−.032188	.011854	.0000000	−.033602	.012911	.0000000	−.035717
.2713249	.014589	.0000000	−.037546	.015954	.0000000	−.040274	.016999	.0000000	−.042365	.018584	.0000000	−.045534
.2913249	.018517	.0000000	−.044001	.020290	.0000000	−.047548	.021659	.0000000	−.050286	.023763	.0000000	−.054493
.3113249	.022023	.0000000	−.049743	.024179	.0000000	−.054053	.025854	.0000000	−.057404	.028462	.0000000	−.062620
.3313249	.025130	.0000000	−.054813	.027637	.0000000	−.059825	.029598	.0000000	−.063749	.032690	.0000000	−.069932
.3513249	.027854	.0000000	−.059245	.030679	.0000000	−.064894	.032903	.0000000	−.069343	.036450	.0000000	−.076437
.3713249	.030209	.0000000	−.063066	.033317	.0000000	−.069283	.035777	.0000000	−.074204	.039745	.0000000	−.082139
.3913249	.032205	.0000000	−.066299	.035560	.0000000	−.073009	.038228	.0000000	−.078345	.042573	.0000000	−.087035
.4113249	.033852	.0000000	−.068963	.037415	.0000000	−.076087	.040259	.0000000	−.081776	.044931	.0000000	−.091121
.4313249	.035158	.0000000	−.071070	.038887	.0000000	−.078530	.041875	.0000000	−.084505	.046818	.0000000	−.094390
.4513249	.036127	.0000000	−.072633	.039982	.0000000	−.080344	.043078	.0000000	−.086536	.048228	.0000000	−.096836
.4713249	.036764	.0000000	−.073659	.040703	.0000000	−.081537	.043871	.0000000	−.087873	.049160	.0000000	−.098452
.4913249	.037071	.0000000	−.074153	.041050	.0000000	−.082112	.044253	.0000000	−.088518	.049611	.0000000	−.099233
.5113249	.037049	.0000000	−.074118	.041025	.0000000	−.082071	.044226	.0000000	−.088472	.049579	.0000000	−.099178
.5313249	.036698	.0000000	−.073554	.040629	.0000000	−.081414	.043789	.0000000	−.087736	.049064	.0000000	−.098286
.5513249	.036018	.0000000	−.072457	.039859	.0000000	−.080139	.042943	.0000000	−.086307	.048069	−.0000000	−.096559

TABLE I.—RESULTS OF CALCULATIONS FOR PARABOLIC-ARC BODY OF FINENESS RATIO 10 AT SUBCRITICAL MACH NUMBERS (PURELY SUBSONIC FLOWS)—Concluded

x/l	(e) $M_\infty = 0.92$			(f) $M_\infty = 0.93$			(g) $M_\infty = 0.934$			(h) $M_\infty = 0.935$		
	u/U_∞	$\Delta/29$	C_p	u/U_∞	$\Delta/29$	C_p	u/U_∞	$\Delta/29$	C_p	u/U_∞	$\Delta/29$	C_p
0.0113249	−0.140235	−0.0001565	0.242261	−0.141412	−0.0001565	0.244616	−0.141909	−0.0001565	0.245610	−0.142036	−0.0001565	0.245863
.0313249	−.106637	−.0000165	.178129	−.107751	−.0000165	.180357	−.108222	−.0000165	.181300	−.108344	−.0000165	.181543
.0513249	−.086335	−.0000041	.140461	−.087372	−.0000041	.142534	−.087812	−.0000041	.143414	−.087924	−.0000041	.143639
.0713249	−.070422	−.0000014	.111443	−.071370	−.0000014	.113337	−.071773	−.0000014	.114144	−.071876	−.0000014	.114351
.0913249	−.056936	−.0000006	.087150	−.057782	−.0000006	.088843	−.058144	−.0000006	.089566	−.058237	−.0000006	.089752
.1113249	−.045071	−.0000003	.065972	−.045806	−.0000003	.067440	−.046121	−.0000003	.068070	−.046202	−.0000003	.068233
.1313249	−.034411	−.0000002	.047074	−.035022	−.0000002	.048297	−.035285	−.0000002	.048824	−.035353	−.0000002	.048959
.1513249	−.024708	−.0000001	.029963	−.025184	−.0000001	.030916	−.025390	−.0000001	.031329	−.025444	−.0000001	.031436
.1713249	−.015804	−.0000001	.014324	−.016134	−.0000001	.014984	−.016278	−.0000001	.015271	−.016315	−.0000001	.015346
.1913249	−.007593		−.000059	−.007764		.000284	−.007839		.000434	−.007859		.000473
.2113249	0		−.013333	0		−.013333	0		−.013333	0		−.013333
.2313249	.007027		−.025605	.007212		−.025974	.007294		−.026138	.007316		−.026181
.2513249	.013527	.0000000	−.036948	.013909	.0000000	−.037713	.014082	.0000002	−.038058	.014127	.0000000	−.038148
.2713249	.019525	.0000000	−.047416	.020119	.0000000	−.048605	.020390	.0000000	−.049147	.020461	.0000000	−.049290
.2913249	.025037	.0000000	−.057042	.025858	.0000000	−.058683	.026237	.0000000	−.059441	.026338	.0000000	−.059642
.3113249	.030075	.0000000	−.065847	.031135	.0000000	−.067967	.031634	.0000000	−.068963	.031767	.0000000	−.069229
.3313249	.034643	.0000000	−.073838	.035956	.0000000	−.076463	.036585	.0000000	−.077721	.036754	.0000000	−.078061
.3513249	.038739	.0000000	−.081014	.040315	.0000000	−.084167	.041088	.0000000	−.085713	.041299	.0000000	−.086135
.3713249	.042358	.0000000	−.087364	.044206	.0000000	−.091061	.045137	−.0000000	−.092923	.045395	−.0000000	−.093440
.3913249	.045491	.0000000	−.092871	.047613	−.0000000	−.097116	.048718	−.0000000	−.099325	.049031	−.0000000	−.099951
.4113249	.048126	.0000000	−.097511	.050517	−.0000000	−.102292	.051809	−.0000000	−.104875	.052186	−.0000000	−.105630
.4313249	.050251	.0000000	−.101256	.052890	.0000000	−.106536	.054380	−.0000000	−.109515	.054833	−.0000000	−.110421
.4513249	.051850	.0000000	−.104080	.054703	.0000000	−.109786	.056390	−.0000000	−.113159	.056933	−.0000001	−.114245
.4713249	.052913	.0000000	−.105957	.055922	.0000000	−.111977	.057779	−.0000000	−.115690	.058424	−.0000001	−.116979
.4913249	.053428	.0000000	−.106868	.056519	.0000001	−.113051	.058478	.0000001	−.116968	.059206	−.0000003	−.118424
.5113249	.053392	.0000000	−.106804	.056477	.0000001	−.112974	.058428	.0000005	−.116876	.059153	.0000010	−.118326
.5313249	.052803	.0000000	−.105764	.055796	.0000000	−.111749	.057633	.0000004	−.115424	.058261	.0000021	−.116680
.5513249	.051669	−.0000000	−.103760	.054548	−.0000019	−.109518	.056158	−.0000005	−.112737	.056692	−.0000024	−.113805

TABLE II.—RESULTS OF CALCULATIONS FOR PARABOLIC-ARC BODY OF FINENESS RATIO 6 AT SUBCRITICAL MACH NUMBERS (PURELY SUBSONIC FLOWS)

x/l	(a) $M_\infty=0.70$			(b) $M_\infty=0.80$			(c) $M_\infty=0.85$			(d) $M_\infty=0.87$			(e) $M_\infty=0.88$		
	u/U_∞	$\Delta/2g$	C_p	u/U_∞	$\Delta/2g$	C_p	u/U_∞	$\Delta/2g$	C_p	u/U_∞	$\Delta/2g$	C_p	u/U_∞	$\Delta/2g$	C_p
0.0113249	−0.290529	−0.0004347	0.474924	−0.300432	−0.0004346	0.494729	−0.306731	−0.0004345	0.507326	−0.309591	−0.0004346	0.513046	−0.311111	−0.0004345	0.516087
.0313249	−.208125	−.0000459	.318625	−.217623	−.0000459	.337621	−.223728	−.0000459	.349831	−.226590	−.0000484	.355556	−.228001	−.0000458	.358377
.0513249	−.162470	−.0000113	.235470	−.171350	−.0000113	.253229	−.177128	−.0000113	.264786	−.179787	−.0000113	.270104	−.181207	−.0000113	.272944
.0713249	−.128800	−.0000039	.175928	−.136901	−.0000039	.192129	−.142246	−.0000039	.202820	−.144727	−.0000039	.207781	−.146057	−.0000039	.210441
.0913249	−.101648	−.0000017	.129066	−.108839	−.0000017	.143449	−.113656	−.0000017	.153083	−.115913	−.0000017	.157597	−.117129	−.0000017	.160030
.1113249	−.078766	−.0000008	.090390	−.084939	−.0000008	.102737	−.089141	−.0000008	.111140	−.091131	−.0000008	.115120	−.092208	−.0000008	.117276
.1313249	−.058984	−.0000005	.057559	−.064047	−.0000005	.067684	−.067552	−.0000004	.074694	−.069231	−.0000004	.078052	−.070146	−.0000004	.079883
.1513249	−.041605	−.0000003	.029176	−.045480	−.0000003	.036927	−.048211	−.0000003	.042389	−.049537	−.0000003	.045040	−.050265	−.0000003	.046496
.1713249	−.026174	−.0000002	.004337	−.028800	−.0000002	.009589	−.030686	−.0000002	.013360	−.031614	−.0000002	.015217	−.032128	−.0000002	.016244
.1913249	−.012381		−.017585	−.013710		−.014927	−.014684		−.012980	−.015170		−.012006	−.015442		−.011463
.2113249	0		−.037037	0		−.037037	0		−.037037	0		−.037037	0		−.037037
.2313249	.011136		−.054354	.012482		−.057048	.013510		−.059103	.014043		−.060168	.014347		−.060776
.2513249	.021153	.0000001	−.069790	.023849	.0000001	−.075182	.025951	.0000001	−.079385	.027061	.0000001	−.081606	.027704	.0000001	−.082893
.2713249	.030151	.0000001	−.083543	.034182	.0000001	−.091605	.037394	.0000001	−.098029	.039128	.0000001	−.101498	.040149	.0000001	−.103539
.2913249	.038207	.0000001	−.095767	.043543	.0000001	−.106440	.047889	.0000001	−.115132	.050292	.0000001	−.119938	.051733	.0000001	−.122819
.3113249	.045383	.0000001	−.106588	.051978	.0000001	−.119777	.057467	.0000001	−.130756	.060581	.0000000	−.136984	.062487	.0000000	−.140796
.3313249	.051729	.0000000	−.116103	.059518	.0000000	−.131680	.066144	.0000000	−.144932	.070005	.0000000	−.152655	.072429	.0000000	−.157502
.3513249	.057285	.0000000	−.124393	.066186	.0000000	−.142197	.073921	.0000000	−.157665	.078558	.0000000	−.166941	.081556	.0000000	−.172936
.3713249	.062081	.0000000	−.131522	.071999	.0000000	−.151358	.080791	.0000000	−.168940	.086221	.0000000	−.179800	.089854	−.0000000	−.187066
.3913249	.066145	.0000000	−.137540	.076967	.0000000	−.159182	.086737	.0000000	−.178724	.092956	.0000000	−.191162	.097290	−.0000000	−.199828
.4113249	.069497	.0000000	−.142489	.081094	.0000000	−.165682	.091739	.0000000	−.186973	.098717	.0000000	−.200928	.103813	−.0000000	−.211120
.4313249	.072152	.0000000	−.146400	.084384	.0000000	−.170863	.095770	.0000000	−.193636	.103439	.0000000	−.208974	.109347	−.0000001	−.220791
.4513249	.074122	.0000000	−.149297	.086838	.0000000	−.174728	.098804	.0000000	−.198662	.107053	.0000001	−.215158	.113783	−.0000002	−.228618
.4713249	.075416	.0000000	−.151198	.088455	.0000000	−.177276	.100819	.0000000	−.202003	.109485	.0000001	−.219336	.116953	−.0000003	−.234272
.4913249	.076040	.0000000	−.152113	.089237	.0000000	−.178507	.101796	.0000000	−.203625	.110676	.0000002	−.221386	.118612	−.0000002	−.237256
.5113249	.075996	.0000000	−.152048	.089181	.0000000	−.178419	.101727	.0000000	−.203510	.110591	.0000002	−.221240	.118495	.0000024	−.237046
.5313249	.075283	.0000000	−.151003	.088289	.0000000	−.177014	.100611	.0000000	−.201659	.109233	.0000001	−.218902	.116612	.0000031	−.233660
.5513249	.073900	−.0000000	−.148971	.086560	−.0000000	−.174292	.098461	−.0000000	−.198092	.106640	−.0000001	−.214451	.113266	−.0000037	−.227703

TABLE III.—RESULTS OF CALCULATIONS FOR PARABOLIC-ARC BODY OF FINENESS RATIO 10 AT MACH NUMBERS ABOVE THE UPPER CRITICAL (PURELY SUPERSONIC FLOWS)

x/l	(a) $M_\infty=1.21$			(b) $M_\infty=1.22$			(c) $M_\infty=1.23$		
	u/U_∞	$\Delta/29$	C_p	u/U_∞	$\Delta/29$	C_p	u/U_∞	$\Delta/29$	C_p
0.0113249	−0.122523	−0.0000057	0.206838	−0.119625	−0.0000021	0.201041	−0.117275	−0.0000010	0.196342
.0313249	−.110329	−.0000011	.185513	−.108363	−.0000006	.181582	−.106645	−.0000003	.178144
.0513249	−.099655	−.0000004	.167101	−.098195	−.0000002	.164181	−.096881	−.0000002	.161552
.0713249	−.089884	−.0000002	.150365	−.088770	−.0000001	.148139	−.087752	−.0000001	.146102
.0913249	−.080765	−.0000001	.134808	−.079914	−.0000001	.133106	−.079127	−.0000001	.131532
.1113249	−.072163	−.0000001	.120154	−.071520	−.0000000	.118870	−.070922	−.0000000	.117674
.1313249	−.063990	−.0000000	.106232	−.063520	−.0000000	.105292	−.063080	−.0000000	.104412
.1513249	−.056188	−.0000000	.092923	−.055863	−.0000000	.092273	−.055557	−.0000000	.091662
.1713249	−.048715	−.0000000	.080145	−.048514	−.0000000	.079743	−.048324	−.0000000	.079364
.1913249	−.041540		.067835	−.041447		.067648	−.041358		.067471
.2113249	−.034641		.055949	−.034641		.055949	−.034641		.055949
.2313249	−.028001		.044451	−.028082		.044615	−.028160		.044771
.2513249	−.021606	.0000000	.033319	−.021760	.0000000	.033626	−.021906	.0000000	.033918
.2713249	−.015450	.0000000	.022532	−.015666	.0000000	.022966	−.015873	.0000000	.023379
.2913249	−.009524	.0000000	.012081	−.009796	.0000000	.012625	−.010055	.0000000	.013144
.3113249	−.003827	.0000000	.001958	−.004147	.0000000	.002598	−.004453	.0000000	.003210
.3313249	.001644	.0000000	−.007839	.001282	.0000000	−.007115	.000936	.0000000	−.006423
.3513249	.006886	.0000000	−.017309	.006488	.0000000	−.016513	.006107	.0000000	−.015752
.3713249	.011898	.0000000	−.026446	.011470	.0000000	−.025588	.011059	.0000000	−.024768
.3913249	.016675	.0000000	−.035240	.016221	.0000000	−.034332	.015786	.0000000	−.033462
.4113249	.021211	.0000000	−.043681	.020737	.0000000	−.042731	.020282	−.0000000	−.041821
.4313249	.025499	.0000000	−.051752	.025007	.0000000	−.050770	.024537	.0000000	−.049828
.4513249	.029527	−.0000000	−.059434	.029024	−.0000000	−.058428	.028542	−.0000000	−.057464
.4713249	.033287	−.0000000	−.066705	.032776	−.0000000	−.065683	.032286	−.0000000	−.064704
.4913249	.036763	−.0000000	−.073538	.036249	−.0000000	−.072510	.035756	−.0000000	−.071524
.5113249	.039942	−.0000000	−.079905	.039428	−.0000000	−.078877	.038935	−.0000000	−.077891
.5313249	.042807	−.0000000	−.085771	.042297	−.0000000	−.084751	.041808	−.0000000	−.083773
.5513249	.045337	−.0000000	−.091096	.044835	−.0000000	−.090092	.044354	−.0000000	−.089130
.5713249	.047512	−.0000000	−.095761	.047022	−.0000000	−.094780	.046552	−.0000000	−.093840
.5913249	.049307	−.0000000	−.099948	.048831	−.0000000	−.098997	.043376	−.0000000	−.098087
.6113249	.050693	−.0000000	−.103368	.050237	−.0000000	−.102456	.049800	−.0000000	−.101583
.6313249	.051639	−.0000000	−.106037	.051206	−.0000000	−.105171	.050791	−.0000000	−.104342
.6513249	.052109	−.0000000	−.107883	.051703	−.0000000	−.107069	.051314	−.0000000	−.106292
.6713249	.052063	−.0000000	−.108823	.051687	−.0000000	−.108070	.051328	−.0000000	−.107352
.6913249	.051453	−.0000000	−.108763	.051111	−.0000000	−.108079	.050785	−.0000000	−.107428
.7113249	.050225	−.0000000	−.107595	.049921	−.0000000	−.106988	.049633	−.0000000	−.106411
.7313249	.048315	−.0000000	−.105192	.048054	−.0000000	−.104671	.047808	−.0000000	−.104177
.7513249	.045649	−.0000000	−.101405	.045436	−.0000000	−.100978	.045234	−.0000000	−.100575
.7713249	.042137	−.0000000	−.096053	.041976	−.0000000	−.095731	.041825	−.0000000	−.095429
.7913249	.037671	−.0000001	−.088922	.037567	−.0000001	−.088714	.037472	−.0000001	−.088523
.8113249	.032118	−.0000001	−.079743	.032076	−.0000001	−.079660	.032042	−.0000001	−.079591
.8313249	.025306	−.0000001	−.068176	.025334	−.0000001	−.068232	.025366	−.0000001	−.068297
.8513249	.017016	−.0000002	−.053781	.017121	−.0000002	−.053990	.017227	−.0000002	−.054202
.8713249	.006949	−.0000004	−.035960	.007139	−.0000004	−.036339	.007327	−.0000004	−.036715
.8913249	−.005318	−.0000007	−.013866	−.005032	−.0000007	−.014438	−.004752	−.0000007	−.014998
.9113249	−.020428	−.0000015	.013786	−.020031	−.0000015	.012992	−.019646	−.0000015	.012221
.9313249	−.039449	−.0000036	.049131	−.038920	−.0000036	.048073	−.038409	−.0000035	.047052
.9513249	−.064442	−.0000107	.096292	−.063743	−.0000105	.094895	−.063074	−.0000104	.093557
.9713249	−.100636	−.0000475	.165728	−.099660	−.0000464	.163777	−.098746	−.0000456	.161948
.9913249									

TABLE III.—RESULTS OF CALCULATIONS FOR PARABOLIC-ARC BODY OF FINENESS RATIO 10 AT MACH NUMBERS ABOVE THE UPPER CRITICAL (PURELY SUPERSONIC FLOWS)—Concluded

x/l	(d) $M_\infty = 1.25$			(e) $M_\infty = 1.30$			(f) $M_\infty = 1.40$		
	u/U_∞	$\Delta/29$	C_p	u/U_∞	$\Delta/29$	C_p	u/U_∞	$\Delta/29$	C_p
0.0113249	−0.113468	−0.0000003	0.188727	−0.106554	−0.0000001	0.174899	−0.097431	−0.0000000	0.156654
.0313249	−.103712	−.0000001	.172279	−.098114	−.0000000	.161083	−.090448	−.0000000	.145751
.0513249	−.094578	−.0000001	.156946	−.090040	−.0000000	.147870	−.083650	−.0000000	.135090
.0713249	−.085938	−.0000000	.142474	−.082282	−.0000000	.135162	−.077022	−.0000000	.124642
.0913249	−.077710	−.0000000	.128697	−.074805	−.0000000	.122888	−.070552	−.0000000	.114381
.1113249	−.069836	−.0000000	.115501	−.067580	−.0000000	.110990	−.064230	−.0000000	.104288
.1313249	−.062275	−.0000000	.102802	−.060587	−.0000000	.099426	−.058049	−.0000000	.094350
.1513249	−.054995	−.0000000	.090539	−.053807	−.0000000	.088163	−.052002	−.0000000	.084553
.1713249	−.047975	−.0000000	.078665	−.047229	−.0000000	.077175	−.046087	−.0000000	.074891
.1913249	−.041194		.067144	−.040843		.066441	−.040301		.065357
.2113249	−.034641		.055949	−.034641		.055949	−.034641		.055949
.2313249	−.028305		.045060	−.028618		.045687	−.029108		.046666
.2513249	−.022179	.0000000	.034464	−.022772	.0000000	.035649	−.023703	.0000000	.037511
.2713249	−.016259	.0000000	.024151	−.017100	.0000000	.025832	−.018427	.0000000	.028487
.2913249	−.010541	.0000000	.014115	−.011602	.0000000	.016237	−.013284	.0000000	.019601
.3113249	−.005026	.0000000	.004356	−.006281	.0000000	.006866	−.008278	.0000000	.010860
.3313249	.000286	.0000000	−.005124	−.001139	.0000000	−.002274	−.003413	−.0000000	.002274
.3513249	.005392	.0000000	−.014321	.003820	.0000000	−.011176	.001304	−.0000000	−.006145
.3713249	.010288	.0000000	−.023225	.008589	.0000000	−.019828	.005866	−.0000000	−.014382
.3913249	.014968	.0000000	−.031826	.013164	−.0000000	−.028217	.010266	−.0000000	−.022421
.4113249	.019425	.0000000	−.040108	.017535	−.0000000	−.036327	.014493	−.0000000	−.030244
.4313249	.023650	.0000000	−.048055	.021692	−.0000000	−.044139	.018538	−.0000000	−.037830
.4513249	.027634	−.0000000	−.055647	.025626	−.0000000	−.051631	.022388	−.0000000	−.045156
.4713249	.031364	−.0000000	−.062859	.029323	−.0000000	−.058778	.026031	−.0000000	−.052194
.4913249	.034826	−.0000000	−.069664	.032770	−.0000000	−.065553	.029452	−.0000000	−.058917
.5113249	.038006	−.0000000	−.076033	.035951	−.0000000	−.071923	.032635	−.0000000	−.065291
.5313249	.040886	−.0000000	−.081930	.038849	−.0000000	−.077855	.035562	−.0000000	−.071281
.5513249	.043447	−.0000000	−.087316	.041444	−.0000000	−.083308	.038213	−.0000000	−.076847
.5713249	.045666	−.0000000	−.092070	.043712	−.0000000	−.088160	.040565	−.0000000	−.081866
.5913249	.047520	−.0000000	−.096374	.045630	−.0000000	−.092595	.042593	−.0000000	−.086521
.6113249	.048979	−.0000000	−.099940	.047170	−.0000000	−.096323	.044271	−.0000000	−.090524
.6313249	.050012	−.0000000	−.102784	.048301	−.0000000	−.099361	.045565	−.0000000	−.093890
.6513249	.050585	−.0000000	−.104833	.048986	−.0000000	−.101636	.046442	−.0000000	−.096548
.6713249	.050655	−.0000000	−.106006	.049186	−.0000000	−.103068	.046860	−.0000000	−.098417
.6913249	.050177	−.0000000	−.106210	.048853	−.0000000	−.103564	.046775	−.0000000	−.099406
.7113249	.049096	−.0000000	−.105337	.047936	−.0000000	−.103017	.046132	−.0000000	−.099410
.7313249	.047350	−.0000000	−.103261	.046370	−.0000000	−.101303	.044872	−.0000000	−.098305
.7513249	.044864	−.0000000	−.099835	.044084	−.0000000	−.098275	.042921	−.0000000	−.095948
.7713249	.041551	−.0000000	−.094881	.040990	−.0000000	−.093759	.040193	−.0000000	−.092165
.7913249	.037304	−.0000001	−.088187	.036982	−.0000001	−.087543	.036585	−.0000001	−.086749
.8113249	.031989	−.0000001	−.079486	.031929	−.0000001	−.079366	.031968	−.0000001	−.079443
.8313249	.025441	−.0000001	−.068446	.025667	−.0000001	−.068898	.026179	−.0000001	−.069922
.8513249	.017442	−.0000002	−.054732	.017981	−.0000002	−.055711	.019008	−.0000002	−.057765
.8713249	.007697	−.0000004	−.037456	.008581	−.0000004	−.039224	.010171	−.0000004	−.042403
.8913249	−.004208	−.0000007	−.016085	−.002941	−.0000007	−.018619	−.000736	−.0000007	−.023030
.9113249	−.018905	−.0000015	.010739	−.017207	−.0000014	.007345	−.014321	−.0000014	.001572
.9313249	−.037437	−.0000035	.045108	−.035245	−.0000034	.040724	−.031594	−.0000034	.033421
.9513249	−.061815	−.0000096	.091038	−.059026	−.0000101	.085461	−.054490	−.0000099	.076389
.9713249	−.097063	−.0000446	.158583	−.093466	−.0000433	.151389	−.087834	−.0000426	.140124
.9913249				−.164899	−.0005193	.291174	−.157350	−.0005067	.276077

TABLE IV.—RESULTS OF CALCULATIONS FOR PARABOLIC-ARC BODIES OF VARIOUS FINENESS RATIOS AT $M_\infty=1$—EQUATION (87)

x/l	(a) $l/d=6$			(b) $l/d=6\sqrt{2}$			(c) $l/d=10$			(d) $l/d=12$			(e) $l/d=14$		
	u/U_∞	$\Delta/29$	C_p	u/U_∞	$\Delta/29$	C_p	u/U_∞	$\Delta/29$	C_p	u/U_∞	$\Delta/29$	C_p	u/U_∞	$\Delta/29$	C_p
0.0113249	−0.402655	−0.0008544	0.699175	−0.227573	−0.0004337	0.402079	−0.171300	−0.0002381	0.304392	−0.127810	−0.0002188	0.229087	−0.098643	−0.0001612	0.177792
.0313249	−.286750	−.0000885	.475875	−.167093	−.0000445	.285374	−.128741	−.0000375	.222337	−.096135	−.0000249	.167864	−.074880	−.0000200	.131830
.0513249	−.231813	−.0000228	.374156	−.136809	−.0000138	.228883	−.106013	−.0000094	.179817	−.079472	−.0000064	.136577	−.062113	−.0000040	.107792
.0713249	−.193750	−.0000073	.305828	−.114881	−.0000021	.188926	−.089070	.0000034	.148738	−.066924	−.0000014	.113430	−.052354	−.0000017	.089707
.0913249	−.163815	−.0000036	.253400	−.097040	−.0000037	.156965	−.075276	−.0000085	.123830	−.056494	−.0000031	.094431	−.044186	−.0000029	.074738
.1113249	−.138764	−.0000028	.210386	−.081740	−.0000018	.129909	−.063247	.0000032	.102324	−.047349	−.0000004	.077913	−.036958	−.0000002	.061585
.1313249	−.116932	−.0000004	.173455	−.068109	−.0000001	.106013	−.052454	−.0000005	.083160	−.039109	−.0000007	.063117	−.030427	−.0000010	.049759
.1513249	−.097439	−.0000014	.140844	−.055784	−.0000017	.084551	−.042662	−.0000012	.065872	−.031588	−.0000010	.049667	−.024445	−.0000009	.038966
.1713249	−.079708	−.0000005	.111405	−.044445	−.0000005	.064883	−.033618	−.0000003	.049952	−.024617	−.0000002	.037230	−.018887	−.0000001	.028955
.1913249	−.063349		.084351	−.033907		.046641	−.025200		.035155	−.018117		.025647	−.013699		.019620
.2113249	−.048113		.059188	−.024056		.029594	−.017321		.021308	−.012028		.014797	−.008837		.010871
.2313249	−.033805		.035528	−.014794		.013546	−.009910		.008270	−.006301		.004582	−.004264		.002636
.2513249	−.020283	.0000003	.013083	−.006046	.0000003	−.001651	−.002918	.0000001	−.004059	−.000902	.0000001	−.005067	.000044	.0000001	−.005137
.2713249	−.007453	.0000007	−.008336	.002226	.0000006	−.016072	.003689	.0000006	−.015746	.004194	.0000004	−.014197	.004107	.0000004	−.012482
.2913249	.004773	−.0000002	−.028899	.010068	.0000001	−.029813	.009935	.0000001	−.026837	.009000	.0000002	−.022838	.007931	.0000003	−.019417
.3113249	.016460	.0000007	−.048741	.017519	.0000006	−.042948	.015858	.0000001	−.037411	.013545	−.0000000	−.031045	.011541	−.0000001	−.025989
.3313249	.027626	.0000003	−.067898	.024569	.0000007	−.055461	.021446	.0000010	−.047445	.017824	.0000009	−.038810	.014935	.0000009	−.032193
.3513249	.038339	−.0000004	−.086503	.031274	−.0000005	−.067461	.026730	−.0000008	−.056997	.021847	−.0000005	−.046151	.018110	.0000002	−.038024
.3713249	.048585	.0000008	−.104529	.037611	.0000011	−.078902	.031718	.0000007	−.066086	.025638	.0000003	−.053115	.021099	.0000001	−.043549
.3913249	.058405	−.0000006	−.122060	.043605	−.0000007	−.089834	.036394	−.0000000	−.074677	.029165	.0000004	−.059643	.023865	.0000008	−.048693
.4113249	.067783	.0000005	−.139060	.049252	.0000006	−.100251	.040791	−.0000003	−.082840	.032469	−.0000006	−.065811	.026445	−.0000009	−.053532
.4313249	.076733	−.0000003	−.155562	.054547	−.0000002	−.110143	.044874	.0000005	−.090503	.035515	.0000007	−.071555	.028815	.0000008	−.058015
.4513249	.085234	.0000003	−.171521	.059498	.0000000	−.119523	.048676	−.0000005	−.097730	.038330	−.0000006	−.076924	.030989	−.0000005	−.062171
.4713249	.093286	−.0000002	−.186938	.064087	.0000001	−.128357	.052161	.0000005	−.104453	.040892	.0000004	−.081875	.032959	.0000003	−.065985
.4913249	.100859	.0000001	−.201752	.068319	−.0000001	−.136655	.055355	−.0000004	−.110721	.043215	−.0000003	−.086438	.034726	−.0000001	−.069459
.5113249	.107943	−.0000001	−.215942	.072173	.0000001	−.144375	.058223	.0000004	−.116466	.045283	.0000002	−.090579	.036292	.0000001	−.072594
.5313249	.114498	.0000001	−.229432	.075654	−.0000001	−.151525	.060794	−.0000004	−.121745	.047107	−.0000002	−.094322			
.5513249	.120509	−.0000001	−.242188	.078739	.0000001	−.158063	.063031	.0000004	−.126484						
.5713249	.125917	−.0000004	−.254095				.064965	−.0000003	−.130667						
.5913249	.130752	−.0000002	−.265211				.066565	.0000006	−.134465						
.6113249	.134910	−.0000002	−.275328				.067894	−.0000007	−.137770						
.6313249							.068918	.0000006	−.140596						
.6513249							.069730	−.0000002	−.143123						
.6713249							.070327	.0000001	−.145350						
.6913249							.070826	−.0000002	−.147508						
.7113249							.071225	−.0000002	−.149596						
.7313249							.071603	−.0000002	−.151768						
.7513249							.071891	.0000001	−.153889						
.7713249							.072110	.0000002	−.156000						

TABLE V.—RESULTS OF CALCULATIONS FOR PARABOLIC-ARC BODIES OF VARIOUS FINENESS RATIOS AT $M_\infty = 1$—EQUATION (42)

x/l	(a) $l/d=6$			(b) $l/d=6\sqrt{2}$			(c) $l/d=10$			(d) $l/d=12$			(e) $l/d=14$		
	u/U_∞	$\Delta/29$	C_p	u/U_∞	$\Delta/29$	C_p	u/U_∞	$\Delta/29$	C_p	u/U_∞	$\Delta/29$	C_p	u/U_∞	$\Delta/29$	C_p
0.3113249							0.004707	−0.0000035	−0.015109						
.3313249							.012865	−.0000006	−.030282						
.3513249							.020017	−.0000002	−.043570						
.3713249							.026487	−.0000001	−.055624						
.3913249							.032397	−.0000000	−.066684						
.4113249							.037806	−.0000000	−.076869						
.4313249							.042748	−.0000000	−.086250						
.4513249							.047241	−.0000000	−.094860						
.4713249							.051294	−.0000000	−.102719						
.4913249							.054908	−.0000000	−.109827						
.5113249							.058078		−.116176				0.036292		−0.072594
.5313249							.060794		−.121745	0.047107		−0.094322	.037617		−.075315
.5513249				0.078739		−0.158063	.063042		−.126505	.048582		−.097456	.038647	0.0000000	−.077509
.5713249				.081411		−.163952	.064802	−.0000000	−.130341	.049676	−0.0000000	−.099917	.039370	−.0000000	−.079155
.5913249				.083450	−0.0000000	−.168753	.066052	−.0000000	−.133438	.050372	−.0000000	−.101671	.039773	−.0000000	−.080228
.6113249	0.134910		−0.275328	.084818	−.0000000	−.172391	.066762	−.0000000	−.135508	.050650	−.0000000	−.102677	.039842	−.0000000	−.080695
.6313249	.138099		−.283863	.085470	−.0000000	−.174773	.066899	−.0000000	−.136558	.050485	−.0000000	−.102886	.039557	−.0000000	−.080522
.6513249	.140087	−0.0000000	−.290351	.085352	−.0000000	−.175792	.066423	−.0000000	−.136510	.049848	−.0000000	−.102241	.038898	−.0000000	−.079664
.6713249	.140754	−.0000000	−.294554	.084398	−.0000000	−.175319	.065285	−.0000000	−.135268	.048706	−.0000000	−.100674	.037838	−.0000000	−.078072
.6913249	.139957	−.0000001	−.296183	.082533	−.0000000	−.173201	.063430	−.0000000	−.132718	.047019	−.0000000	−.098105	.036348	−.0000000	−.075684
.7113249	.137524	−.0000001	−.294890	.079666	−.0000000	−.169255	.060791	−.0000000	−.128727	.044737	−.0000000	−.094437	.034391	−.0000000	−.072429
.7313249	.133249	−.0000001	−.290280	.075685	−.0000001	−.163262	.057284	−.0000000	−.123130	.041804	−.0000000	−.089554	.031925	−.0000000	−.068218
.7513249	.126877	−.0000001	−.281827	.070456	−.0000001	−.154949	.052810	−.0000001	−.115727	.038147	−.0000000	−.083312	.028894	−.0000000	−.062944
.7713249	.118094	−.0000002	−.268906	.063809	−.0000001	−.143977	.047243	−.0000001	−.106265	.033674	−.0000001	−.075528	.025229	−.0000001	−.056469
.7913249	.106495	−.0000004	−.250710	.055523	−.0000002	−.129906	.040417	−.0000002	−.094413	.028266	−.0000002	−.065962	.020839	−.0000001	−.048607
.8113249	.091545	−.0000007	−.226166	.045298	−.0000005	−.112134	.032102	−.0000004	−.079712	.021752	−.0000003	−.054273	.015592	−.0000003	−.039096
.8313249	.072486	−.0000014	−.193761	.032686	−.0000012	−.089767	.021947	−.0000011	−.061459	.013860	−.0000010	−.039917	.009266	−.0000010	−.027493
.8513249	.048118	−.0000041	−.151093	.016876	−.0000046	−.061180	.009244	−.0000052	−.038237	.003941	−.0000067	−.021596	.001190	−.0000098	−.012456
.8713249	.015770	−.0000244	−.092820												

TABLE VI.—RESULTS OF CALCULATIONS FOR PARABOLIC-ARC BODIES OF VARIOUS FINENESS RATIOS AT $M_\infty = 1$—EQUATION (29)

z/l	(a) $l/d=6$			(b) $l/d=6\sqrt{2}$			(c) $l/d=10$			(d) $l/d=12$			(e) $l/d=14$		
	u/U_∞	$\Delta/29$	C_p	u/U_∞	$\Delta/29$	C_p	u/U_∞	$\Delta/29$	C_p	u/U_∞	$\Delta/29$	C_p	u/U_∞	$\Delta/29$	C_p
0				0		−0.029985	0		−0.021073	0		−0.014206	0		−0.010205
.85357										−.002284					
.85757						−.020971	−.006891		−.008280			−.009919	−.003525		−.003807
.86132															
.86492															
.86783				0			0								
.87132				−.004835		−.003135	−.014153		.005041	−.013050		.009943	−.011700		.011530
.87853	0		−0.063681												
.88132	−.006720		−.051187	−.014589		−.013970	−.021310		.018118	−.018333		.019650	−.015789		.019076
.88132	−.024220		−.019620	−.024000		−.031041	−.028536		.031302	−.022704	−0.0000007	.029512	−.019963	−0.0000002	.026779
.90132	−.040900		.010217	−.033416		.048471	−.035946	−0.0000005	.044823	−.029230	−.0000004	.039661	−.024265	−.0000002	.034720
.91132	−.057576		.039957	−.043034	−0.0000013	.066562	−.043641	−.0000003	.058880	−.034976	−.0000002	.050228	−.028742	−.0000001	.042993
.92132	−.074710	−0.0000032	.070525	−.053005	−.0000008	.085638	−.051731	−.0000002	.073696	−.041014	−.0000001	.061357	−.033443	−.0000001	.051700
.93132	−.092881	−.0000019	.102677	−.063490	−.0000004	.106091	−.060355	−.0000003	.089548	−.047441	−.0000002	.073240	−.038441	−.0000001	.060983
.94132	−.111919	−.0000012	.137274	−.074886	−.0000004	.128486	−.069715	−.0000005	.106840	−.054394	−.0000003	.086154	−.043834	−.0000002	.071039
.95132	−.132997	−.0000015	.175463	−.086876	−.0000007	.153714	−.080132	−.0000010	.126213	−.062096	−.0000007	.100546	−.049788	−.0000005	.082202
.96132	−.156821	−.0000029	.219055	−.100504	−.0000014	.183419	−.092197	−.0000027	.148850	−.070658	−.0000019	.117234	−.056602	−.0000014	.095069
.97132	−.185030	−.0000076	.271328	−.116392	−.0000038	.221309	−.107245	−.0000098	.177423	−.081909	−.0000068	.138077	−.064961	−.0000050	.111010
.98132	−.221334	−.0000272	.339703	−.136396	−.0000136	.280397	−.129979	−.0000651	.221333	−.098214	−.0000452	.169606	−.077263	−.0000332	.134820
.99132	−.278766	−.0001808	.450242	−.167021	−.0000897										

U.S. GOVERNMENT PRINTING OFFICE: 1959